

Equation of state for dense matter from finite nuclei to neutron star mergers

THESIS

Submitted in partial fulfillment
of the requirements for the degree of
DOCTOR OF PHILOSOPHY

by

Tuhin Malik 

(Roll No. 2014PHXF0402G)

Under the guidance of

Dr. Tarun Kumar Jha (Supervisor)

and

Prof. Bijay Kumar Agrawal (Co-supervisor)



DEPARTMENT OF PHYSICS

BIRLA INSTITUTE OF TECHNOLOGY AND SCIENCE, PILANI

December - 2019

Dedicated to my parents

and

brother

**BIRLA INSTITUTE OF TECHNOLOGY AND SCIENCE, PILANI
(RAJASTHAN)**

CERTIFICATE

This is to certify that the thesis entitled “**Equation of state for dense matter from finite nuclei to neutron star mergers**” submitted by **TUHIN MALIK**, ID No 2014PHXF0402G for award of **Ph.D.** of the Institute embodies original work done by him under our supervision.



Signature of the Supervisor

Name: **Dr. Tarun Kumar Jha**

Designation: Assistant professor

Affiliation: BITS Pilani, Goa, India

Date: 10/12/2019



Signature of the Co-Supervisor

Name: **Prof. Bijay Kumar Agrawal**

Designation: Professor 'H'


Affiliation: Saha Institute of Nuclear Physics
Kolkata, India

Date: 10/12/2019

Abstract

Equation of state (EOS) of dense matter has been constrained from the experimental data available on the properties of finite nuclei and neutron stars. Towards this purpose, a diverse set of nuclear energy density functionals based on relativistic and non-relativistic mean field models have been employed. These EOSs are so chosen that they are consistent with the bulk properties of the finite nuclei. The values of various nuclear matter parameters which predominantly govern the behaviour of the EOS are determined through their correlations with the properties of the neutron stars such as radii, tidal deformability and maximum mass of the neutron stars. The nuclear matter parameters considered are incompressibility, symmetry energy and their density derivatives which appear in the expansion of the EOS around the saturation density. The radii and tidal deformability of the neutron star with the canonical mass display strong correlations with the linear combinations of slopes of the incompressibility and symmetry energy coefficients. Similar correlations with the curvature of the symmetry energy coefficient are also observed indicating that the properties of the neutron stars are sensitive to the high density behaviour of the symmetry energy. It is also shown that the giant resonances in nuclei are instrumental in limiting the tidal deformability parameter and the radius of a neutron star in somewhat narrower bounds. The outcomes of the present thesis is important in view of the fact that the accurate values of the various neutron star observables as considered are expected to be available in near future.

Declaration of Academic Integrity

I, **Tuhin Malik** , S/o Mr. Sibnath Malik, declare that this written submission represents my ideas in my own words and where others ideas or words have been included, I have adequately cited and referenced the original sources. I also declare that I have adhered to all principles of academic honesty and integrity and have not misrepresented or fabricated or falsified any idea/data/fact/source in my submission. I understand that any violation of the above will be cause for disciplinary action as per rules of regulations of the Institute.

Tuhin Malik
Tuhin Malik 

Acknowledgement

I express my deepest love and respect towards my parents and my brother for providing me all kinds of support throughout my life. The journey during my Ph.D. has been full of many ups and downs. It was the journey undertaken together with my whole family. **Baba-Ma, Dida, Masi, and Korobi**, I wish I could show my admiration more!

Foremost, I take this opportunity to express my profound sense of gratitude to my thesis advisor **Dr. Tarun Kumar Jha**, Department of Physics, BITS Pilani K K Birla Goa Campus. He introduces me to the fantastic world of neutron stars. His constant advice, continuous encouragement, friendly attitude, and patience at every stage inspired me a lot. The relationship with him was never limited to the academic discussion. Probably he is the coolest gentleman I ever met in my life. The biggest lesson I learned from him is that always be relaxed in the tough situation of life.

Probably no gratitude is enough for the constant support provided by **Prof. Bijay Kumar Agrawal**, who has been one of the advisors for this thesis. The amount of inquisitiveness and enthusiasm he has to offer towards the subject is genuinely inspiring. I am forever in debt to him for making me love the subject. I much appreciate him for his tireless support, constant encouragement, and extraordinary mentorship throughout my Ph.D. tenure. Our both academic and non-academic discussions over the years have been of great value to me. Without his ever-present guidance, this work would not have been a reality. I also acknowledge the fatherly advice and care of **Prof. Jadunath De** and **Prof. Santosh Samaddar**, with whom I was so privileged to collaborate for several occasions. The wisdom and the stories that they shared will always bring a joyous smile in my face. I also acknowledge the help provided by **Mrs. Tanuja Agrawal** to present the results in the manuscript of the calculations more attractively.

I would like to sincerely thank my collaborators, **Prof. Constança Providência**, and **Dr. Morgane Fortin**, for collaborating at different phases of this thesis work. I am very grateful to them for their immense help and precious advice. Prof. C. Providência hosted twice during my visit to the University of Coimbra, Portugal, offering very warm hospitality during Aug 2018 and July 2019. I

take this opportunity to thank all my other collaborators **Dr. Chiranjib Mondal**(Chiru Da) and **Dr. Naosad Alam** (Naosad Da), as they are not only collaborators but also good friends.

I should remain thankful to my collaborator **Prof. Hiranmaya Mishra** for arranging a visit to Physical Research Laboratory, Ahmedabad. His excellent knowledge in Physics inspired me and helped me a lot to deal with the critical research problem. **Prof. Suresh Kumar Patra** of Institute of Physics, Bhubaneswar, also be thanked for inviting me for a visit. I must thank my other collaborators, **Dr. Bharat Kumar, Dr. Arpan Das, and Dr. Alekha Naik**, for their support during the different phases of this work.

I am also indebted to the members of my doctoral committee, **Dr. V Sunil Kumar, Prof. Chandradew Sharma**, for their encouraging words and thoughtful criticism. I would also like to thank all the other faculty members of the department for their continuous encouragement and support. I am very much thankful to all faculty members of this department. I am fortunate to be a part of this department. The faculty and student relations in this department not just limited to discussion about physics.

Especially, I would like to express my deepest gratefulness and love to **Dr. Kinjal Banerjee and Dr. Rudranil Basu** for their unconditional support, love, and patience. They are not just faculty members of my department even friends as well. I am also grateful to **Dr. Debdulal Thakur** (Former faculty Economics, BITS Goa), **Dr. Soumodip Bandhopadhyay** (Computer Sc, BITS Goa), **Mrs. Nilanajona Goswami, Dr. Rajashree Sengupta** (Economics, BITS Goa), whom I got as friends and guardians during my Ph.D. I am very much fortunate that I got so many good peoples around me as friends during 5 years of my Ph.D. journey. They all have contributions to this thesis in different ways.

Life has blessed me with a lot of good friends, who often showed the best ways to deal with a problem. **Subhas, Koushik** without your friendship life would not be this beautiful. Throughout my research career, my colleagues **Selvaganapathy and Akhila, Arunkarthick, Bijeesh M. M., A. Venkatesan, Souvik Da, Sreemanta Da, Atanu, Chithira, Shakhi, Dhavala, Malati, Mouna, Deepak, Aditya, Saumyen, Anu, Malavika, Sumit, Kiran, Sharvari, Sourav, Abhay** needs to be spacial thanked. **Avijit**, it has been a pleasure to having him as a friend and thanks for his supports. Someone needs to be specially thanked for teaching me about both good and hard lessons of life.

I would like to thank **Prof. Souvik Bhattacharyya** (Vice-Chancellor, BITS Pilani), **Prof. Raghurama G.** (Director, BITS Pilani, K K Birla Goa Campus), **Prof. Sasikumar Punnekkat** (Former Director, BITS Pilani, K K Birla Goa Campus), **Prof. Srinivas Krishnaswamy** (Dean, Academic Graduate Studies and Research Division, BITS Pilani), **Prof. Bharat Deshpande** (Associate Dean,

Academic Graduate Studies and Research Division) and **Prof. Prasanta Kumar Das** (Former Associate Dean, Academic Graduate Studies and Research Division).

I am also thankful to all my school and college teachers. Without their diligent teaching, I never would be able to come to this stage. **Dr Saurav Palit** (Saurav Da) needs to be specially thanked for encouraging me about the fun of physics and he is the one who inspired me first to chose Physics Honours. In my college days, I got all the faculty members of the Physics Department, Scottish Church College around me as best teachers and friends as well. The contribution of **Dr. Arup Roy, Dr. Bibhas Bhattacharya, and Dr. Satadal Bhattacharyya** is unforgettable to my life.

Now comes the funding agencies, without funding support this thesis work impossible. I would like to thank DAE-BRNS for its support (**2013/37P/5/BRNS**) during the first year and BITS Pilani for the remaining year of my Ph.D. SCIENCE & ENGINEERING RESEARCH BOARD (SERB), Govt. of India needs to be thanked for awarding me International Travel Support (**ITS2018002448**) to participate XXII International Conference on Few-Body Problems in Physics (FB22), France (09 July 2018 to 13 July 2018). I acknowledge the COUNCIL OF SCIENTIFIC AND INDUSTRIAL RESEARCH (CSIR), HUMAN RESOURCE DEVELOPMENT, Govt. of India for International Travel Grant (**TG1054219-HRD**) awarded to participate TALENT course 11 Learning from Data: Bayesian Methods and Machine Learning, in University of York, UK, June 10-28, 2019.

Finally, I must thank *Rimpa* for each and every encouragement I received. I am fortunate to have you as a wife in the last but not least stage of this thesis.

Date: December 10, 2019

Tuhin Malik
Tuhin Malik 

Contents

List of Tables	vii
List of Figures	x
Nomenclature	xiv
Abbreviation	xv
Keywords	xvii
List of Publication	xviii
1 Introduction	1
1.1 Opening words	1
1.2 Constraints from terrestrial and astrophysical Data	3
1.2.1 Finite nuclei	3
1.2.2 HIC and <i>ab-initio</i> methods	4
1.2.3 Neutron Star mass and radius	7
1.2.4 Multi messenger era	8
1.3 Objectives	9
1.4 Organization of the Thesis	11
2 Formalism	12
2.1 Field theoretical models	12
2.1.1 Effective Chiral Model (ECM)	13
2.1.2 Relativistic Mean Field Model (RMF)	14
2.2 Non relativistic Model	15

2.3	Nuclear matter parameter (NMP)	16
2.4	Structure and dynamics of neutron star	18
2.4.1	Tidal deformability	18
3	Nuclear interactions at high densities in effective chiral model	20
3.1	Background	20
3.2	Mesonic cross coupling	21
3.3	Symmetric nuclear matter properties	24
3.4	Density dependence of symmetry energy $S(\rho)$	24
3.5	Equation of state	27
3.6	Neutron star mass-radius relationship	29
3.7	Summary	33
4	Correlations of nuclear matter parameters with astrophysical observations	35
4.1	Background	35
4.2	Nuclear models and EOS parameters	36
4.3	Tidal deformability and Love Number	41
4.4	Nuclear mater parameters and astrophysical observable	43
4.5	Constraining M_0 and $K_{\text{sym},0}$	49
4.6	Neutron star radius and tidal deformability	52
4.7	Summary	54
5	Constraining dense matter EOS from terrestrial and astrophysical observations	55
5.1	Motivation from existing trends	57
5.2	Constraining tidal deformability from measured properties of finite nuclei	61
5.3	Summary	64
6	Conclusion	65
7	Future Scope of the Work	68
A	Mass dependence of correlations parameters	71
B	The properties of finite nuclei, nuclear matter, and neutron stars	72

List of Tables

1.1	The present nuclear constants pertaining to SNM (ϵ_0 and K_0) and density dependent symmetry energy (J_0 , L_0 and $K_{\text{sym},0}$) at saturation density ρ_0	5
1.2	The present empirical constant on EOS ($P(\rho)$, $\epsilon_n(\rho)$ and $S(\rho)$ represent pressure, energy per particle and symmetry energy respectively) corresponding to the symmetric nuclear matter (SNMX), pure neutron matter (PNMX) and symmetry energy coefficient (SYMX) together with the range of densities in which they are determined.	5
1.3	Present constraint on tidal deformability from GW170817 [Abbott et al. 2019]	9
3.1	List of the model parameters determined from the properties of SNM such as, energy per nucleon $E_0 = -16$ MeV, nuclear incompressibility $K = 247$ MeV and the nucleon effective mass $Y = m^*/m = 0.864$ at the saturation density $\rho_0 = 0.153$ fm ⁻³ . The scalar and vector meson coupling parameters are $C_\sigma = g_\sigma^2/m_\sigma^2$ and $C_\omega = g_\omega^2/m_\omega^2$ respectively. $B = b/m^2$ and $C = c/m^4$ are the parameters for the higher order self-couplings of the scalar field with m being the nucleon mass. The nucleon, ω meson and σ meson masses are 939 MeV, 783 MeV and 469 MeV respectively.	24
3.2	The values of the coupling constants C_ρ , η_1 and η_2 are determined from various symmetry energy elements. The mass of the ρ meson is 770 MeV. The values of C_ρ are in units of fm ² , η_1 and η_2 are dimensionless. All the symmetry energy elements are in units of MeV.	25
3.3	The maximum mass and radius of NS composed of β - equilibrated matter are listed. The total mass and radii following the ZFH method are obtained by using Eqs. 3.14-3.16. These are compared with the ones calculated from the BPS and polytropic EOSs for the outer and inner crusts, respectively. ρ_{cc}/ρ_0 is the scaled transition density. M_{max} , R_{max} and $R_{1.4}$ are the NS maximum mass, radius at maximum mass and the radius at $1.4 M_\odot$ respectively.	32

4.1	The nuclear matter properties for a representative set of RMF models calculated at the saturation density ρ_0 . The quantities listed below are the energy per nucleon e_0 , incompressibility coefficient (K_0), skewness parameter(Q_0) for the symmetric nuclear matter. The symmetry energy coefficient (J_0), its slope (L_0) and the curvature ($K_{\text{sym},0}$) determining the density dependence of the symmetry energy.	38
4.2	Same as table 4.1, but , for SHF models.	39
4.3	The Pearson correlation coefficients, \mathcal{R} obtained for the correlations between various NS and nuclear matter properties. The values of tidal deformability Λ , radius R and the Love number k_2 are evaluated for the NS masses $1.2 - 1.6 M_\odot$. The nuclear matter incompressibility K_0 , the skewness Q_0 , slope of incompressibility M_0 , symmetry energy J_0 , slope of symmetry energy L_0 and the curvature parameters $K_{\text{sym},0}$	45
4.4	The values of the coefficients \mathcal{R} obtained for the correlations of Λ , R and k_2 with various linear combinations of EOS parameters. The calculations are performed for the NS masses $1.2 - 1.6 M_\odot$	46
4.5	Values for the correlations coefficients for $\Lambda_{1.4}$ and $k_{2,1.4}$ with $M_0 + \beta L_0$ and $M_0 + \eta K_{\text{sym},0}$ obtained separately for the RMF and SHF models. The values of the correlation coefficients corresponding to all the models (ALL) are also listed.	49
4.6	The empirical values of M_0 and $K_{\text{sym},0}$ derived for different limits on $\Lambda_{1.4}$ and L_0 . The bounds on $\Lambda_{1.4} > 344$ and $< 687(859)$ obtained from Fig. 4.9 are considered. The ranges of $L_0 = 40 - 62$ MeV and $L_0 = 30 - 86$ MeV are taken from Refs. [Lattimer & Lim 2013, Oertel <i>et al.</i> 2017].	52
5.1	Parameters for the model Sk Λ 267 and the resulting nuclear matter and neutron star properties along with their errors in the parenthesis. J_0 is the symmetry energy coefficient, L_0 is related to its density derivative [Malik <i>et al.</i> 2018b].	61
B.1	Some selected properties of nuclear matter such as binding energy per nucleon e_0 , nuclear matter incompressibility coefficient K_0 , its skewness Q_0 , symmetry energy coefficient J_0 , its slope L_0 , effective mass $\frac{m_0^*}{m}$, isovector splitting of nucleon effective mass $\frac{\Delta m_0^*}{\delta}$ calculated at saturation density density ρ_0 for the representative set of Skyrme models considered. The models are arranged according to increasing order of $\frac{m_0^*}{m}$. The values for various quantities associated with ^{208}Pb nucleus and those for neutron star as employed in Fig.1 of the main text are also listed.	74

B.2	Experimental values of the fit data and adopted errors on them for Sk Λ 267. For Sk Λ 484 we have taken additional fit data $\Lambda_{1,4} = 500 \pm 100$	75
B.3	Dipole polarizability α_D , peak energy of IVGDR $E_{\text{GDR}}^{\text{p}}$, centroid energy of ISGMR $E_{\text{GMR}}^{\text{c}}$ for different nuclei [Col <i>et al.</i> 2013] and neutron skin thickness Δr_{np} of ^{208}Pb are listed for Sk Λ 267 and Sk Λ 484 models. The corresponding experimental values are also provided for comparison.	76
B.4	Values of the parameters for the Sk Λ 267 and Sk Λ 484 models along with their errors. Different properties of nuclear matter and neutron star resulting from both the parameter sets are also listed. Definitions of the different nuclear matter properties are used as in Ref. [Dutra <i>et al.</i> 2012].	77

List of Figures

1.1	Experimental constraints for symmetry energy parameters from different experiments [Lattimer & Prakash 2016]	6
1.2	The constraint on the pressure $P(\rho)$ for SNM (left upper panel), PNM (left lower panel), energy per neutron ϵ_n of PNM (right upper panel) and symmetry energy coefficient $S(\rho)$ (right lower panel) as a function of baryon density ρ (see Table 1.2).	7
2.1	Effective potential (a) No spontaneous symmetry braking (b) spontaneous symmetry breaking [Koch 1997].	14
3.1	Symmetry energy as a function of scaled density (ρ/ρ_0) is plotted for three different variants of the effective chiral model as labeled by NCC, SR and WR obtained in the present work and are compared with those for a few selected RMF models NL3, IUFSU, BSP and BKA22. The constraints on the symmetry energy from IAS [Danielewicz & Lee 2014], HIC Sn+Sn [Tsang <i>et al.</i> 2009] and ASY-EOS experimental data [Russotto <i>et al.</i> 2016] are also displayed. The inset shows the blown up behavior of symmetry energy at low densities.	26
3.2	The values of K and K_τ from different models as labeled in [Colo <i>et al.</i> 2014, Sagawa <i>et al.</i> 2007] are compared with our models (NCC, SR and WR). The vertical and horizontal dashed lines represent the empirical ranges for K and K_τ respectively.	28
3.3	Energy per neutron as a function of scaled neutron density (ρ_n/ρ_0) for three different variants of the effective chiral model as labeled by NCC, SR and WR obtained in the present work and for a few RMF models NL3, IUFSU, BSP and BKA22 are compared with microscopic calculations [Gezerlis & Carlson 2010, Hebeler <i>et al.</i> 2013] as shown by the shaded region. . .	29

3.4	The pressure as a function of scaled density (ρ/ρ_0) for the SNM (left) and the PNM (right). The SNM EOS for the NCC, SR and WR models are exactly the same and is labeled by “this work”. For the comparison the SNM and PNM EOSs for a few RMF models NL3, IUFSU, BSP and BKA22 are displayed. The SNM and PNM EOSs shown by shaded regions are taken from Ref. [Danielewicz <i>et al.</i> 2002] (see text for details)	30
3.5	The mass-radius relationships for the NCC, SR and WR models are displayed. The effects of the crustal EOSs are incorporated by using explicitly the BPS and polytropic EOSs (solid lines) at low densities and alternatively using the ZFH method (dashed lines).	33
4.1	Probability distributions of energy per nucleon e_0 , saturation density (ρ_0), incompressibility coefficient (K_0) and skewness parameter(Q_0) corresponding to the symmetric nuclear matter obtained for a representative set of RMF and SHF models. The values of mean (μ) and the standard deviations (σ) for each of the NMP is also given. The NMPs as displayed along the abscissa are obtained by appropriate transformation so that the spread in their values can be compared. (see text for details).	37
4.2	Same as Fig. 4.1, but, for symmetry energy coefficient (J_0), its slope (L_0) and the curvature ($K_{\text{sym},0}$) which determine the density dependence of the symmetry energy coefficient.	40
4.3	Plots for the (a) pressure p as a function of the energy density, and (b) $dp/d\varepsilon$ as a function of the baryonic number density for beta equilibrated NS matter obtained using a representative set of RMF (black dashed lines) and SHF models (red lines). The circles in right panel correspond to the central densities and the slopes $dp/d\varepsilon$ at the maximum NS mass for each of the EOS. The BSk20 and BSk26 EOSs are marginally acausal at the NS maximum masses $\sim 2.2 M_\odot$ [Alam <i>et al.</i> 2016, Fortin <i>et al.</i> 2016].	41
4.4	(a) Tidal deformability Λ and (b) the Love number k_2 as a function of the NS mass (m) for a representative set of relativistic and non-relativistic models. The SHF model, SkI5, displays markedly different behavior for Λ as well as for k_2	42
4.5	Tidal deformability parameters for the case of high mass (Λ_1) and low mass (Λ_2) components of the observed GW170817. The 90%(dot-dot-dashed) and 50% (dot) confidence lines are taken from Ref. [Abbott <i>et al.</i> 2017a] corresponding to the low spin priors.	43

4.6	Correlation coefficients \mathcal{R} for (a-c) the tidal deformability Λ , (d-f) the radius R , and (g-i) the Love number k_2 with different individual nuclear matter parameters as well as with some selected linear combinations of them obtained for the NS masses $1.2 M_\odot$ (top), $1.4 M_\odot$ (middle) and $1.6 M_\odot$ (bottom). Results are plotted only for the cases with $\mathcal{R} > 0.5$ (see tables 4.3 and 4.4 for details).	44
4.7	The probability distribution for the correlations of $\Lambda_{1.4}$ with $M_0 + \beta L_0$ (left) and $M_0 + \eta K_{\text{sym},0}$ (right) calculated using bootstrap method (see text for details).	47
4.8	(a-b) The $M_0 + \beta L_0$ and (c-d) $M_0 + \eta K_{\text{sym},0}$ versus the tidal Love number $k_{2,1.4}$ (top panels) and dimensionless tidal deformability $\Lambda_{1.4}$ (bottom panels) for a $1.4 M_\odot$ NS, using a set of RMF and SHF models.	48
4.9	The tidal deformability $\Lambda_{1.4}$ versus the weighted average $\tilde{\Lambda}$ as defined in Eq.(2.39) for all the RMF and SHF models. The solid line represents the best fit. The arrows pointing right and up indicate the lower bounds on $\tilde{\Lambda}$ and $\Lambda_{1.4}$, respectively. The upper bounds on $\tilde{\Lambda}$ and $\Lambda_{1.4}$ are denoted by left and down arrows, respectively.	50
4.10	Plots for the incompressibility slope parameter M_0 versus tidal deformability $\Lambda_{1.4}$ at fixed values of symmetry energy slope parameter L_0 (solid lines) obtained using Eq.(4.1). The choices for the values of L_0 are discussed in the text. The dot-dot-dashed lines represent the bounds obtained in Fig. 4.9.	51
4.11	(a) The variation of tidal Love number $k_{2,1.4}$ and (b) the dimensionless tidal deformability $\Lambda_{1.4}$ with the radius $R_{1.4}$ obtained for the RMF (black squares) and SHF (red circles) models. The solid lines in the top and bottom panels are the best fitted linear and curve lines, respectively. The horizontal dot-dot-dashed lines represent the bounds obtained in Fig. 4.9.	53
5.1	The maximum neutron star mass $M_{\text{NS}}^{\text{max}}$ versus the tidal deformability parameter $\Lambda_{1.4}$ obtained from the 28 selected EDFs. The red dashed lines refer to $1.97 M_\odot$, the observed lower bound for $M_{\text{NS}}^{\text{max}}$. For more details, see text.	59
5.2	Correlation of $E_{\text{GDR}}^{\text{p}}$ and $M_{\text{NS}}^{\text{max}}$ obtained using (a) the set of selected models as in Fig.5.1 with effective mass m_0^*/m in the range 0.65 -0.75 and (b) a set of systematically varied models with chosen fixed effective masses in the present work.	62
5.3	Pressure of β -equilibrated neutron star matter displayed as a function of density. The shaded region represents the constraints from GW170817 event (B.P. Abbott <i>et al</i> 2018: [Abbott <i>et al.</i> 2018]).	63

A.1	The values of α , β and η obtained by optimizing the the correlations of Λ with the linear combinations $K_0 + \alpha L_0$, $M_0 + \beta L_0$ and $M_0 + \eta K_{\text{sym},0}$ are plotted as a function of NS mass.	71
B.1	Deviations of the dipole polarizability $\Delta\alpha_D$ and the peak energy ΔE_{GDR}^p from their experimental values obtained with the Sk Λ 267 and Sk Λ 484 parameter sets are plotted for different nuclei.	73
B.2	The pressure $P(\rho)$ for SNM (upper panel) and PNM (lower panel) as a function of baryon density ρ for the parameter sets Sk Λ 267 and Sk Λ 484. Constraints from different previous studies e.g. Kaon exp [Fantina <i>et al.</i> 2014, Fuchs 2006], HIC [Danielewicz <i>et al.</i> 2002] and N3LO [Hebeler <i>et al.</i> 2013] are provided for comparison.	73

Nomenclature

Physical constants

Quantity	Symbol	Value
speed of light in vacuum	c	$299,792,458 \text{ m/s}$
Planck constant	h	$6.62607 \times 10^{-34} \text{ Js}$
Planck constant, reduced	\hbar	$1.0545 \times 10^{-34} \text{ Js}$
electron charge magnitude	e	$1.6021 \times 10^{-19} \text{ C}$
conversion constant	$\hbar c$	197.326 MeV fm
conversion constant	$(\hbar c)^2$	$0.3893 \text{ GeV}^2 \text{ mbarn}$
electron mass	m_e	$0.510 \text{ MeV}/c^2$
proton mass	m_p	$938.272 \text{ MeV}/c^2$
fine-structure constant	$\alpha = e^2/4\pi\epsilon_0\hbar c$	$1/137.035$
Fermi coupling constant	$G_F/(\hbar c)^3$	$6.6740 \times 10^{-11} \text{ m}^3 \text{ Kg}^{-1} \text{ s}^{-2}$

Abbreviation

ANM	Asymmetric Nuclear matter
BCS	Bardeen-Cooper-Schrieffer
BNS	Binary Neutron Star
BPS	Baym-Pethick-Sutherland
CMB	Cosmic Microwave Background
DM	Dark Matter
ECM	Effective Chiral Model
EFT	Effective Field Theory
EOS	Equation of State
FAIR	Facility for Antiproton and Ion Research
FRIB	Facility for Rare Isotope Beams
GEO	Gravitational-Wave Observatory
GTR	General Theory of Relativity
GW	Gravitational Wave
ISGMR	Iso-scalar Giant Monopole Resonance
IVGDR	Iso-vector Giant Dipole Resonance
LHC	Large Hadron Collider
LIGO	Laser Interferometer Gravitational-Wave Observatory
NICER	Neutron Star Interior Composition Explorer
NN	nucleon-nucleon
NS	Neutron Star

NSM	Neutron Star Matter
PNM	Pure Neutron Matter
PSR	Pulsar
QCD	Quantum Chromodynamics
QGP	Quark-Gluon Plasma
RHIC	Relativistic Heavy Ion Collider
RMF	Relativistic Mean Field
RNS	Rotating Neutron Star
RPA	Random Phase Approximation
SNM	Symmetric Nuclear Matter
TOV	Tolman-Oppenheimer-Volkoff
WIMP	Weakly interacting massive particles

Keywords

Equations of state; Compact stars; Neutron Star; Neutron-star mergers; Gravitational-wave observations; Effective Chiral Model; Relativistic Mean field theory; Chiral Symmetry; Saturated Nuclear Matter; Dense Nuclear Matter; Properties of Neutron Star

List of Publications

1. **“Tides in merging neutron stars: Consistency of the GW170817 event with experimental data on finite nuclei”**
T. Malik, B. K. Agrawal, J. N. De, S. K. Samaddar, C. Providência, C. Mondal and T. K. Jha.
Phys. Rev. C **99**, no. 5, 052801 (R) (2019)
2. **“Nucleon effective mass and its isovector splitting”**
T. Malik, C. Mondal, B. K. Agrawal, J. N. De and S. K. Samaddar.
Phys. Rev. C **98**, no. 6, 064316 (2018)
3. **“GW170817: constraining the nuclear matter equation of state from the neutron star tidal deformability”**
T. Malik, N. Alam, M. Fortin, C. Providência, B. K. Agrawal, T. K. Jha, B. Kumar and S. K. Patra.
Phys. Rev. C **98**, no. 3, 035804 (2018)
4. **“Confronting nuclear equation of state in the presence of dark matter using GW170817 observation in relativistic mean field theory approach”**
A. Das, T. Malik and A. C. Nayak.
Phys. Rev. D **99**, no. 4, 043016 (2019)
5. **“Nuclear symmetry energy with mesonic cross-couplings in the effective chiral model”**
T. Malik, K. Banerjee, T. K. Jha and B. K. Agrawal.
Phys. Rev. C **96**, no. 3, 035803 (2017)
6. **“Spectroscopy of low-lying states in odd-odd ^{146}Eu ”**
T. Bhattacharjee *et al.*.
Phys. Rev. C **88**, no. 1, 014313 (2013).

This thesis is based on following publications

1. **“Nuclear symmetry energy with mesonic cross-couplings in the effective chiral model”**

T. Malik, K. Banerjee, T. K. Jha and B. K. Agrawal.

Phys. Rev. C **96**, no. 3, 035803 (2017)

2. **“GW170817: constraining the nuclear matter equation of state from the neutron star tidal deformability”**

T. Malik, N. Alam, M. Fortin, C. Providência, B. K. Agrawal, T. K. Jha, B. Kumar and S. K. Patra.

Phys. Rev. C **98**, no. 3, 035804 (2018)

3. **“Tides in merging neutron stars: Consistency of the GW170817 event with experimental data on finite nuclei”**

T. Malik, B. K. Agrawal, J. N. De, S. K. Samaddar, C. Providência, C. Mondal and T. K. Jha.

Phys. Rev. C **99**, no. 5, 052801(R) (2019)

Chapter 1

Introduction

1.1 Opening words

Ernest Rutherford discovered the atomic nucleus in 1911 from the scattering of alpha particles by gold foil. The nucleus contains positively charged protons and electrically neutral neutrons. The neutron was discovered in 1932 by James Chadwick. The entire mass of an atom is concentrated on nucleus whose dimension is few femtometers (10^{-15} meters) whereas the size of an atom is few angstroms (10^{-10} meters). An atom denoted by A_ZX , has mass number $A = (N + Z)$, where N is the number of neutrons, and Z is the number of protons. The number of electrons is the same as protons. From various scattering experiments, the nuclear radius is found to be $r \simeq r_0 \times A^{1/3}$, where r_0 is the radius constant and is ~ 1.15 fm. Considering a nucleus to be a classical spherical system the volume will be $V = \frac{4}{3}\pi r^3 = \frac{4}{3}\pi(r_0 A^{1/3})^3 = \frac{4}{3}\pi(r_0^3 A)$. The average nucleon density in the nucleus is $\rho_0 = A/V = (4/3\pi r_0^3)^{-1}$, which is approximately constant and independent of mass number A of nuclei. The constant value $\rho_0 \sim 0.16 \text{ fm}^{-3}$ identified as the saturation density of a hypothetical system called nuclear matter, an infinite system of an equal number of neutrons and protons where the Coulomb interaction is switched off.

On the other extreme, compact stars such as neutron stars (NS), observed as pulsars, are believed to contain matter at few times nuclear saturation density in its core. Neutron stars (NSs) are the ideal cosmic laboratories to shed light directly or indirectly on different theories of physics as well as on the physics beyond the standard scenario. To explain and understand the extreme properties of such stars, one needs to connect different branches of physics including low energy nuclear physics, QCD under extreme conditions, general theory of relativity (GR) *etc.* Born out of Supernova, neutron stars represent one the densest form of matter in the observable universe. Observed masses lie in the range

of $\sim (1 - 2)M_{\odot}$ with radii $\sim (10 - 15)\text{km}$, where M_{\odot} is the mass of the sun. The typical values of the surface magnetic field of neutron stars may range from $(10^{12} - 10^{18})$ Gauss. Those with the strongest magnetic field are called magnetars, and generally, they belong to Soft Gamma Repeaters (SGRs) or Anomalous X-ray Pulsars (AXPs) [Gomes *et al.* 2017]. Typical examples of such magnetars are the 1E 1048.1 – 5937 and 1E 2259 + 586 with surface magnetic field $B_{\text{surf}} \sim 10^{14}$ Gauss [Melatos 1999], 4U 0142 + 61 ($B_{\text{surf}} \sim 10^{16}$ Gauss) [Makishima *et al.* 2014] and SGR 1806 – 20 ($B_{\text{surf}} \sim 10^{14}$ Gauss) [Kouveliotou *et al.* 1998] *etc.* One can refer to the magnetars catalog available online for more such examples [Olausen & Kaspi 2014].

The internal structure of the NS depends on the hydrostatic equilibrium between the inward gravitational pull of matter and the outward neutron degeneracy pressure. If we assumed the correctness of GR, to understand the internal structure of NS predominantly, one needs the theory of the behavior of matter at extreme conditions, i.e., the theory of infinite nuclear matter equation of state (EOS). At such high densities, the presence of exotic matter in the core can not be ruled out. A soup of particle resonances such as Λ^0 , $\Sigma^{-,0,+}$, $\Xi^{-,0}$, *etc* or of quarks represents an exciting possibility. A star mainly composed of neutrons will have neutrons at very high chemical potential compared to those of protons. To maintain chemical potential, eventual β - decay of neutrons can lead to some fraction of protons and electrons as,

$$n \rightarrow p + e^{-} + \bar{\nu}, \quad (1.1)$$

$$n + \nu \rightarrow p + e^{-}. \quad (1.2)$$

To maintain the neutron star matter charge neutral, muons (μ) will appear when the chemical potential of the electrons reaches the muon rest mass ($m_{\mu} = 106 \text{ MeV}$). For a given baryon density ($\rho = \rho_n + \rho_p$), the charge neutrality is given as,

$$\rho_p = \rho_e + \rho_{\mu} \quad (1.3)$$

where ρ_n , ρ_p and ρ_{μ} are the number density of neutron, proton and muons respectively. The β -equilibrium condition is given as,

$$\mu_n = \mu_p + \mu_e \quad \text{and} \quad \mu_e = \mu_{\mu} \quad (1.4)$$

where μ_n, μ_p, μ_e and μ_{μ} are the chemical potential of neutron, proton, electron and muon respectively.

Terrestrially high density matter can be produced and probed by heavy-ion collision experiments, but the main difficulty is that the asymmetry is usually small. Neutron stars being highly asymmetric,

we need to understand the nuclear EOS, conventionally defined as energy (or pressure) as a function of density, over a wide range of densities. To a good approximation, the EOS can be decomposed into two parts, (i) EOS for symmetric nuclear matter $e(\rho, 0)$ (ii) and another part that contains the density dependent symmetry energy coefficient $S(\rho)$,

$$e(\rho, \delta) \simeq e(\rho, 0) + S(\rho)\delta^2, \quad (1.5)$$

where $e(\rho, \delta)$ is the energy per nucleon at a given density $\rho = \rho_n + \rho_p$ with ρ_n and ρ_p being the neutron and proton densities, respectively, and $\delta = (\rho_n - \rho_p)/\rho$ is the isospin asymmetry. We can recast the EOS with various bulk nuclear matter properties at saturation density for the symmetric nuclear matter, the energy per nucleon e_0 , incompressibility coefficient $K_0 = 9\rho_0^2 \left(\frac{\partial^2 \epsilon(\rho, 0)}{\partial \rho^2} \right)_{\rho_0}$, skewness parameter $Q_0 = 27\rho_0^3 \left(\frac{\partial^3 \epsilon(\rho, 0)}{\partial \rho^3} \right)_{\rho_0}$ etc, along with parameters pertaining to asymmetric matter like the symmetry energy coefficient $J_0 = \frac{1}{2} \left(\frac{\partial^2 \epsilon(\rho, \delta)}{\partial \delta^2} \right)_{\delta=0} [= S(\rho_0)]$, its slope $L_0 = 3\rho_0 \left(\frac{\partial S(\rho)}{\partial \rho} \right)_{\rho_0}$ and the curvature $K_{\text{sym},0} = 9\rho_0^2 \left(\frac{\partial^2 S(\rho)}{\partial \rho^2} \right)_{\rho_0}$ etc. These parameters are density derivatives with of the energy and symmetry energy.

Therefore, by constraining the nuclear matter properties at saturation density we can constrain the density dependent of the EOS for the asymmetric matter. It is difficult to calculate the EOS from *ab initio* QCD calculations, especially at supra-saturation densities ($\rho \gg \rho_0$) because of the complicated nonperturbative feature of QCD. And this is the one fundamental issue in nuclear physics, particle physics, and astrophysics, which is yet to be explored.

1.2 Constraints from terrestrial and astrophysical Data

Data from terrestrial experiments such as finite nuclei, Heavy Ion Collision (HIC) as well as astrophysical observations like neutron stars properties are particularly important to constrain the nuclear matter EOS as well as nucleon-nucleon interactions at high densities. We now outline those empirical constraints till date in the subsequent sections.

1.2.1 Finite nuclei

At saturation density, the present nuclear constants pertaining to SNM (ϵ_0 and K_0) and symmetry energy coefficients (J_0 , L_0 and $K_{\text{sym},0}$), which determine the density dependent of symmetry energy are listed in Table 1.2.1. These values refer to infinite nuclear matter, but with roots embedded in finite nuclear observables. To gain accurate knowledge of these parameters, one should also revert to the

indirect methods such as the correlations of the finite nuclei observables with them at saturation density. The coefficients pertaining to SNM and symmetry energy relate to the nuclear masses, isoscalar giant monopole resonances (ISGMR) and isovector giant dipole resonances (IVGDR) energies of finite nuclei *etc.* The values of $\epsilon_0 = -15.88 \pm 0.24$ MeV and $\rho_0 = 0.163 \pm 0.005$ fm⁻³ are the averages of the 'best-selected' nuclear EOSs that give the best fit to the selected nuclear data [Dutra *et al.* 2012]. The value of nuclear incompressibility K_0 can be settled to $K_0 \sim 240 \pm 20$ MeV [Avogadro & Bertulani 2013, Niksic *et al.* 2008, Todd-Rutel & Piekarewicz 2005], which gives good agreement with the experimentally determined centroids of ISGMR, in particular, for ²⁰⁸Pb, ⁹⁰Zr and ¹⁴⁴Sm nuclei. In Jiang *et al.* [2012], we find $J_0 = 32.10 \pm 0.31$ by analyzing the compact correlation between the experimental double differences of symmetry energies of finite nuclei and their mass number. The recent development of various experiments can probe L_0 , but values differ from one another. Results from measurements from different experimental observables such as Neutron-skin thickness [Roca-Maza *et al.* 2011], Nuclear masses [Lattimer & Prakash 2016, and references therein], iso-vector giant dipole resonances [Lattimer & Prakash 2016, and references therein], iso-vector giant quadruple resonances [Lattimer & Prakash 2016, and references therein] are presented in Fig.1.1. The overlapping white region of all experiment in Fig.1.1, is said to be the region of 70% confidence ($L_0 \sim 40 - 65$ MeV). A recent attempt to tighten the bound on L_0 from nuclear masses have been made by microscopic calculations [Agrawal *et al.* 2012a, 2013] on the neutron skin of heavy nuclei and value of L_0 is found to be 59 ± 13 MeV. Other recent attempts from the analysis of the iso-vector giant dipole and quadruple resonance in the 208Pb Nucleus [Roca-Maza *et al.* 2013a, b] give $L_0 = 43 \pm 26$ MeV and 37 ± 18 MeV respectively. The value of $K_{\text{sym},0}$ plays quite a significant role in determining the density dependent symmetry energy behavior, at densities $\rho \gg \rho_0$. The value of $K_{\text{sym},0}$ is poorly known since one does not know of any probe which is sensitive to it. Across several nuclear models the values of $K_{\text{sym},0}$ lie within a wide range, -700 MeV $< K_{\text{sym},0} < 400$ MeV. In recent studies [Mondal *et al.* 2017], a strong correlation has been found between $K_{\text{sym},0}$ and $3J_0 - L_0$ by analyzing 500 nuclear models and the value of $K_{\text{sym},0}$ is constrained to be -111.8 ± 71.3 MeV.

1.2.2 HIC and *ab-initio* methods

The present empirical constraint on EOS (barring the ones at the saturation density) are listed in Table 1.2. The rows and columns are self explanatory. The first two rows refer to the pressure of symmetric nuclear matter (SNM). They are obtained from the analysis of directed and elliptic flow [Danielewicz *et al.* 2002] and kaon production [Fantina *et al.* 2014, Fuchs 2006] in heavy ion collisions

Table 1.1: The present nuclear constants pertaining to SNM (ϵ_0 and K_0) and density dependent symmetry energy (J_0 , L_0 and $K_{\text{sym},0}$) at saturation density ρ_0 .

NMP	empirical value (MeV)	References
e_0	-15.88 ± 0.24	Dutra et al. 2012
K_0	$240 \pm 20 \text{ MeV}$	Stone et al. 2014
J_0	32.10 ± 0.31	Jiang et al. 2012
L_0	40 ± 20	Lattimer & Prakash 2016
$K_{\text{sym},0}$	-111.8 ± 71.8	Mondal et al. 2017

Table 1.2: The present empirical constant on EOS ($P(\rho)$, $\epsilon_n(\rho)$ and $S(\rho)$ represent pressure, energy per particle and symmetry energy respectively) corresponding to the symmetric nuclear matter (SNMX), pure neutron matter (PNMX) and symmetry energy coefficient (SYMX) together with the range of densities in which they are determined.

	Quantity	Density region (fm^{-3})	Band/Range (MeV)	References
SNM1	$P(\rho)$	0.32 to 0.74	HIC	Danielewicz et al. 2002
SNM2	$P(\rho)$	0.19 to 0.33	Kaon exp	Fantina et al. 2014 , Fuchs 2006
PNM1	$\epsilon_n(\rho)$	0.1	10.9 ± 0.5	Brown 2013
PNM2	$\epsilon_n(\rho)$	0.03 to 0.17	N ³ LO	Hebeler et al. 2013
PNM3	$P(\rho)$	0.32 to 0.73	HIC	Danielewicz et al. 2002
PNM4	$P(\rho)$	0.03 to 0.17	N ³ LO	Hebeler et al. 2013
SYM1	$S(\rho)$	0.1	24.1 ± 0.8	Trippa et al. 2008
SYM2	$S(\rho)$	0.01 to 0.19	IAS,HIC	Danielewicz & Lee 2014 , Tsang et al. 2009
SYM3	$S(\rho)$	0.01 to 0.31	ASY-EOS	Russotto et al. 2016

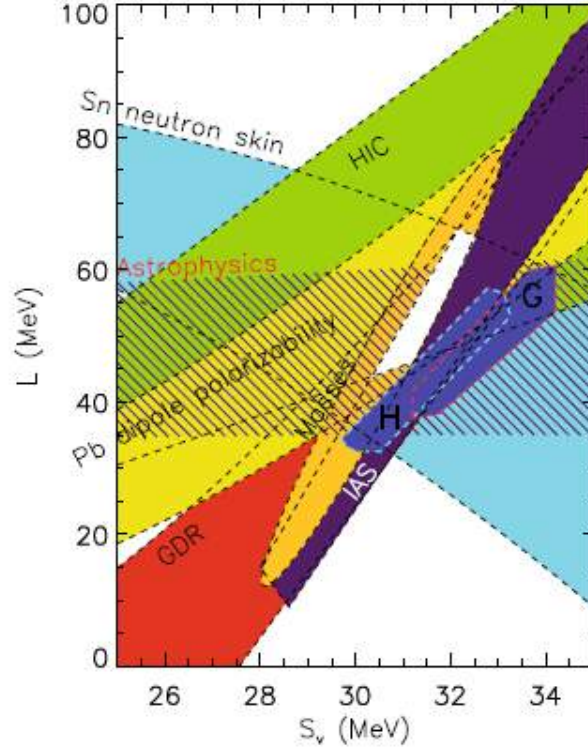


Figure 1.1: Experimental constraints for symmetry energy parameters from different experiments [Lattimer & Prakash 2016]

(HIC). The next four rows correspond to pure neutron matter (PNM). Its energy at a density $\rho = 0.1 \text{ fm}^{-3}$ is taken from the 'best-fit' Skyrme EDFs [Brown 2013]. The information on the energy and pressure of low density neutron matter is taken from high precision predictions at next-to-next-to-next-to-leading order (N^3LO) in chiral effective field theory [Hebeler *et al.* 2013, Sammarruca *et al.* 2015]. The pressure of PNM is the excess over the pressure of SNM due to symmetry energy. It is constructed theoretically with two extreme parameterizations, the soft (Asy Soft) and the stiff (Asy Stiff) symmetry energy [Prakash *et al.* 1988]. Its values are taken from Ref. [Danielewicz *et al.* 2002]. The last three rows refer to the symmetry energy coefficients $S(\rho)$ at the densities mentioned in the Table. They come from three different sources, namely, simulation of low energy HIC in $^{112}\text{Sn}+^{112}\text{Sn}$ and $^{124}\text{Sn}+^{124}\text{Sn}$ [Tsang *et al.* 2009, 2010], nuclear structure studies involving Isobaric Analogue States (IAS) [Danielewicz & Lee 2014] and Asy-EOS experiments at GSI [Russotto *et al.* 2016]. In addition, the value of $S(\rho)$ at $\rho = 0.1 \text{ fm}^{-3}$ quoted from microscopic analysis of IVGDR in ^{208}Pb is taken [Trippa *et al.* 2008] into consideration. These are shown pictorially in Fig. 1.2. Since much of the data are theoretical, inputs from astrophysical observations are crucial in further constraining the dense matter EOS.

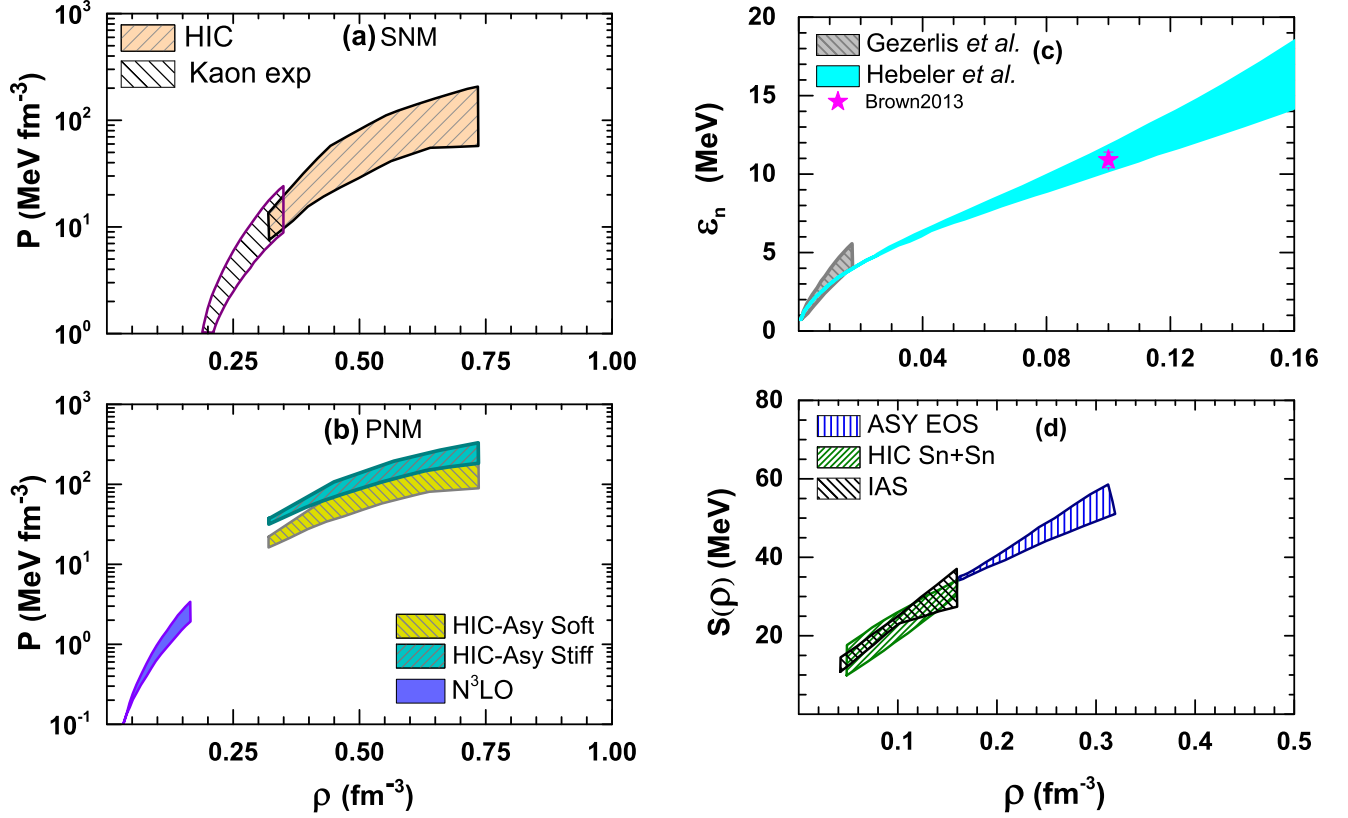


Figure 1.2: The constraint on the pressure $P(\rho)$ for SNM (left upper panel), PNM (left lower panel), energy per neutron ϵ_n of PNM (right upper panel) and symmetry energy coefficient $S(\rho)$ (right lower panel) as a function of baryon density ρ (see Table 1.2).

1.2.3 Neutron Star mass and radius

Theoretically, the maximum allowable mass and radius depend on nuclear EOS at both low and high densities. Analogously, precise measurements of both neutron star mass and radii can constrain the nuclear EOS. Because of enormous distances, the direct measurement of the neutron star radius is a difficult proposition. However, masses are precisely measured. Future observations such as those planned by NICER (Neutron star Interior Composition Explorer) mission [Arzoumanian *et al.* 2014, Gendreau *et al.* 2016], eXTP (enhanced X-ray Timing and Polarimetry) Mission [Watts *et al.* 2019], LOFT (Large Observatory For X-ray Timing) satellite [Wilson-Hodge *et al.* 2016], and ATHENA (Advanced Telescope for High Energy Astrophysics) [Motch *et al.* 2013] may provide the possible range for radius of a canonical NS ($M = 1.4M_\odot$) ‘ $R_{1.4}$ ’. However, the empirical estimates of $R_{1.4}$ are equal to $R_{1.4} \simeq (11.9 \pm 1.22)$ km [Bauswein *et al.* 2017, Lim & Holt 2018, Malik *et al.* 2018a, Most *et al.* 2018, Radice & Dai 2019]. Lately, Precise observations of high mass pulsars such as PSR

$J1614-2230$ ($M = 1.97 \pm 0.04$) M_{\odot} [Demorest *et al.* 2010], PSR $J0348+0432$ ($M = 2.01 \pm 0.04$) M_{\odot} [Antoniadis & *et al.* 2013] and the recently detected MSP $J0740 + 6620$ with a mass $2.14^{+0.10}_{-0.09} M_{\odot}$ [Cromartie *et al.* 2019] have put a bound on the nuclear EOS, which led to serious considerations on the role of strong interactions at high densities. The mastery of the behavior of EOS of dense matter relevant to neutron stars (NSs) is one of the main objectives of both nuclear physics and astrophysics to date [Haensel *et al.* 2007, Rezzolla *et al.* 2018b]. Due to the lack of detailed knowledge of the nuclear interactions at densities typical of the NS interior, many theoretical models have been exploited [Dutra *et al.* 2012, 2014].

1.2.4 Multi messenger era

On August 2017, the Advanced LIGO and Advanced Virgo gravitational-wave observatories detected for the first time gravitational waves (GWs) emitted from the inspiral of two low-mass compact objects which is consistent with a binary neutron star (BNS) merger [Abbott *et al.* 2017a] and subsequently the electromagnetic counterparts are also observed [Abbott *et al.* 2017b, c, Coulter *et al.* 2017, Goldstein *et al.* 2017, Haggard *et al.* 2017, Hallinan *et al.* 2017, Troja *et al.* 2017]. This discovery opens a new window to look into the nuclear matter theories relevant to NS. The tidal deformations of the NSs that come into the analysis of this GW observation data provide relevant constraints on the uncertainty of parameters of the nuclear equation of matter EOS.

Astrophysical observations are complementary probes for the information in the region of the dense-matter EOS, which is not experimentally accessible in the laboratory [Rezzolla *et al.* 2018b]. The NSs are massive and compact astrophysical objects, the coalescence of binary NS systems is one of the most promising sources of gravitational waves (GWs) observable by ground-based detectors [Brillet & *et al.* Virgo Collaboration, Cutler *et al.* 1993, Drever 1983, Hough & *et al.* 1989, Taylor & Weisberg 1982, Thorne 1987]. The GW signals emitted during a NS merger depends on the behavior of neutron star matter at high densities. Therefore, its detection opens the possibility of constraining the nuclear matter parameters (NMP) characterizing the EOS [Duez 2010, Faber 2009]. During the last stages of the inspiral motion of the coalescing neutron stars (NSs), the strong gravity of each of them induces a tidal deformation in the companion star. Decoding the gravitational wave phase evolution caused by that deformation allows the determination of the dimensionless tidal deformability parameter [Binnington & Poisson 2009, Damour & Nagar 2009, Flanagan & Hinderer 2008, Hinderer 2008, Hinderer *et al.* 2010]. It is a measure of the response to the gravitational pull on the neutron star surface correlating with pressure gradients inside the NS and, therefore, it has been proposed as an effective

Table 1.3: Present constraint on tidal deformability from GW170817 [Abbott *et al.* 2019]

Chrip Mass $\mathcal{M} = \frac{(m_1 m_2)^{3/5}}{(m_1 + m_2)^{1/5}}$	$1.186_{-0.001}^{+0.001} M_\odot$
mass ratio $q = m_1/m_2$	0.73 – 1.00
m_1	(1.16 to 1.36) M_\odot
m_2	(1.36 to 1.60) M_\odot
Combined Tidal deformability $\tilde{\Lambda}$	300_{-230}^{+420}

probe of the equation of state (EOS) of nuclear matter relevant for neutron stars [De *et al.* 2018, Malik *et al.* 2018a, 2019b]. In the recent studies possible correlations between the tidal deformability of a NS with the properties of infinite nuclear matter such as the slope and curvature of the symmetry energy coefficient have been explored widely [Carson *et al.* 2019, Fattoyev *et al.* 2018, Malik *et al.* 2018a, 2019b, Zhang & Li 2019a, b].

1.3 Objectives

The equation state of nuclear matter determines the properties of microscopic nuclei and also macroscopic celestial objects such as neutron stars, supernova and neutron star merger. The EOS of neutron-rich nucleonic matter, relevant for neutron star, remains very uncertain at supra-saturation densities. Some progress has been made in constraining the neutron-rich nucleonic matter EOS over the years. In particular, the EOS parameters like the nuclear incompressibility K_0 , symmetry energy J_0 and its slope L_0 at saturation density are constrained well by the analysis of the terrestrial nuclear experiment and astrophysical observations. However, the parameters characterizing the high density behavior of neutron-rich matter, such as the skewness Q_0 of SNM, the curvature parameter $K_{\text{sym},0}$ and the skewness parameter $Q_{\text{sym},0}$ of the symmetry energy are only loosely known till date. The analysis of directed and elliptic flow [Danielewicz *et al.* 2002] and kaon production [Fantina *et al.* 2014, Fuchs 2006] in heavy ion collisions (HIC) provides a reasonably tight bound for the EOS of SNM up to about $4.5\rho_0$. On the contrary, results from the efforts to constrain the EOS of dense neutron-rich matter using heavy-ion reactions that may involve rare isotopes with large neutron/proton ratios, currently are not in general agreement from the analysis of limited data available [Li 2017].

Observables related to neutron stars such as the mass, radius and quadrupole deformation of

merging neutron stars depend significantly on the EOS of dense neutron rich matter. The very precise measured most massive pulsar has put a serious constraint on neutron-rich EOS. Future observations such as those planned by NICER (Neutron star Interior Composition Explorer) mission are expected to provide the more precise value of neutron star radii in the coming year. In August 2017, the Advanced LIGO and Advanced Virgo gravitational-wave observatories detected for the first time GWs emitted from a binary NS inspiral. Remarkably, this discovery opened a new window in the field of multi-messenger astronomy and nuclear physics. The analysis of GW170817 predicts that the combined dimensionless tidal deformability of the NS merger $\tilde{\Lambda}$ equals to 300^{+420}_{-230} .

Studies of the correlations between nuclear matter parameters and the tidal deformability, based on a few selected relativistic mean field models, have shown that measurements of the latter can constrain the high density behavior of the nuclear symmetry energy [Fattoyev *et al.* 2013] as well as impose bounds on the value of neutron skin thickness [Fattoyev *et al.* 2018]. In subsequent studies, it was found that correlations between the various properties of NS and nuclear matter EOS parameters are significantly affected when a more diverse set of models are employed [Alam *et al.* 2015, Fortin *et al.* 2016]. These preliminary studies need to be validated, further using a more diverse set of models for the nuclear EOS.

It is also essential to investigate the compatibility of the value of tidal deformability obtained from astrophysical observations with the EOS constrained by laboratory data on light nuclei. Through a combination of laboratory data on light nuclei and sophisticated microscopic modeling of the sub-saturation EOS from CEFT [Lim & Holt 2018, 2019, Tews *et al.* 2018, 2019], attempts have been made to arrive at values of the tidal deformability. The connection of the tidal deformability to the laboratory data is not yet fully explored. The main objectives, in view of the recent observation GW170817, of this thesis, are:

- To explore the dependence of the tidal deformability on the various nuclear matter parameters describing the EOS.
- To perform calculations for tidal deformability and various properties of finite nuclei, in particular, monopole and dipole giant resonances in addition to binding energy and charge radii using a diverse set of nuclear models.
- To find the agreement of the nuclear equation of state (EOS) deduced from the GW170817 based tidal deformability with the one obtained from empirical data on microscopic nuclei.

1.4 Organization of the Thesis

Broadly, this thesis aims to connect the various aspects of nuclear matter paradigm from properties of finite nuclei to high density aspects obtained from both experiments and observation of neutron stars. Here we tried to establish the connection between astrophysical observations to the possible fundamental nuclear interactions at high densities. And therefore, after introducing the relevant aspects of nuclear matter in Chapter 1 here, we discuss the theoretical formalism in Chapter 2. Subsequently, Chapter 3 is dedicated to the study of possible nuclear interactions at high densities, particularly to the effect of mesonic cross couplings. The correlations of neutron star properties to the underlying EOS parameters are presented in Chapter 4. In Chapter 5 we have discussed the possible ways to constrain the dense matter EOS relevant to neutron stars from the terrestrial and astrophysical observations, including the recent results from GW170817. The finding of our work and investigations is concluded in Chapter 6.

Chapter 2

Formalism

There are four fundamental forces in nature: electromagnetic, gravitational, weak and strong, of which strong force is the most dominant one in the nuclear range. This is the force which holds nucleons together inside the nucleus. Thus obtaining the nuclear matter EOS is the nuclear many body dynamics. In general the models for nuclear EOS can be broadly categorized into two groups (i) the relativistic and (ii) the non relativistic models. The theoretical frameworks to calculate the EOS and neutron star properties employed in the present thesis are briefly outline as follows.

2.1 Field theoretical models

The force between two nucleons is realized by the the exchange of mediating particles called mesons when the nucleons are close together of the order of femtometer ($10^{-15}m$). This is the basis of nuclear interaction in relativistic framework. The prominent masons are the σ, ω and ρ mesons [Boguta & Bodmer 1977, Boguta & Stoecker 1983, Serot & Walecka 1997, Walecka 1974]. The σ mesons creates a strong attractive central force and influences the spin-orbit potential, on the other hand ω -mesons are responsible for the repulsive short range force. The protons and neutrons only differ in terms of their isospin projections, the ρ mesons are included to distinguish between these baryons. In this approach, the nuclear interactions are described by a Lagrangian densities \mathcal{L} and in the co-variant formalism the Euler-Lagrange equation for a field φ is given by,

$$\partial_\mu \left(\frac{\partial \mathcal{L}}{\partial (\partial_\mu \varphi)} \right) = \frac{\partial \mathcal{L}}{\partial \varphi} \quad (2.1)$$

and the stress-energy tensor $T^{\mu\nu}$ is,

$$T^{\mu\nu} = \frac{\partial \mathcal{L}}{\partial (\partial_\mu \varphi)} \partial^\nu \varphi - g^{\mu\nu} \mathcal{L} \quad (2.2)$$

where $g^{\mu\nu}$ are the components of metric tensor and is given by $g^{\mu\nu} = \text{Diag}[1 - 1 - 1 - 1]$. The energy ε and pressure P of the system in static case is then,

$$\begin{aligned}\varepsilon &= \langle T_{00} \rangle \\ P &= \frac{1}{3} \langle T_{ii} \rangle\end{aligned}\quad (2.3)$$

We have employed two types of Lagrangian densities depending on their symmetries which are described below.

2.1.1 Effective Chiral Model (ECM)

The Chiral Symmetry is a global symmetry of strong interactions in the strong coupling limit. The axial vector current is conserved under this symmetry. The model contains chiral symmetry at the Lagrangian level. However, spontaneous symmetry breaking at ground state leads to a mass-less mode called Goldstone-Boson mode. The models based on chiral symmetry was introduced by Gell-Mann & Levy [Gell-Mann & Levy 1960].

The complete Lagrangian for the effective model is [Jha *et al.* 2006]

$$\begin{aligned}\mathcal{L} &= \bar{\psi}_B \left[\left(i\gamma_\mu \partial^\mu - g_\omega \gamma_\mu \omega^\mu - \frac{1}{2} g_\rho \vec{\rho}_\mu \cdot \vec{\tau} \gamma^\mu \right) - g_\sigma (\sigma + i\gamma_5 \vec{\tau} \cdot \vec{\pi}) \right] \psi_B + \frac{1}{2} (\partial_\mu \vec{\pi} \cdot \partial^\mu \vec{\pi} + \partial_\mu \sigma \partial^\mu \sigma) \\ &\quad - \frac{\lambda}{4} (x^2 - x_0^2)^2 - \frac{\lambda b}{6m^2} (x^2 - x_0^2)^3 - \frac{\lambda c}{8m^4} (x^2 - x_0^2)^4 - \frac{1}{4} F_{\mu\nu} F^{\mu\nu} + \frac{1}{2} g_\omega^2 x^2 (\omega_\mu \omega^\mu) \\ &\quad - \frac{1}{4} \vec{R}_{\mu\nu} \cdot \vec{R}^{\mu\nu} + \frac{1}{2} m_\rho^2 (\vec{\rho}_\mu \cdot \vec{\rho}^\mu)\end{aligned}\quad (2.4)$$

The first line of the above Lagrangian ψ along with its adjoint $\bar{\psi} = \psi^\dagger \gamma^0$ represent the nucleon isospin doublet, where γ^μ are the Dirac matrices and τ are the Pauli matrices. In this model for hadronic matter, the nucleons interact via the exchange of scalar (σ), vector (ω) and isospin triplet (ρ) mesons. g_σ , g_ω and g_ρ are the meson nucleon coupling strength of scalar, vector and the iso-vector fields, respectively. In the Lagrangian above the vector (ω) meson mass is dynamically generated here and the non linear term in Lagrangian density is able to produce many body interaction, which is very relevant in high density condition such as the density in the interior Neutron star.

The potential in the Lagrangian density is a *Mexican-Hat* type potential (Fig. 2.1), which is spontaneously broken at ground state vacuum expectation value x_0 through interaction of the scalar and the pseudo scalar mesons with the vector boson. The masses of the scalar mesons (m_σ), vector mesons (m_ω) and nucleons (m_B) are then related to vacuum expectation value of scalar field (x_0) and are given by

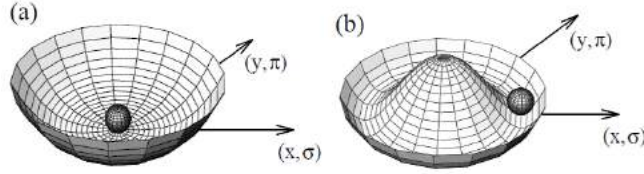


Figure 2.1: Effective potential (a) No spontaneous symmetry braking (b) spontaneous symmetry breaking [Koch 1997].

$$m = g_\sigma x_0, m_\sigma = \sqrt{(2\lambda)}x_0 \text{ and } m_\omega = g_\omega x_0$$

where, $x^2 = \vec{\pi}^2 + \sigma^2$, $\lambda = \frac{(m_\sigma^2 - m_\pi^2)}{2f_\pi^2}$ and $f_\pi = x_0$ is the pion decay constant. In the mean field treatment the explicit roll of pion is ignored and hence $m_\pi = 0$. The mesonic fields are then the classical fields i.e., without any quantum fluctuation.

2.1.2 Relativistic Mean Field Model (RMF)

The effective Lagrangian for the RMF models, we have employed in the present work can be grouped into two categories, namely (i) the coupling constants are independent of the density and the mesonic field couples linearly to the nucleons describing their interactions along with the non-linear terms as well, and (ii) density dependent couplings. The Lagrangian density will be $\mathcal{L} = \mathcal{L}_B + \mathcal{L}_{int}$, where

$$\mathcal{L}_B = \bar{\psi} \left[\gamma^\mu \left(i\partial_\mu - g_v V_\mu - g_\rho \vec{\tau} \cdot \vec{b}_\mu \right) - (M_n + g_s \phi) \right] \psi. \quad (2.5)$$

and

$$\begin{aligned} \mathcal{L}_{int} = & \bar{\psi} \left[g_\sigma \sigma - \gamma^\mu \left(g_\omega \omega_\mu + \frac{1}{2} g_\rho \tau \cdot \rho_\mu + \frac{e}{2} (1 + \tau_3) A_\mu \right) \right] \psi - \frac{\kappa_3}{6M} g_\sigma m_\sigma^2 \sigma^3 \\ & - \frac{\kappa_4}{24M^2} g_\sigma^2 m_\sigma^2 \sigma^4 + \frac{1}{24} \zeta_0 g_\omega^2 (\omega_\mu \omega^\mu)^2 + \frac{\eta_{2\rho}}{4M^2} g_\omega^2 m_\rho^2 \omega_\mu \omega^\mu \rho_\nu \rho^\nu \end{aligned} \quad (2.6)$$

Where the symbols have usual meaning and the details can be found in Refs. [Boguta & Bodmer 1977, Boguta & Stoecker 1983, Furnstahl *et al.* 1997, Todd-Rutel & Piekarewicz 2005]. The parameters g_σ , g_ω and g_ρ describe the strength of the couplings of baryon(ψ) with σ , ω and ρ mesons.

For the density-dependent meson-exchange model [Lalazissis *et al.* 2005] interaction part of the Lagrangian does not contain any non-linear term, but, the meson-nucleon strengths g_σ , g_ω and g_ρ have an explicit density dependence in the following form:

$$g_i(\rho) = g_i(\rho_0) f_i(x), \quad \text{for } i = \sigma, \omega \quad (2.7)$$

where the density dependence is given by

$$f_i(x) = a_i \frac{1 + b_i(x + d_i)^2}{1 + c_i(x + e_i)^2} \quad (2.8)$$

in which x is given by $x = \rho/\rho_0$, and ρ_0 denotes the baryon density at saturation in symmetric nuclear matter. For the ρ meson, density dependence is of exponential form and given by

$$f_\rho(x) = \exp(-a_\rho(x - 1)) \quad (2.9)$$

The coupling strengths in Eqs. (2.5) and (2.6) are usually calibrated to reproduce the measured binding energies, charge radii and the properties of giant resonances.

2.2 Non relativistic Model

The non relativistic models are based on the use of nucleon-nucleon potential together with variational method. The Skyrme-Hartree-Fock model (SHF) is most popular non-relativistic self-consistent method. Skyrme force is an effective nucleon-nucleon interaction which was originally introduced by Skyrme in 1956 [Skyrme 1956]. It is a widely used energy density functional which is a zero-range momentum dependent method employed to describe the gross properties of finite nuclei. This zero-range interaction is easy to handle in the Hartree-Fock calculation. However, the momentum dependence of the zero-range force accounts for the finite-range effect between the nucleons. In the Skyrme force, the effects of many-body interaction are also included through the density dependent two body interaction. The total energy E of the system can be expressed as,

$$E = \int \mathcal{H}(r) d^3r \quad (2.10)$$

where, the Skyrme energy density functional $\mathcal{H}(r)$ is given by [Chabanat *et al.* 1997, Vautherin & Brink 1972],

$$\mathcal{H} = \mathcal{K} + \mathcal{H}_0 + \mathcal{H}_3 + \mathcal{H}_{\text{eff}} + \mathcal{H}_{\text{fin}} + \mathcal{H}_{\text{so}} + \mathcal{H}_{\text{sg}} + \mathcal{H}_{\text{Coul}} \quad (2.11)$$

where, $\mathcal{K} = \frac{\hbar^2}{2m}\tau$ is the kinetic energy term, \mathcal{H}_0 is the zero-range term, \mathcal{H}_3 the density dependent term, \mathcal{H}_{eff} an effective-mass term, \mathcal{H}_{fin} a finite-range term, \mathcal{H}_{so} a spin-orbit term, \mathcal{H}_{sg} a term due to tensor coupling with spin and gradient and $\mathcal{H}_{\text{Coul}}$ is the contribution to the energy density due to the Coulomb interaction. For the Skyrme interaction we have,

$$\mathcal{H}_0 = \frac{1}{4}t_0 [(2 + x_0)\rho^2 - (2x_0 + 1)(\rho_p^2 + \rho_n^2)], \quad (2.12)$$

$$\mathcal{H}_3 = \frac{1}{24} t_3 \rho^\alpha [(2 + x_3) \rho^2 - (2x_3 + 1)(\rho_p^2 + \rho_n^2)], \quad (2.13)$$

$$\mathcal{H}_{\text{eff}} = \frac{1}{8} [t_1(2 + x_1) + t_2(2 + x_2)] \tau \rho + \frac{1}{8} [t_2(2x_2 + 1) - t_1(2x_1 + 1)] (\tau_p \rho_p + \tau_n \rho_n), \quad (2.14)$$

$$\begin{aligned} \mathcal{H}_{\text{fin}} &= \frac{1}{32} [3t_1(2 + x_1) - t_2(2 + x_2)] (\nabla \rho)^2 \\ &\quad - \frac{1}{32} [3t_1(2x_1 + 1) + t_2(2x_2 + 1)] [(\nabla \rho_p)^2 + (\nabla \rho_n)^2], \end{aligned} \quad (2.15)$$

$$\mathcal{H}_{\text{so}} = \frac{W_0}{2} [\mathbf{J} \cdot \nabla \rho + \mathbf{J}_p \cdot \nabla \rho_p + \mathbf{J}_n \cdot \nabla \rho_n], \quad (2.16)$$

$$\mathcal{H}_{\text{sg}} = -\frac{1}{16} (t_1 x_1 + t_2 x_2) \mathbf{J}^2 + \frac{1}{16} (t_1 - t_2) [\mathbf{J}_p^2 + \mathbf{J}_n^2]. \quad (2.17)$$

Here, $\rho = \rho_p + \rho_n$, $\tau = \tau_p + \tau_n$, and $\mathbf{J} = \mathbf{J}_p + \mathbf{J}_n$ are the particle number density, kinetic energy density and spin density with p and n denoting the protons and neutrons, respectively. We have used the value of $\hbar^2/2m = 20.734 \text{ MeVfm}^2$ in our calculations. For the case of uniform matter, \mathcal{H}_{fin} , \mathcal{H}_{so} , \mathcal{H}_{sg} and $\mathcal{H}_{\text{Coul}}$ do not contribute.

Further, the $\mathcal{H}(\nabla)$ depends only on the ρ_p and ρ_n and is independent of position coordinate r , $\mathcal{H}(r) \rightarrow \mathcal{E}(\rho_p, \rho_n)$. The energy per nucleon, $\epsilon(\rho_p, \rho_n) = \frac{\mathcal{E}(\rho_p, \rho_n)}{\rho}$ can be expressed in terms of the total density ρ and the asymmetry parameter $\delta = \frac{\rho_n - \rho_p}{\rho}$ as,

$$\begin{aligned} \epsilon(\rho, \delta) &= \frac{3}{5} \frac{\hbar^2}{2m} \left(\frac{3\pi^2}{2} \right)^{2/3} \rho^{2/3} F_{5/3} + \frac{1}{8} t_0 \rho [2(x_0 + 2) - (2x_0 + 1) F_2] \\ &\quad + \frac{1}{48} t_3 \rho^{\sigma+1} [2(x_3 + 2) - (2x_3 + 1) F_2] \\ &\quad + \frac{3}{40} \left(\frac{3\pi^2}{2} \right)^{2/3} \rho^{5/3} \left\{ [t_1(x_1 + 2) + t_2(x_2 + 2)] F_{5/3} + \frac{1}{2} [t_2(2x_2 + 1) - t_1(2x_1 + 1)] F_{3/2} \right\} \\ F_m(\delta) &= \frac{1}{2} [(1 + \delta)^m + (1 - \delta)^m] \end{aligned} \quad (2.19)$$

Once the Skyrme parameters are known, the EOS for nuclear matter at any given asymmetry δ can be obtained using Eq. (2.18). To a good approximation, the EOS can also be expressed in terms of various nuclear matters calculated at the saturation density ρ_0 .

2.3 Nuclear matter parameter (NMP)

The EOS to a good approximation can be decomposed into the EOS for the symmetric matter and the density dependent symmetry energy as,

$$\epsilon(\rho, \delta) = \epsilon(\rho, \delta = 0) + S(\rho)\delta^2 \quad (2.20)$$

The EOS for the symmetric nuclear matter $\epsilon(\rho, \delta = 0)$ and symmetry energy $S(\rho)$ can be further expressed in terms of the nuclear matter properties at the saturation density ρ_0 as,

$$\epsilon(\rho, 0) = \epsilon_0 + \frac{1}{2}K_0 \left(\frac{\rho - \rho_0}{3\rho_0} \right)^2 + \frac{1}{6}Q_0 \left(\frac{\rho - \rho_0}{3\rho_0} \right)^3, \quad (2.21)$$

$$S(\rho) = J_0 + L_0 \left(\frac{\rho - \rho_0}{3\rho_0} \right) + \frac{1}{2}K_{\text{sym},0} \left(\frac{\rho - \rho_0}{3\rho_0} \right)^2. \quad (2.22)$$

$$\epsilon_0 = \epsilon(\rho_0, \delta = 0) \quad (2.23)$$

The quantities appearing in Eqs. (2.21) and (2.23) are the incompressibility coefficient (K_0), skewness parameter(Q_0), symmetry energy coefficient (J_0), it's slope (L_0) and the curvature parameters ($K_{\text{sym},0}$). They are defined as follows,

$$K_0 = 9\rho_0^2 \left(\frac{\partial^2 \epsilon(\rho, 0)}{\partial \rho^2} \right)_{\rho_0} \quad (2.24)$$

$$Q_0 = 27\rho_0^3 \left(\frac{\partial^3 \epsilon(\rho, 0)}{\partial \rho^3} \right)_{\rho_0} \quad (2.25)$$

$$M_0 = 12K_0 + Q_0 \quad (2.26)$$

$$J_0 = \frac{1}{2} \left(\frac{\partial^2 \epsilon(\rho_0, \delta)}{\partial \delta^2} \right)_{\delta=0} \quad (2.27)$$

$$L_0 = 3\rho_0 \left(\frac{\partial S(\rho)}{\partial \rho} \right)_{\rho_0} \quad (2.28)$$

$$K_{\text{sym},0} = 9\rho_0^2 \left(\frac{\partial^2 S(\rho)}{\partial \rho^2} \right)_{\rho_0} \quad (2.29)$$

Similarly, the nuclear incompressibility (K) of asymmetric nuclear matter can also be expanded in terms of δ at ρ_0 as $K(\delta) = K + K_\tau \delta^2 + \mathcal{O}(\delta^4)$, where $\delta = \frac{(\rho_n - \rho_p)}{\rho}$ is the isospin asymmetry and K_τ is given by [Chen *et al.* 2009]

$$K_\tau = K_{\text{sym},0} - 6L_0 - \frac{Q_0 L_0}{K_0}, \quad (2.30)$$

2.4 Structure and dynamics of neutron star

The properties of neutron stars can be obtained by solving Tolman-Oppenheimer-Volkoff (TOV) equations [Weinberg 1972]. The TOV Equation for static and spherical case is,

$$\frac{dP}{dr} = -\frac{G\epsilon(r)m(r)}{c^2r^2} \left[1 + \frac{P(r)}{\epsilon(r)}\right] \left[1 + \frac{4\pi r^3 P(r)}{m(r)c^2}\right] \left[1 - \frac{2Gm(r)}{c^2r}\right] \quad (2.31)$$

$$\frac{dm}{dr} = 4\pi r^2 \epsilon(r) \quad (2.32)$$

where, G and c are the gravitational constant and speed of light respectively. $P(r)$, $\epsilon(r)$ and $m(r)$ are the pressure, energy density and mass of the neutron star which is the function of distance r from the center of the spherical star. The boundary conditions $p(0) = p_c$ and $m(0) = 0$, where p_c and $m(0)$ are the pressure and mass at the center of the NS. The main physics input to the TOV equations is the EOS, which are calculated using the models as described in the preceding sections. The solutions of the TOV equations are the mass-radius for a sequence of static star. These solutions are also used to calculate the tidal deformability parameter as discussed bellow.

2.4.1 Tidal deformability

The gravitational wave form evolution caused by the tidal deformation of BNS systems depend on the EOS of high density matter. The tidal deformation during the last orbits before merger has been studied [Annala *et al.* 2018, Damour & Nagar 2009, Damour *et al.* 2012, Favata 2014, Flanagan & Hinderer 2008, Harry & Hinderer 2018, Hinderer 2008, Hinderer *et al.* 2010, Messenger & Read 2012, Narikawa *et al.* 2018, Read *et al.* 2009, 2013]. The tidal deformability parameter λ is defined as

$$Q_{ij} = -\lambda \mathcal{E}_{ij}, \quad (2.33)$$

where Q_{ij} is the induced quadrupole moment of a star in a binary due to the static external tidal field \mathcal{E}_{ij} of the companion star. The parameter λ can be expressed in terms of the dimensionless quadrupole tidal Love number k_2 as

$$\lambda = \frac{2}{3} k_2 R^5, \quad (2.34)$$

where R is the radius of the NS. The value of k_2 is typically in the range $\simeq 0.05 - 0.15$ [Hinderer 2008, Hinderer *et al.* 2010, Postnikov *et al.* 2010] for NSs and depends on the stellar structure. This quantity can be calculated using the following expression [Hinderer 2008]

$$k_2 = \frac{8C^5}{5} (1 - 2C)^2 [2 + 2C(y_R - 1) - y_R] \times \quad (2.35)$$

$$\left\{ \begin{aligned} &2C(6 - 3y_R + 3C(5y_R - 8)) \\ &+ 4C^3 [13 - 11y_R + C(3y_R - 2) + 2C^2(1 + y_R)] \\ &+ 3(1 - 2C)^2 [2 - y_R + 2C(y_R - 1)] \log(1 - 2C) \end{aligned} \right\}^{-1},$$

where $C (\equiv m/R)$ is the compactness parameter of the star of mass m . The quantity $y_R (\equiv y(R))$ can be obtained by solving the following differential equation

$$r \frac{dy(r)}{dr} + y(r)^2 + y(r)F(r) + r^2 Q(r) = 0, \quad (2.36)$$

with

$$F(r) = \frac{r - 4\pi r^3 (\epsilon(r) - p(r))}{r - 2m(r)}, \quad (2.37)$$

$$\begin{aligned} Q(r) = & \frac{4\pi r \left(5\epsilon(r) + 9p(r) + \frac{\epsilon(r)+p(r)}{\partial p(r)/\partial \epsilon(r)} - \frac{6}{4\pi r^2} \right)}{r - 2m(r)} \\ & - 4 \left[\frac{m(r) + 4\pi r^3 p(r)}{r^2 (1 - 2m(r)/r)} \right]^2. \end{aligned} \quad (2.38)$$

In the previous equations, $m(r)$ is mass enclosed within the radius r , and $\epsilon(r)$ and $p(r)$ are, respectively, the energy density and pressure in terms of radial coordinate r of a star. These quantities are calculated within the nuclear matter model chosen to describe the stellar EOS. For a given EOS, Eq.(2.36) can be integrated together with the TOV with the boundary conditions $y(0) = 2$, $p(0) = p_c$ and $m(0) = 0$, where $y(0)$, p_c and $m(0)$ are the dimensionless quantity, pressure and mass at the center of the NS, respectively. One can then define the dimensionless tidal deformability: $\Lambda = \frac{2}{3} k_2 C^{-5}$. The tidal deformabilities of the NSs present in the binary neutron star system can be combined to yield the weighted average as,

$$\tilde{\Lambda} = \frac{16}{13} \frac{(12q + 1)\Lambda_1 + (12 + q)q^4\Lambda_2}{(1 + q)^5}, \quad (2.39)$$

where Λ_1 and Λ_2 are the individual tidal deformabilities corresponding to the two components in the NS binary with masses m_1 and m_2 , respectively [Favata 2014, Flanagan & Hinderer 2008] with $q = m_2/m_1 < 1$.

Chapter 3

Nuclear interactions at high densities in effective chiral model

3.1 Background

The models based on chiral symmetry was introduced by Gell-Mann & Levy [[Gell-Mann & Levy 1960](#)]. The importance of chiral symmetry in the study of nuclear matter was emphasized by Lee & Wick [[Lee & Wick 1974](#)]. However, the linear chiral sigma models fail to describe properties of finite nuclei. In such models, the normal vacuum jumps to a chirally restored abnormal vacuum (Lee-Wick vacuum)[[Lee & Margulies 1975](#), [Lee & Wick 1974](#)]. This phenomenon is referred to as chiral collapse problem [[Thomas *et al.* 2004](#)] and it can be overcome mainly in two ways. One of the approaches is to incorporate logarithmic terms of the scalar field in chiral potentials [[Furnstahl & Serot 1993](#), [Heide *et al.* 1994](#), [Mishustin *et al.* 1993](#), [Papazoglou *et al.* 1997, 1998](#)] which prevents the normal vacuum from collapsing. This class of chiral models are phenomenologically successful in describing finite nuclei [[Schramm 2002](#), [Tsubakihara & Ohnishi 2007](#), [Tsubakihara *et al.* 2007, 2010](#)]. However, these models explicitly break the chiral symmetry and are divergent when chiral symmetry is restored [[Furnstahl & Serot 1993](#)].

Alternatively, the chiral collapse problem is prevented by generating the isoscalar-vector meson mass dynamically via Spontaneous Symmetry Breaking (SSB) by coupling the isoscalar-vector mesons with the scalar mesons [[Boguta 1983](#), [Sahu *et al.* 1993](#)]. However, the main drawback of all these models was the unrealistic high nuclear incompressibility (K). Later on, in several attempts, the higher order terms of scalar meson field [[Jha & Mishra 2008](#), [Sahu & Ohnishi 2000](#), [Sahu *et al.* 2004](#)] were introduced to ensure a reasonable K at saturation density. The non-linear terms in the chiral Lagrangian

can provide the three-body forces [Logoteta *et al.* 2015] which might have important roles to play at high densities. The effective chiral model has been used to study nuclear matter aspects such as matter at low density and finite temperature [Sahu *et al.* 2004], NS structure and composition [Jha *et al.* 2006] and nuclear matter saturation properties. As emphasized in Ref. [Sahu *et al.* 2004], the model parameters are constrained and related to the vacuum expectation value of the scalar field. Since the mass of the isoscalar-vector meson is dynamically generated, practically there are very few free parameters to adjust the saturation properties. However, this type of models had a couple of drawbacks. They yield the symmetry energy slope parameter, $L \sim 90$ MeV, which is a little too large. Also, the symmetry energy at 0.1 fm^{-3} baryon density is ~ 22 MeV, which is lower than the presently estimated value [Roca-Maza *et al.* 2013a, Trippa *et al.* 2008].

In this chapter, we employ the effective chiral model in which chiral symmetry breaks spontaneously. We extend this model by including the cross-couplings of σ and ω mesons with the ρ meson. We would like to see whether these terms in the interaction help in fixing the values of symmetry energy and its slope parameter at the saturation density. We study the effects of the cross-couplings on the Equation of State (EOS) for Asymmetric Nuclear Matter (ANM). The effects of the crustal EOS on the mass and the radius of NS are evaluated using the method suggested recently by Zdunik *et al.* [Zdunik *et al.* 2017].

3.2 Mesonic cross coupling

The complete Lagrangian density for the effective chiral model which includes the various cross-coupling terms is given by,

$$\mathcal{L} = \mathcal{L}_l + \mathcal{L}_\times, \quad (3.1)$$

where,

$$\begin{aligned} \mathcal{L}_l = & \bar{\psi}_B \left[\left(i\gamma_\mu \partial^\mu - g_\omega \gamma_\mu \omega^\mu - \frac{1}{2} g_\rho \vec{\rho}_\mu \cdot \vec{\tau} \gamma^\mu \right) \right. \\ & \left. - g_\sigma (\sigma + i\gamma_5 \vec{\tau} \cdot \vec{\pi}) \right] \psi_B + \frac{1}{2} (\partial_\mu \vec{\pi} \cdot \partial^\mu \vec{\pi} + \partial_\mu \sigma \partial^\mu \sigma) \\ & - \frac{\lambda}{4} (x^2 - x_0^2)^2 - \frac{\lambda b}{6m^2} (x^2 - x_0^2)^3 \\ & - \frac{\lambda c}{8m^4} (x^2 - x_0^2)^4 - \frac{1}{4} F_{\mu\nu} F^{\mu\nu} + \frac{1}{2} g_\omega^2 x^2 (\omega_\mu \omega^\mu) \\ & - \frac{1}{4} \vec{R}_{\mu\nu} \cdot \vec{R}^{\mu\nu} + \frac{1}{2} m_\rho'^2 \vec{\rho}_\mu \cdot \vec{\rho}^\mu, \end{aligned} \quad (3.2)$$

and

$$\mathcal{L}_\times = \eta_1 \left(\frac{1}{2} g_\rho^2 x^2 \vec{\rho}_\mu \cdot \vec{\rho}^\mu \right) + \eta_2 \left(\frac{1}{2} g_\rho^2 \vec{\rho}_\mu \cdot \vec{\rho}^\mu \omega_\mu \omega^\mu \right). \quad (3.3)$$

Here, ψ_B is the nucleon isospin doublet interacting with different mesons σ , ω and ρ , with the respective coupling strengths g_i , with $i = \sigma, \omega$ and ρ . The b and c are the strength for self couplings of scalar fields. The γ^μ are the Dirac matrices and τ are the Pauli matrices. \mathcal{L}_l (Eq. (3.2)) is the original Lagrangian given in Ref. [Jha *et al.* 2006]. Note that potential for the scalar fields (π, σ) are written in terms of a chiral invariant field x given by $x^2 = \pi^2 + \sigma^2$.

\mathcal{L}_\times (Eq. (3.3)) is the new additional piece we add to the original Lagrangian given in [Jha *et al.* 2006]. It contains cross-coupling terms between ρ and ω and also between ρ and σ . The coupling strength for $\sigma - \rho$ and $\omega - \rho$ are given by $\eta_1 g_\rho^2$ and $\eta_2 g_\rho^2$ respectively. The interaction of the scalar (σ) and the pseudo-scalar (π) mesons with the isoscalar-vector meson (ω) generates a dynamical mass for the ω meson through SSB of the chiral symmetry with scalar field attaining the vacuum expectation value x_0 . Then the mass of the nucleon (m), the scalar (m_σ) and the vector meson mass (m_ω), are related to x_0 (vacuum expectation of x) through

$$m = g_\sigma x_0, \quad m_\sigma = \sqrt{2\lambda} x_0, \quad m_\omega = g_\omega x_0, \quad (3.4)$$

where, $\lambda = \frac{(m_\sigma^2 - m_\pi^2)}{2f_\pi^2}$ and $f_\pi = x_0$ is the pion decay constant, which reflects the strength of SSB. In Eq. (3.3) when $\eta_1 \neq 0$ there is a cross-interaction between ρ and σ . Hence a fraction of ρ meson mass will come from SSB. The mass of ρ meson (m_ρ) in this model then will be related to vacuum expectation of x through

$$m_\rho^2 = m_\rho'^2 + \eta_1 g_\rho^2 x_0^2. \quad (3.5)$$

In the mean field treatment the explicit role of pion mass is ignored and hence $m_\pi = 0$ and mesonic field is assumed to be uniform, i.e., without any quantum fluctuation. Then, the isoscalar-vector field ω is of the form $\omega_\mu = \omega_0 \delta_\mu^0$, where δ_μ^0 is Kronecker delta. Note that ω_0 does not depend on space-time but it depends on baryon density (ρ). The vector field (ω), scalar field (σ) and isovector field (ρ_3^0) equations (in terms of $Y = x/x_0 = m^*/m$) are, respectively, given by:

$$\left[m_\omega^2 Y^2 + \eta_2 C_\rho m_\rho^2 (\rho_3^0)^2 \right] \omega_0 = g_\omega \rho, \quad (3.6)$$

$$(1 - Y^2) - \frac{b}{m^2 C_\omega} (1 - Y^2)^2 + \frac{c}{m^4 C_\omega^2} (1 - Y^2)^3 + \frac{2C_\sigma m_\omega^2 \omega_0^2}{m^2} + \frac{2\eta_1 C_\sigma C_\rho m_\rho^2 (\rho_3^0)^2}{C_\omega m^2} - \frac{2C_\sigma \rho_s}{mY} = 0, \quad (3.7)$$

$$m_\rho^2 \left[1 - \eta_1(1 - Y^2)C_\rho/C_\omega + \eta_2 C_\rho \omega_0^2 \right] \rho_3^0 = \frac{1}{2} g_\rho (\rho_p - \rho_n). \quad (3.8)$$

The quantity ρ and ρ_S are the baryon and the scalar density defined as,

$$\rho = \frac{\gamma}{(2\pi)^3} \int_0^{k_F} d^3k, \quad (3.9)$$

$$\rho_s = \frac{\gamma}{(2\pi)^3} \int_0^{k_F} \frac{m^*}{\sqrt{m^{*2} + k^2}} d^3k, \quad (3.10)$$

where, k_F is the baryon fermi momentum and γ (for example, $\gamma = 4$ for Symmetric Nuclear Matter (SNM)) is the spin degeneracy factor. $C_\sigma \equiv g_\sigma^2/m_\sigma^2$, $C_\omega \equiv g_\omega^2/m_\omega^2$ and $C_\rho \equiv g_\rho^2/m_\rho^2$ are the scalar, vector and isovector coupling parameters. The energy density (ϵ) and pressure (p) for a given baryon density (in terms of $Y = m^*/m$) in this model is obtained from the stress-energy tensor, which is given as

$$\begin{aligned} \epsilon = & \frac{1}{\pi^2} \sum_{k_n, k_p} \int_0^{k_F} k^2 \sqrt{k^2 + m^{*2}} dk + \frac{m^2}{8C_\sigma} (1 - Y^2)^2 \\ & - \frac{b}{12C_\sigma C_\omega} (1 - Y^2)^3 + \frac{c}{16m^2 C_\sigma C_\omega^2} (1 - Y^2)^4 + \frac{1}{2} m_\omega^2 \omega_0^2 Y^2 \\ & + \frac{1}{2} m_\rho^2 \left[1 - \eta_1(1 - Y^2)(C_\rho/C_\omega) + 3\eta_2 C_\rho \omega_0^2 \right] (\rho_3^0)^2, \end{aligned} \quad (3.11)$$

$$\begin{aligned} p = & \frac{1}{3\pi^2} \sum_{k_n, k_p} \int_0^{k_F} \frac{k^4}{\sqrt{k^2 + m^{*2}}} dk - \frac{m^2}{8C_\sigma} (1 - Y^2)^2 \\ & + \frac{b}{12C_\sigma C_\omega} (1 - Y^2)^3 - \frac{c}{16m^2 C_\sigma C_\omega^2} (1 - Y^2)^4 + \frac{1}{2} m_\omega^2 \omega_0^2 Y^2 \\ & + \frac{1}{2} m_\rho^2 \left[1 - \eta_1(1 - Y^2)(C_\rho/C_\omega) + \eta_2 C_\rho \omega_0^2 \right] (\rho_3^0)^2. \end{aligned} \quad (3.12)$$

For SNM we have to set $k_n = k_p$ and $\rho_3^0 = 0$. As our present knowledge of nuclear matter is mainly confined to normal nuclear matter density (ρ_0), coupling constants $C_\sigma \equiv g_\sigma^2/m_\sigma^2$ and $C_\omega \equiv g_\omega^2/m_\omega^2$ are not free parameters in the Eqs.(3.11,3.12). To obtain C_σ and C_ω , we solve the field equations (Eqs. (3.6-3.8)) self consistently while satisfying the nuclear saturation properties. Note that for different values of $Y = x_0/x = m^*/m$, we get different values of C_σ and C_ω .

After inclusion of cross interactions \mathcal{L}_\times (Eq. (3.3)) the modified symmetry energy $S(\rho)$ in this model is

$$S(\rho) = \frac{k_F^2}{6\sqrt{k_F^2 + m^{*2}}} + \frac{C_\rho k_F^3}{12\pi^2 (m_\rho^*/m_\rho)^2} + \frac{\eta_2 C_\rho^2 \omega_0^2 k_F^3}{6\pi^2 (m_\rho^*/m_\rho)^4} - \frac{2\eta_2 C_\rho^2 C_\omega k_F^9}{27\pi^6 m_\omega^2 Y^4 (m_\rho^*/m_\rho)^4}, \quad (3.13)$$

where, $m_\rho^{*2} = m_\rho^2 \left[1 - \eta_1(1 - Y^2)(C_\rho/C_\omega) + \eta_2 C_\rho \omega_0^2 \right]$ and $k_F = (3\pi^2 \rho/2)^{1/3}$. The coupling parameters C_ρ, η_1 and η_2 can be evaluated numerically by fixing symmetry energy $S(\rho)$ and its slope parameter L at saturation density (ρ_0). Without cross-couplings ($\eta_1 = \eta_2 = 0$) we revert back to the Lagrangian given in [Jha et al. 2006]

Table 3.1: List of the model parameters determined from the properties of SNM such as, energy per nucleon $E_0 = -16$ MeV, nuclear incompressibility $K = 247$ MeV and the nucleon effective mass $Y = m^*/m = 0.864$ at the saturation density $\rho_0 = 0.153$ fm $^{-3}$. The scalar and vector meson coupling parameters are $C_\sigma = g_\sigma^2/m_\sigma^2$ and $C_\omega = g_\omega^2/m_\omega^2$ respectively. $B = b/m^2$ and $C = c/m^4$ are the parameters for the higher order self-couplings of the scalar field with m being the nucleon mass. The nucleon, ω meson and σ meson masses are 939 MeV, 783 MeV and 469 MeV respectively.

C_σ	C_ω	B	C
(fm 2)	(fm 2)	(fm 2)	(fm 4)
7.057	1.757	-5.796	0.001

3.3 Symmetric nuclear matter properties

As can be seen from the preceding section that the EOS of the SNM are determined by the coupling parameters C_σ , C_ω , b and c (Eqs. (3.11,3.12)). The values of these coupling parameters and resulting SNM properties at the saturation density are listed in Table 3.1. The values of the model parameters lie in the stable region [Sahu *et al.* 2010].

3.4 Density dependence of symmetry energy $S(\rho)$

The density dependence of symmetry energy $S(\rho)$ is obtained by using three different variants of the present model. We consider the case of no cross-coupling (NCC), the $\sigma - \rho$ cross-coupling (SR) and the $\omega - \rho$ cross-coupling (WR). Since the NCC model has only one free parameter (i.e., C_ρ) there is not enough freedom to vary J_0 and L independently. However, the SR and WR models can provide some flexibility to adjust them. Note that, in comparison to the earlier models (i.e., NCC type), the inclusion of cross-couplings have important implications on $S(\rho)$. The effects of the cross-couplings grow stronger at high densities which are relevant for the study of NS properties.

In Table 3.2 we list the values of coupling constants (C_ρ , η_1 and η_2) and the resulting nuclear matter properties: J_0 , L , K_{sym} , Q_{sym} and K_τ at the saturation density ρ_0 and J_1 - the symmetry energy at $\rho_1 = 0.1$ fm $^{-3}$. For the NCC, C_ρ is adjusted to yield $J_0 = 32.5$ MeV. For SR(WR) model, the value of C_ρ and $\eta_1(\eta_2)$ are adjusted to yield $J_0 = 32.5$ MeV and $L = 65$ MeV. These values are compatible with $J_0 = 31.6 \pm 2.66$ MeV and $L = 58.9 \pm 16$ MeV obtained by analyzing various terrestrial experimental informations and astrophysical observations [Li & Han 2013]. It may be noted that the

Table 3.2: The values of the coupling constants C_ρ, η_1 and η_2 are determined from various symmetry energy elements. The mass of the ρ meson is 770 MeV. The values of C_ρ are in units of fm^2 , η_1 and η_2 are dimensionless. All the symmetry energy elements are in units of MeV.

		NCC	SR	WR
Parameters	C_ρ	5.14	12.28	6.08
	η_1	0	-0.79	0
	η_2	0	0	6.49
Nuclear Matter	J_0	32.5	32.5	32.5
	J_1	22.30	24.49	23.68
	L	87	65	65
	K_{sym}	-20.09	-59.16	-204.78
	Q_{sym}	58.73	356.11	-88.04
	K_τ	-434	-368	-513

value of J_1 obtained for the NCC model shows a significant deviation from 24.1 ± 0.8 MeV [Trippa *et al.* 2008] and 23.6 ± 0.3 MeV [Roca-Maza *et al.* 2013a] obtained by analyzing the experimental data on isovector giant resonances, whereas, J_1 is in good agreement in case of SR and WR models. The value of L obtained with NCC model is also a little too large. By inclusion of cross-couplings (SR and WR models) the value of L is reduced by $\sim 25\%$ keeping J_0 fixed. In what follows, we shall present our results for the density dependence of symmetry energy, EOSs for the SNM and PNM and the NS properties obtained using the NCC, SR and WR models. We shall also compare our EOSs and the density dependence of symmetry energy with those calculated for a few selected RMF models, namely, NL3 [Lalazissis *et al.* 1997], IUFSU [Fattoyev *et al.* 2010], BSP [Agrawal *et al.* 2012b] and BKA22 [Agrawal 2010]. The NL3 model does not include any cross-coupling, the IUFSU and BSP models include the cross-coupling between ω and ρ mesons, while, BKA22 model is obtained by including the coupling of ρ mesons with the σ mesons.

A lot of progress, both theoretically and experimentally, has been made to constrain symmetry energy at sub saturation densities. We consider the data from three important sources: simulations of low energy Heavy Ion Collisions (HIC) in ^{112}Sn and ^{124}Sn [Tsang *et al.* 2009]; nuclear structure studies by excitation energies to Isobaric Analog States (IAS) [Danielewicz & Lee 2014] and ASY-EOS experiment at GSI [Russotto *et al.* 2016]. The density dependences of the symmetry energy

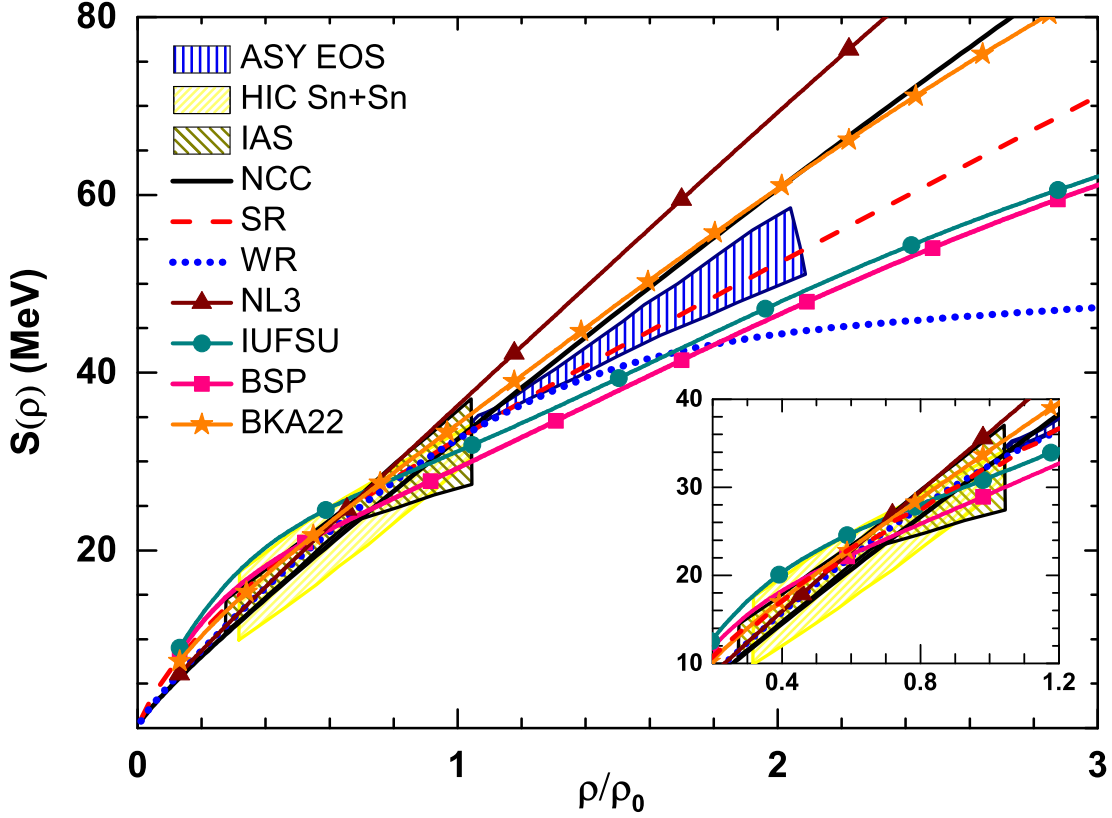


Figure 3.1: Symmetry energy as a function of scaled density (ρ/ρ_0) is plotted for three different variants of the effective chiral model as labeled by NCC, SR and WR obtained in the present work and are compared with those for a few selected RMF models NL3, IUFSU, BSP and BKA22. The constraints on the symmetry energy from IAS [Danielewicz & Lee 2014], HIC Sn+Sn [Tsang *et al.* 2009] and ASY-EOS experimental data [Russotto *et al.* 2016] are also displayed. The inset shows the blown up behavior of symmetry energy at low densities.

for NCC, SR, WR and selected RMF models are displayed in Fig. 3.1. For comparison we have depicted the IAS [Danielewicz & Lee 2014], HIC Sn+Sn [Tsang *et al.* 2009] and ASY-EOS [Russotto *et al.* 2016] data in the figure. It is evident that in the absence of any cross-couplings (NCC), the behavior of symmetry energy as a function of density is not very much compatible with those obtained by analyzing diverse experimental data. Remarkably the SR model satisfies all the above mentioned constraints. None of the considered RMF models satisfy all the symmetry energy constraints.

The effects of various cross-couplings on the symmetry energy grow stronger at $\rho > \rho_0$. The symmetry energy is effectively low in WR model compared to NCC and SR models. Thus one may expect significant differences in the properties of NS obtained for the SR and WR models. This will be explored later in the paper.

The symmetry energy elements L and K_{sym} predominantly determine the value of K_τ (Eq. (2.30)) which is required to evaluate the incompressibility of ANM. In Fig. 3.2 we compare our values of K_τ with various Skyrme and RMF model predictions in K vs K_τ plot [Sagawa *et al.* 2007]. The dashed lines represent the constraints on K_τ from -840 MeV to -350 MeV [Li *et al.* 2010, Pearson *et al.* 2010, Stone *et al.* 2014] and K from 220 MeV to 260 MeV [Shlomo *et al.* 2006] which have been determined using various experimental data on isoscalar giant monopole resonances. All the three models NCC, SR and WR satisfy these bounds of K and K_τ . It is to be noted that the models with a larger nuclear incompressibility (K) tend to have lower K_τ value. As can be seen from Fig. 3.2, several Skyrme models but only three RMF models (NLC, DDME1 and DDME2) satisfy the bounds for K and K_τ simultaneously. The values of L for the nonlinear model NLC with constant coupling is 107.97 MeV [Dutra *et al.* 2014] and that for the DDME models with density dependent coupling constants are $51 - 55$ MeV [Dutra *et al.* 2014]. The value of L for NLC model is very large compared to presently accepted range. We have also looked into the values of K_τ and K for the several nonlinear RMF models [Alam *et al.* 2016]. Among them a few models (BSR type) have L between $60 - 70$ MeV and satisfy the constraints on K and K_τ . These models includes $\sigma - \rho$ and $\omega - \rho$ both cross-couplings.

3.5 Equation of state

In Fig. 3.3 we plot low density EOS for PNM for all of our three models (NCC, SR and WR). The low density behavior of energy per neutron for SR model is in good agreement with the results obtained by microscopic calculations [Gezerlis & Carlson 2010, Hebeler *et al.* 2013] as shown by the shaded region. The PNM EOS for NCC and WR models do not have much overlap with the shaded region. The results for few selected RMF models are also displayed in the figure. Only the BSP model shows marginal overlap with the shaded region. In Ref. [Alam *et al.* 2017] two different families of systematically varied models with $\sigma - \rho$ and $\omega - \rho$ cross-couplings have been employed to study the low density behavior of asymmetric nuclear matter. It was found that none of the models with $\sigma - \rho$ cross-coupling satisfy the low density behavior of the PNM as predicted by Hebeler *et al.* [Hebeler *et al.* 2013]. However this constraint on the PNM EOS at low densities are satisfied by a couple of RMF models with $\omega - \rho$ cross-coupling having $L \sim 45 - 65$ MeV. The EOS with the current parameterization is compared in Fig. 3.4 with the experimental flow data obtained from the HIC [Danielewicz *et al.* 2002] for SNM and PNM EOSs. The later one is constructed theoretically with

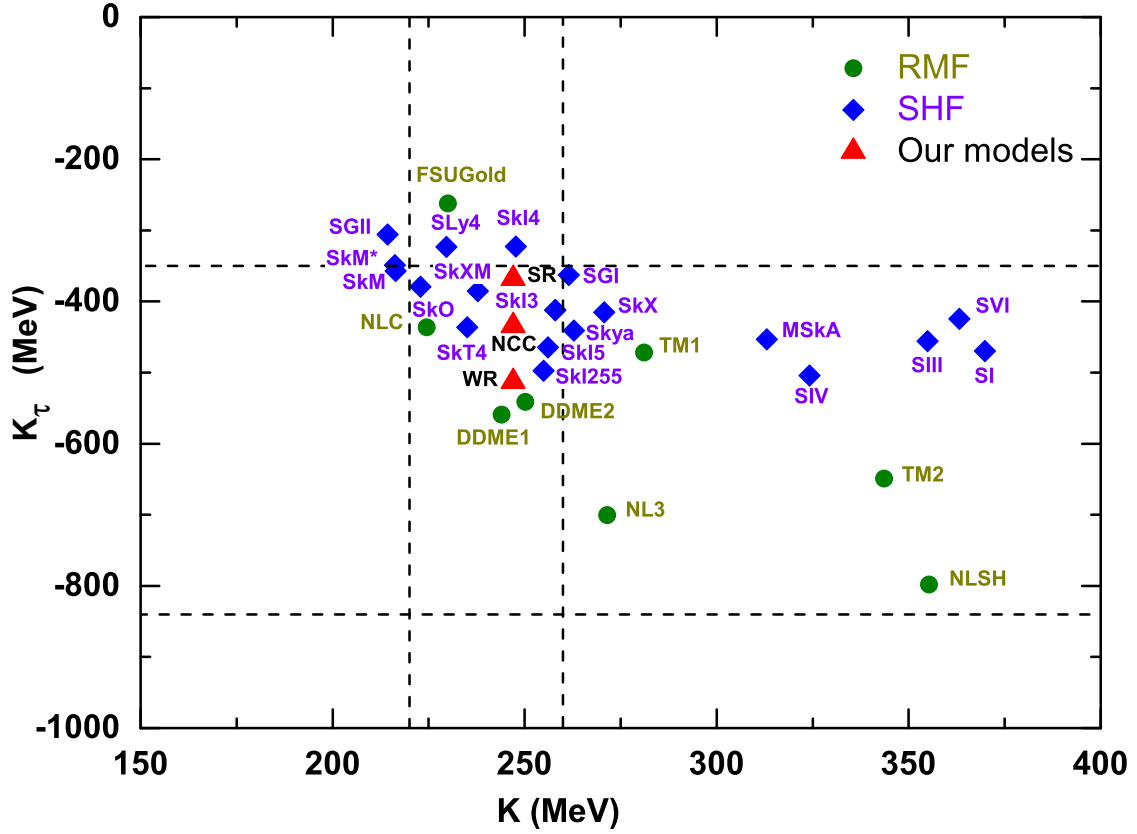


Figure 3.2: The values of K and K_τ from different models as labeled in [Colo *et al.* 2014, Sagawa *et al.* 2007] are compared with our models (NCC, SR and WR). The vertical and horizontal dashed lines represent the empirical ranges for K and K_τ respectively.

two extreme parameterizations, the weakest (Asy soft) and strongest (Asy stiff) of symmetry energy as proposed in [Prakash *et al.* 1988] and as reported in [Danielewicz *et al.* 2002]. The SNM EOS is identical for all of our three models, since, the SNM properties are same. It is passing well through the experimental HIC data. In case of the PNM, the resulting EOSs for NCC and SR models pass through the upper end of HIC-Asy soft and lower end of HIC-Asy stiff, whereas, the PNM EOS for the WR model passes through the HIC-Asy soft only. As can be seen from Fig. 3.4 that the influence of cross-couplings in the effective chiral model at high density is quite strong in comparison to RMF models with similar type of cross-couplings. The PNM EOS for the WR model is quite softer than BSP and IUFSU at high densities. Similar differences can also be seen in the case of SR and BKA22 models.

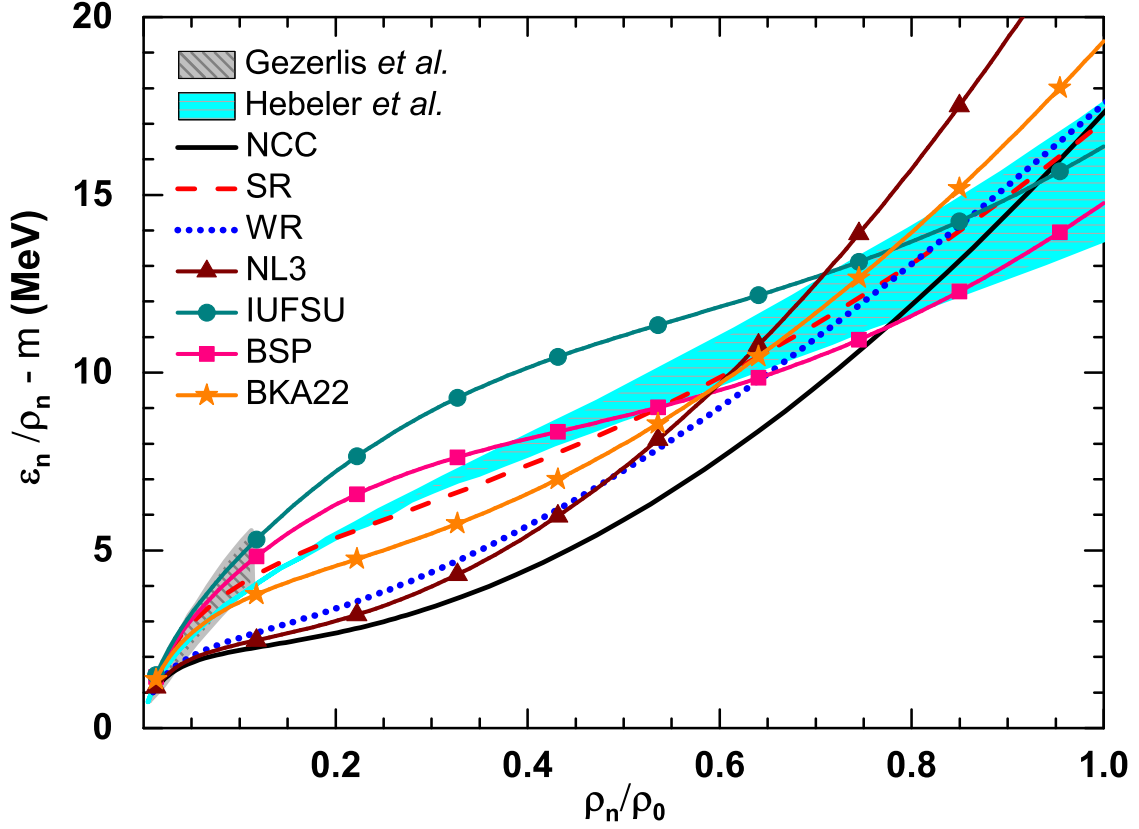


Figure 3.3: Energy per neutron as a function of scaled neutron density (ρ_n/ρ_0) for three different variants of the effective chiral model as labeled by NCC, SR and WR obtained in the present work and for a few RMF models NL3, IUFSU, BSP and BKA22 are compared with microscopic calculations [Gezerlis & Carlson 2010, Hebel *et al.* 2013] as shown by the shaded region.

3.6 Neutron star mass-radius relationship

We extend our analysis to study the mass-radius relationship for static NS composed of beta equilibrated charge neutral matter. The EOS for the core is obtained from the effective chiral model. The effects of crustal EOS at low densities on the mass and the radius of NS are considered in two different ways. We model the crust EOS using BPS EOS [Baym *et al.* 1971] in the density range $\rho \sim 4.8 \times 10^{-9} \text{ fm}^{-3}$ to $2.6 \times 10^{-4} \text{ fm}^{-3}$. The crust and the core are joined using the polytropic form [Carriere *et al.* 2003] $p(\epsilon) = a_1 + a_2\epsilon^\gamma$, where the parameters a_1 and a_2 are determined in such a way that the EOS for the inner crust for a given γ matches with that for the inner edge of the outer crust at one end and with the edge of the core at the other end. The polytropic index γ is taken to be equal to $4/3$. For $\gamma = 4/3$, the values of radius $R_{1.4}$ corresponding to the canonical mass of NS for

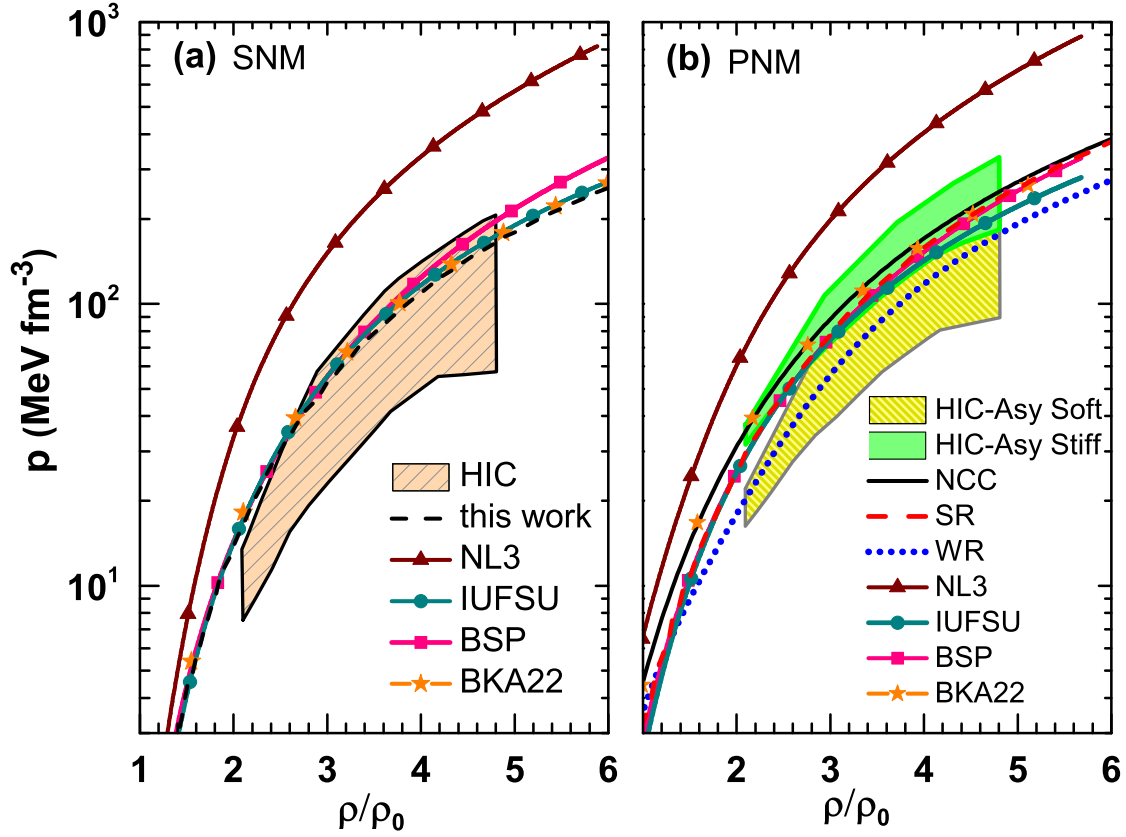


Figure 3.4: The pressure as a function of scaled density (ρ/ρ_0) for the SNM (left) and the PNM (right). The SNM EOS for the NCC, SR and WR models are exactly the same and is labeled by “this work”. For the comparison the SNM and PNM EOSs for a few RMF models NL3, IUFSU, BSP and BKA22 are displayed. The SNM and PNM EOSs shown by shaded regions are taken from Ref. [Danielewicz *et al.* 2002] (see text for details)

the NL3 [Carriere *et al.* 2003] and IUFSU [Piekarewicz *et al.* 2014] RMF models are within $\sim 2\%$ in comparison to those obtained by treating the inner crust in the Thomas Fermi approach [Grill *et al.* 2014]. Alternatively, we estimate the contributions of the crust EOS to the NS radius and mass using the core crust approximation approach given in [Zdunik *et al.* 2017] referred hereafter ZFH method. This method enables one to estimate total mass and radius of a NS including the crust contributions very accurately for NS mass larger than $1 M_\odot$. In the ZFH method the radius and the mass of NS are given by

$$R = \frac{R_{core}}{1 - (\alpha - 1)(R_{core}c^2/2GM - 1)}, \quad (3.14)$$

$$M = M_{crust} + M_{core}, \quad (3.15)$$

with,

$$M_{crust} = \frac{4\pi P_{cc} R_{core}^4}{GM_{core}} \left(1 - \frac{2GM_{core}}{R_{core}c^2}\right). \quad (3.16)$$

In the above equations $\alpha = (\mu_{cc}/\mu_0)^2$, μ_{cc} and μ_0 are the chemical potential at transition density (ρ_{cc}) and at neutron star surface respectively. R_{core} and M_{core} are the radius and mass of NS core. P_{cc} is pressure at transition density. The transition density (ρ_{cc}) is mostly in the range 0.4 to 0.6 ρ_0 for L typically ranging from 30 to 120 MeV [Ducoin *et al.* 2011]. In the present work we have taken $\rho_{cc}/\rho_0 = 0.3, 0.4$ and 0.5 .

Comparison of the results of the two approaches is given in Table 3.6. The maximum mass of the NS is sensitive neither to the methods used to estimate the crust effects nor to the choice of transition density. The WR model, which includes $\omega - \rho$ cross-coupling, does not satisfy the maximum mass constraint as imposed by PSR J0348 + 0432 ($M = 2.01 \pm 0.04 M_\odot$) [Antoniadis & *et al.* 2013]. This disfavors the WR model. The values of $R_{1.4}$ obtained using BPS EOS for the outer crust and polytropic EOS for the inner crust are little too large compared to those for the ZFH method. We find that by including $\sigma - \rho$ coupling (SR) $R_{1.4}$ are smaller compare to the NCC model which does not include any cross-coupling term. The radius of NS is sensitive to transition density. Using the strong correlation between transition density (ρ_{cc}) and L , we found the values of ρ_{cc} to be 0.061 fm^{-3} ($\sim 0.4 \rho_0$) for NCC and 0.077 fm^{-3} ($\sim 0.5 \rho_0$) for SR and WR models respectively [Grill *et al.* 2014]. The mass radius relationship for the NS for all of our three models obtained using respective values of the transition densities are plotted in Fig. 3.5. The dashed lines are obtained using the ZFH method in which the effects of the crust EOS were approximated and the solid lines are obtained using BPS and the polytropic EOSs for the outer and the inner crust respectively. It is found that the value of $R_{1.4}$ is decreased by ~ 0.5 km in SR model compared to NCC model. The $R_{1.4}$ of SR is consistent with 11.9 ± 1.22 km (90% confidence) obtained by constraining symmetry energy at saturation density from various experimental information and theory [Lattimer & Lim 2013]. The NS maximum mass $M_{\max} = 2.79, 1.94, 2.02, 2.04 M_\odot$ and the radius $R_{1.4} = 14.66, 12.49, 12.64, 13.28$ km for the selected RMF models NL3, IUFSU, BSP and BKA22 respectively. The RMF models such as IUFSU and BSP with $\omega - \rho$ cross-coupling readily yield $M_{\max} \sim 2 M_\odot$, since, the softening of the EOS due to the inclusion of this cross-coupling is not as strong as in the case of effective chiral model.

Table 3.3: The maximum mass and radius of NS composed of β -equilibrated matter are listed. The total mass and radii following the ZFH method are obtained by using Eqs. 3.14-3.16. These are compared with the ones calculated from the BPS and polytropic EOSs for the outer and inner crusts, respectively. ρ_{cc}/ρ_0 is the scaled transition density. M_{max} , R_{max} and $R_{1.4}$ are the NS maximum mass, radius at maximum mass and the radius at $1.4 M_{\odot}$ respectively.

$\frac{\rho_{cc}}{\rho_0}$	Model	BPS+polytropic EOS			ZFH method		
		M_{max}	R_{max}	$R_{1.4}$	M_{max}	R_{max}	$R_{1.4}$
		M_{\odot}	km	km	M_{\odot}	km	km
0.3	NCC	1.97	11.55	13.31	1.97	11.48	13.12
	SR	1.97	11.24	12.75	1.97	11.20	12.71
	WR	1.84	10.74	12.22	1.84	10.67	12.03
0.4	NCC	1.97	11.64	13.57	1.97	11.48	13.12
	SR	1.97	11.28	12.87	1.97	11.21	12.72
	WR	1.84	10.83	12.41	1.84	10.67	12.03
0.5	NCC	1.97	11.77	13.90	1.97	11.50	13.13
	SR	1.97	11.35	13.04	1.97	11.24	12.72
	WR	1.84	10.92	12.62	1.84	10.67	12.03

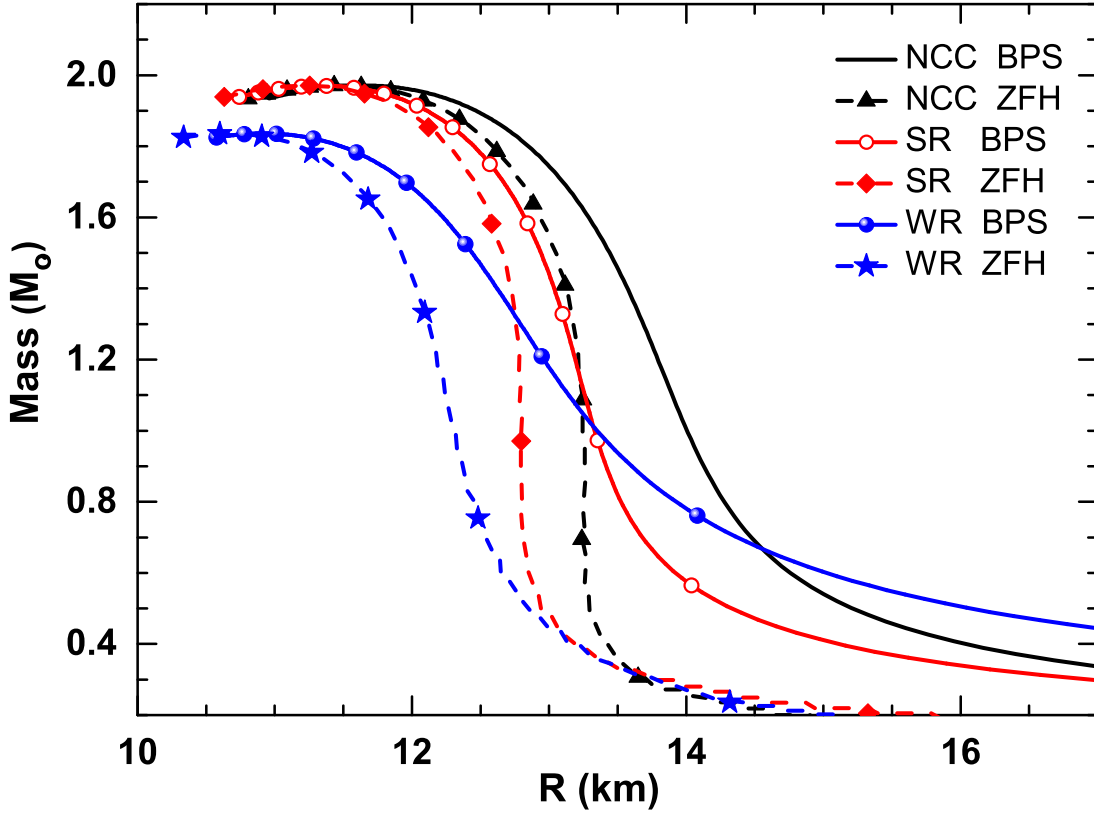


Figure 3.5: The mass-radius relationships for the NCC, SR and WR models are displayed. The effects of the crustal EOSs are incorporated by using explicitly the BPS and polytropic EOSs (solid lines) at low densities and alternatively using the ZFH method (dashed lines).

3.7 Summary

Results obtained for the SR model can be summarized in the following way. It yields symmetry energy $J_0 = 32.5$ MeV, symmetry energy slope parameter $L = 65$ MeV, nuclear incompressibility $K = 247$ MeV and the asymmetry term of nuclear incompressibility $K_\tau = -368$ MeV at saturation density $\rho_0 = 0.153$ fm⁻³. It also yields symmetry energy $J_1 = 24.49$ MeV at density 0.1 fm⁻³, NS maximum mass $1.97 M_\odot$ and radius $R_{1.4} = 12.72$ km. All these values are within presently accepted range. The SR model also satisfies all the discussed constraints from microscopic calculations for low density PNM EOS, density dependence of symmetry energy, HIC data for SNM EOS and HIC-Asy stiff data for PNM EOS.

The contributions of the exotic degrees of freedom, such as hyperons, kaons etc. to the properties of NS are not considered in the present work. In general, the presence of strange particles softens the

EOS and reduce the NS maximum mass. In particular, the inclusion of hyperons in the effective chiral model (i.e. NCC type) tend to reduce the NS maximum mass by $\sim 0.3 M_{\odot}$ [Jha *et al.* 2006]. The influence of hyperons on the NS properties, however, are very sensitive to the choice of the meson-hyperon couplings. It has been shown that sizable fraction of hyperons may exist in the NS with a mass $2 M_{\odot}$, provided, strong repulsive hyperon-hyperon interaction is introduced through strange ϕ mesons [Bizarro *et al.* 2015, Sulaksono & Agrawal 2012, Weissenborn *et al.* 2012].

Chapter 4

Correlations of nuclear matter parameters with astrophysical observations

4.1 Background

Astrophysical observations are the complementary probe for the information in the region of the dense-matter EOS which is not experimentally accessible in the laboratory [Rezzolla *et al.* 2018b]. The NSs are massive and compact astrophysical objects, the coalescence of binary NS systems is one of the most promising sources of gravitational waves (GWs) observable by ground-based detectors [Brillet & *et al.* Virgo Collaboration, Cutler *et al.* 1993, Drever 1983, Hough & *et al.* 1989, Taylor & Weisberg 1982, Thorne 1987]. The GW signals emitted during a NS merger depends on the behavior of neutron star matter at high densities. Therefore, its detection opens the possibility of constraining the nuclear matter parameters (NMP) characterizing the EOS [Duez 2010, Faber 2009]. During the last stages of the inspiral motion of the coalescing neutron stars(NSs), the strong gravity of each of them induces a tidal deformation in the companion star. Decoding the gravitational wave phase evolution caused by that deformation allows the determination of the dimensionless tidal deformability parameter [Binnington & Poisson 2009, Damour & Nagar 2009, Flanagan & Hinderer 2008, Hinderer 2008, Hinderer *et al.* 2010]. It is a measure of the response to the gravitational pull on the neutron star surface correlating with pressure gradients inside the NS and, therefore, it has been proposed as an effective probe of the equation of state (EOS) of nuclear matter relevant for neutron stars [De *et al.* 2018, Malik *et al.* 2018a, 2019b].

Studies of the correlations between nuclear matter parameters and the tidal deformability, based on a few selected relativistic mean field models, have shown that measurements of the latter can con-

strain the high density behavior of the nuclear symmetry energy [Fattoyev *et al.* 2013] as well as put bounds on the value of neutron skin thickness [Fattoyev *et al.* 2018]. These preliminary studies need to be validated further using a more diverse set of models for the nuclear EOS. In earlier studies it was found that correlations between the various properties of NS and nuclear matter EOS parameters are significantly affected when a more diverse set of models are employed [Alam *et al.* 2015, Fortin *et al.* 2016]. Recently, astrophysical observations of NS, in particular, the maximum mass, the radius of a canonical $1.4 M_{\odot}$ NS, and the tidal deformability, have been used to constrain various parameters of the EOS [Zhang *et al.* 2018a]. However, within their assumptions, they found that the tidal deformability obtained from GW170817 is not very restrictive.

In view of the recent observation GW170817, in this chapter, we will study the dependence of the tidal deformability Λ on the NMPs describing the EOS. In other words, we shall examine if there is a unique dependence of Λ on the various nuclear matter properties obtained for a diverse set of nuclear models. One of the simplest approach is to find then correlation between NS properties and nuclear matter properties in a diverse set of nuclear models that are constrained by the bulk properties of finite nuclei [Dutra *et al.* 2012, 2014] and the observed $\approx 2M_{\odot}$ NS maximum mass [Antoniadis & *et al.* 2013]. We have employed diverse set Relativistic and non relativistic mean field models. For all of these models, both the NS and nuclear matter properties vary over a wide range [Alam *et al.* 2016].

4.2 Nuclear models and EOS parameters

The correlations of the properties of neutron stars with the various nuclear matter parameters of the EOS are studied using a set of eighteen relativistic and twenty-four non-relativistic nuclear models. These models have been employed for the study of finite nuclei and NS properties. Our set of models are based on RMF and SHF frameworks. The employed RMF models are BSR2, BSR3, BSR6 [Agrawal 2010, Dhiman *et al.* 2007], FSU2 [Chen & Piekarewicz 2014], GM1 [Glendenning & Moszkowski 1991], NL3 [Lalazissis *et al.* 1997], NL3 $\sigma\rho$ 4, NL3 $\sigma\rho$ 6 [Pais & Providência 2016], NL3 $\omega\rho$ 02 [Horowitz & Piekarewicz 2001], NL3 $\omega\rho$ 03 [Carriere *et al.* 2003], TM1 [Y.Sugahara & H.Toki 1994], and TM1-2 [Providência & Rabhi 2013] and DD2 [Typel *et al.* 2010], DDH δ [Gai-tanos *et al.* 2004], DDH δ Mod [Ducoin *et al.* 2011], DDME1 [Niksic *et al.* 2002], DDME2 [Lalazissis *et al.* 2005], and TW [Typel & Wolter 1999]. The considered SHF models are the SKa, SKb [Kohler 1976], SkI2, SkI3, SkI4, SkI5 [Reinhard & Flocard 1995], SkI6 [Nazarewicz *et al.* 1996], Sly2, Sly9 [Chabanat 1995], Sly230a [Chabanat *et al.* 1997], Sly4 [Chabanat *et al.* 1998], SkMP [Bennour *et al.*

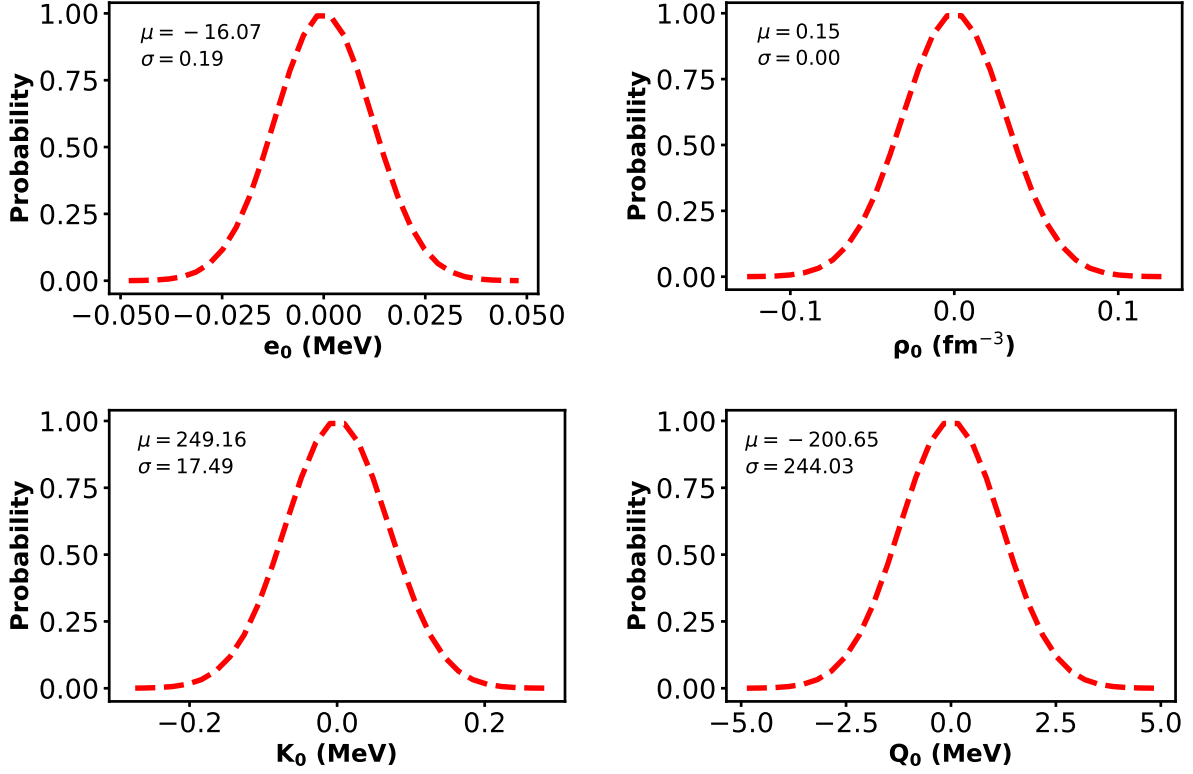


Figure 4.1: Probability distributions of energy per nucleon e_0 , saturation density (ρ_0), incompressibility coefficient (K_0) and skewness parameter (Q_0) corresponding to the symmetric nuclear matter obtained for a representative set of RMF and SHF models. The values of mean (μ) and the standard deviations (σ) for each of the NMP is also given. The NMPs as displayed along the abscissa are obtained by appropriate transformation so that the spread in their values can be compared. (see text for details).

1989], SKOp [Reinhard 1999], KDE0V1 [Agrawal *et al.* 2005], SK255, SK272 [Agrawal *et al.* 2003], Rs [Friedrich & Reinhard 1986], BSk20, BSk21 [Goriely *et al.* 2010], BSk22, BSk23, BSk24, BSk25, and BSk26 [Goriely *et al.* 2013]. The values of the nuclear matter properties, such as, K_0 , Q_0 , M_0 , J_0 , L_0 and $K_{\text{sym},0}$ vary over a wide range for our representative set of EOSs as can be seen from Table 4.1 and 4.2 for RMF and SHF models, respectively. Further details of the models can be found in [Alam *et al.* 2016] and references therein.

In Fig. 4.1, we plot the distributions of e_0 , ρ_0 , K_0 and Q_0 pertaining to the symmetric nuclear matter obtained using the models listed in Tables 4.1 and 4.2. Similar plots for J_0 , L_0 and $K_{\text{sym},0}$ are shown in Fig. 4.2. The mean (μ) and the standard deviation (σ) for each of the NMPs are indicated in their respective plots. For the comparison of the spread in the values of these nuclear matter parameters relative to each other, their values in the figures are transformed as $\frac{x-\mu}{\mu}$, where, x denotes a NMP. It is evident that the values of e_0 , ρ_0 and K_0 are better constrained relative to other nuclear matter

Table 4.1: The nuclear matter properties for a representative set of RMF models calculated at the saturation density ρ_0 . The quantities listed below are the energy per nucleon e_0 , incompressibility coefficient (K_0), skewness parameter (Q_0) for the symmetric nuclear matter. The symmetry energy coefficient (J_0), its slope (L_0) and the curvature ($K_{\text{sym},0}$) determining the density dependence of the symmetry energy.

Model	ρ_0 (fm^{-3})	e_0 (MeV)	K_0 (MeV)	Q_0 (MeV)	M_0 (MeV)	J_0 (MeV)	L_0 (MeV)	$K_{\text{sym},0}$ (MeV)
BSR2	0.149	-16.03	240	-52.1	2829	31.4	62.2	-3.4
BSR3	0.15	-16.09	230.6	-119.4	2648	32.6	70.5	-7.8
BSR6	0.149	-16.13	235.9	-11.4	2820	35.4	85.6	-47.8
DD2	0.149	-16.02	242.2	167.4	3076	31.7	55	-93.4
DDH δ	0.153	-16.25	240.2	-539.8	2343	25.6	48.6	80.7
DDH δ Mod	0.153	-16.25	240.2	-539.8	2343	31.9	57.5	80.3
DDME1	0.152	-16.23	243.9	316.2	3249	33.1	55.4	-101.3
DDME2	0.152	-16.14	251.3	479	3493	32.3	51.3	-87.5
FSU2	0.15	-16.28	237.8	-156.1	2698	37.6	112.7	25.4
GM1	0.153	-16.3	300.1	-215.1	3387	32.5	93.9	18
NL3	0.148	-16.25	271.6	205.5	3464	37.4	118.5	100.9
NL3 $\sigma\rho4$	0.148	-16.25	271.6	205.5	3464	33	68.3	-26.8
NL3 $\sigma\rho6$	0.148	-16.25	271.6	205.5	3464	31.5	55.4	25
NL3 $\omega\rho02$	0.148	-16.25	271.6	205.5	3464	33.1	68.2	-53.1
NL3 $\omega\rho03$	0.148	-16.25	271.6	205.5	3464	31.7	55.3	-7.5
TM1	0.145	-16.26	281.2	-286.3	3088	36.9	110.8	33.6
TM1-2	0.145	-16.26	281.2	-199.3	3175	36.9	111.4	41.9
TW	0.153	-16.25	240.2	-539.8	2343	32.8	55.3	-124.8

Table 4.2: Same as table 4.1, but , for SHF models.

Model	ρ_0 (fm ⁻³)	e_0 (MeV)	K_0 (MeV)	Q_0 (MeV)	M_0 (MeV)	J_0 (MeV)	L_0 (MeV)	$K_{\text{sym},0}$ (MeV)
SKa	0.155	-15.99	263.2	-300.3	2858	32.91	74.62	-78.46
SKb	0.155	-16	263	-300.3	2856	23.88	47.6	-78.5
SkI2	0.1575	-15.77	241	-340	2552	33.4	104.3	70.7
SkI3	0.1577	-15.98	258.2	-303.7	2795	34.83	100.5	73
SkI4	0.16	-15.95	247.95	-329	2646	29.5	60.39	-40.56
SkI5	0.156	-15.85	255.8	-302.1	2768	36.64	129.3	159.5
SkI6	0.159	-15.89	248.17	-327.8	2650	29.9	59.24	-46.77
Sly2	0.161	-15.99	229.92	-370.3	2389	32	47.46	-115.13
Sly230a	0.16	-15.99	229.9	-364.2	2394	31.99	44.3	-98.3
Sly4	0.159	-15.97	230	-362.9	2397	32.04	46	-119.8
Sly9	0.151	-15.8	229.84	-355.6	2402	31.98	54.86	-81.42
SkMP	0.157	-15.56	230.87	-342.7	2428	29.89	70.31	-49.82
SKOp	0.16	-15.75	222.36	-390.8	2277	31.95	68.94	-78.82
KDE0V1	0.165	-16.23	227.54	-384.9	2346	34.58	54.69	-127.12
SK255	0.157	-16.33	254.96	-350.2	2709	37.4	95	-58.3
SK272	0.155	-16.28	271.55	-305.2	2953	37.4	91.7	-67.8
Rs	0.158	-15.53	236.7	-348.3	2492	30.58	85.7	-9.1
Bsk20	0.16	-16.08	241.4	-282.1	2615	30	37.4	-136.5
Bsk21	0.158	-16.05	245.8	-274.1	2676	30	46.6	-37.2
Bsk22	0.1578	-16.09	245.9	-275.4	2675	32	68.5	13
Bsk23	0.1578	-16.07	245.7	-274.9	2674	31	57.8	-11.3
Bsk24	0.1578	-16.05	245.5	-274.4	2672	30	46.4	-37.6
Bsk25	0.1587	-16.03	236	-316.3	2516	29	36.9	-28.5
Bsk26	0.1589	-16.06	240.8	-282.8	2607	30	37.5	-135.6

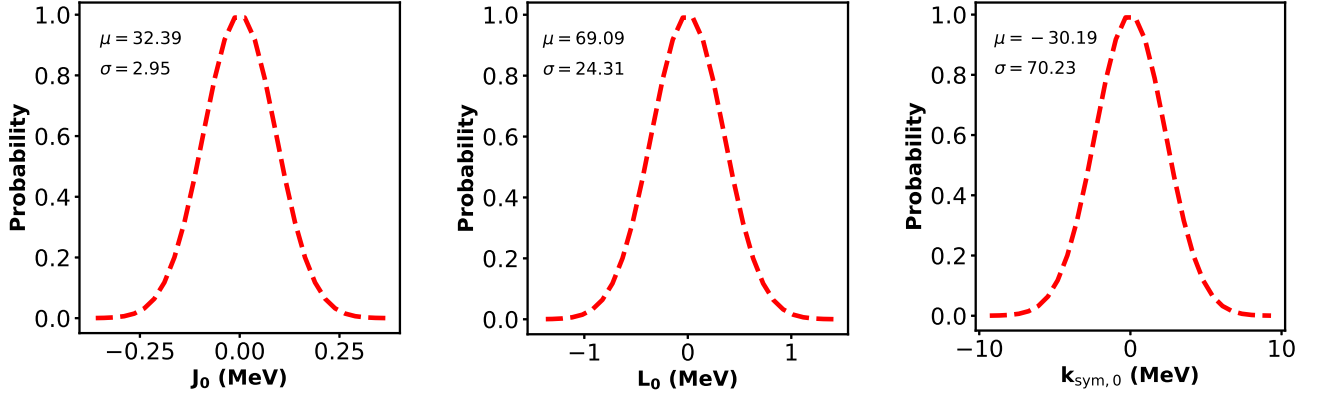


Figure 4.2: Same as Fig. 4.1, but, for symmetry energy coefficient (J_0), its slope (L_0) and the curvature ($K_{\text{sym},0}$) which determine the density dependence of the symmetry energy coefficient.

parameters. The values of Q_0 , L_0 and $K_{\text{sym},0}$ are poorly constrained. The later quantities are crucial in determining the behavior of the EOS for the asymmetric nuclear matter. In what follows, we shall demonstrate how the accurate knowledge of tidal deformability for the neutron stars are essential to constrain these NMPs which would enable one to understand the behaviour the EOS for the asymmetric nuclear matter.

As the mass of the stars in the GW170817 binary is $1.6 M_\odot$ or smaller, we only consider nucleonic degrees of freedom. However, a NS with a mass of $1.6 M_\odot$ could have non-nucleonic degrees of freedom [Dhiman *et al.* 2007, Fortin *et al.* 2017].

The EOSs considered for all the models are consistent with the observational constraint provided by the existence of $2 M_\odot$ NS [Alam *et al.* 2016, Fortin *et al.* 2016]. Moreover, the considered SHF models do not become acausal for masses below $2 M_\odot$. We have taken unified inner-crust core EOS for all the models [Fortin *et al.* 2016] and the EOS of Baym-Pethick-Sutherland [Baym *et al.* 1971] is used for the outer crust.

In Fig. 4.3, we plot for NS matter the variation of pressure (p) with the energy density (ε) in the left panel and the variation of $dp/d\varepsilon$ with the baryon number density in the right panel for our representative set of models. The black circles denote the central density corresponding to the NS maximum mass for each EOS. The dashed line indicates the causality limit (i.e. $dp/d\varepsilon = 1$). The values of $dp/d\varepsilon$ for SHF models are larger at higher densities ($\rho \gg \rho_0$) than those for the RMF models. The maximum mass NS configurations of all models studied are within the causality limit except for BSk20 and BSk26 EOSs, which are marginally acausal.

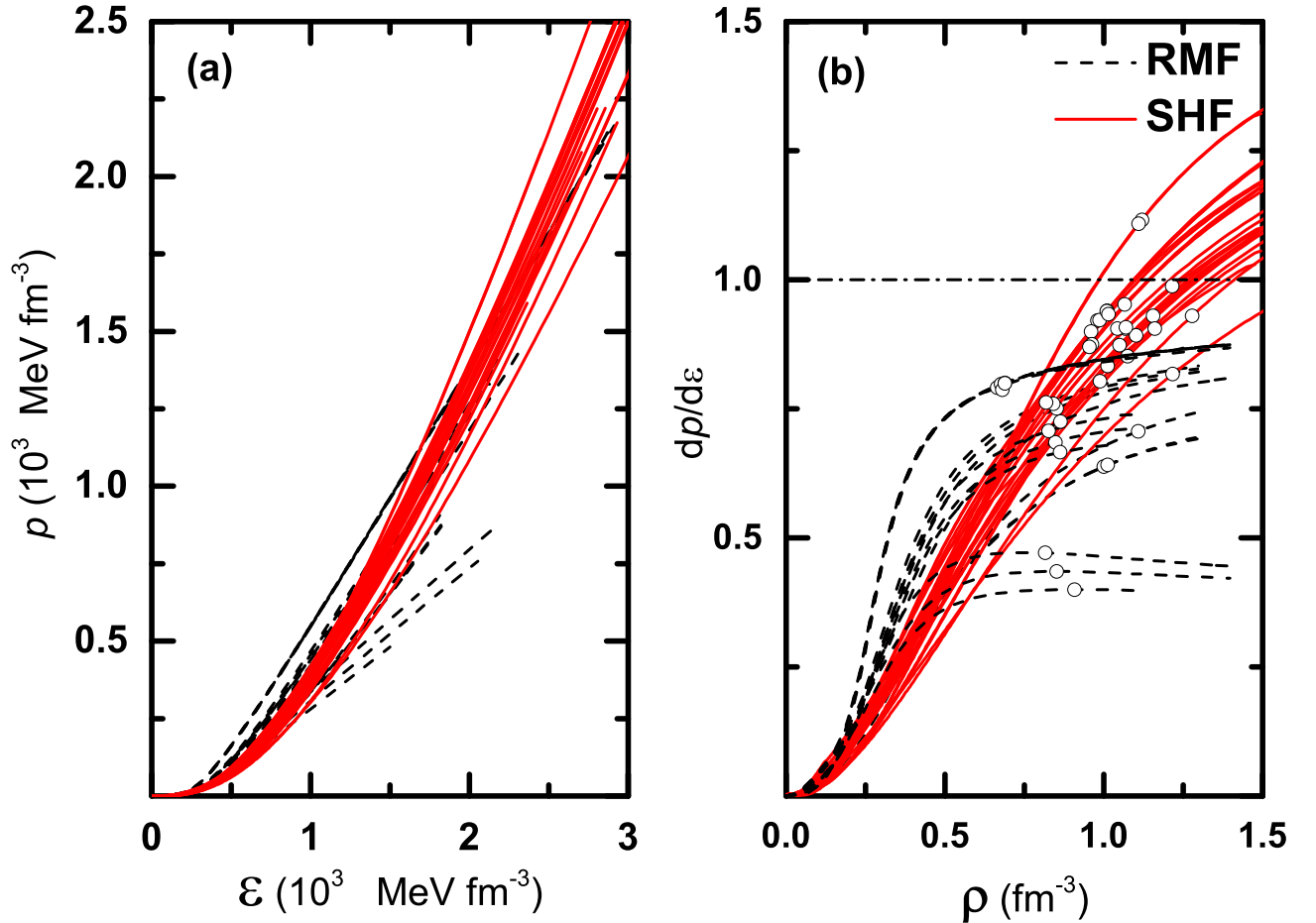


Figure 4.3: Plots for the (a) pressure p as a function of the energy density, and (b) $dp/d\varepsilon$ as a function of the baryonic number density for beta equilibrated NS matter obtained using a representative set of RMF (black dashed lines) and SHF models (red lines). The circles in right panel correspond to the central densities and the slopes $dp/d\varepsilon$ at the maximum NS mass for each of the EOS. The BSk20 and BSk26 EOSs are marginally acausal at the NS maximum masses $\sim 2.2 M_{\odot}$ [Alam *et al.* 2016, Fortin *et al.* 2016].

4.3 Tidal deformability and Love Number

One of the main focus of the present work is to study the sensitivity of the tidal deformability to the properties of nuclear matter at saturation density. To facilitate our discussions in the next section, in Fig. 4.4 the dimensionless tidal deformability Λ (left) and tidal Love number k_2 (right) obtained for our set of EOSs are plotted as a function of the NS mass. The values of k_2 show a noticeable spread across the various models. For instance, at $1.4 M_{\odot}$, the values of k_2 are in the range of 0.07 to 0.11. For the smaller masses the spread in k_2 is larger for the SHF models, but for the larger masses RMF models give on average larger values of k_2 . One can also see from Fig. 1 of reference [Alam *et al.* 2016] that the RMF models predict larger radii, in particular, for large NS masses. Consequently, the

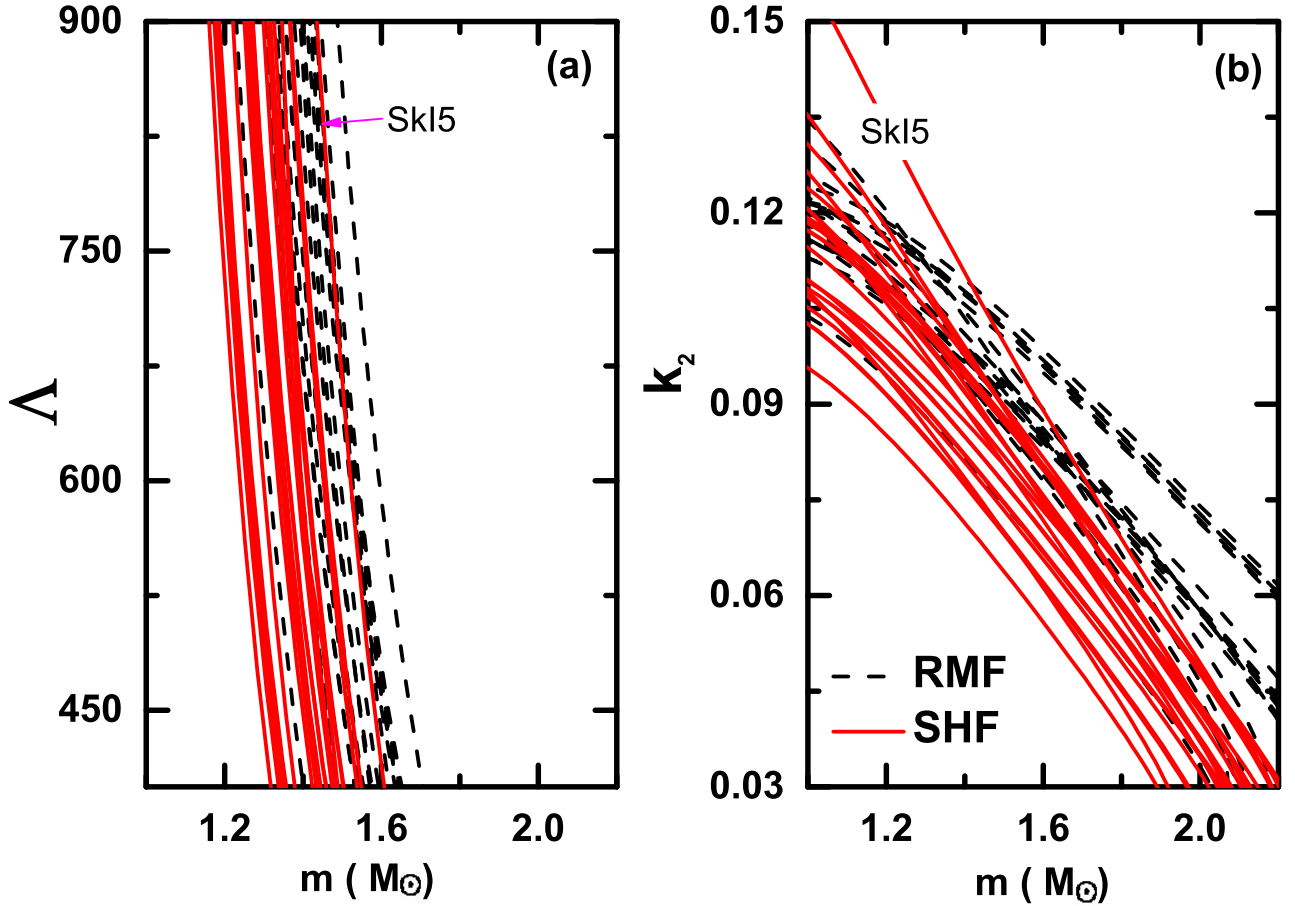


Figure 4.4: (a) Tidal deformability Λ and (b) the Love number k_2 as a function of the NS mass (m) for a representative set of relativistic and non-relativistic models. The SHF model, SkI5, displays markedly different behavior for Λ as well as for k_2 .

parameter Λ tends to be larger for the RMF models than for the SHF models. In the following, we will examine the dependence of Λ on both k_2 and R in detail.

In Fig. 4.5 we plot the tidal deformabilities in the phase space of Λ_1 and Λ_2 associated, respectively, with the high-mass m_1 and the low-mass m_2 components of the binary, for all the considered RMF and SHF models. The curves corresponding to every EOS are obtained by varying the high mass (m_1) independently in the range $1.365 < m/M_\odot < 1.60$ obtained for GW170817 whereas the low mass (m_2) is determined by keeping the chirp mass $\mathcal{M} = (m_1 m_2)^{3/5} (m_1 + m_2)^{-1/5}$ fixed at the observed value $1.188 M_\odot$ [Abbott *et al.* 2017a]. The dot-dot-dashed and the dot lines represent, respectively, the 90% and 50% confidence limits obtained from the GW170817 for the low spin priors. One can note that the 90% confidence limit suggests that SkI5 and the family of models NL3X and TM1X are ruled out except for NL3 $\omega\rho$ 03. For the SkI5 the values of M_0 and L_0 are 2745 MeV and 129

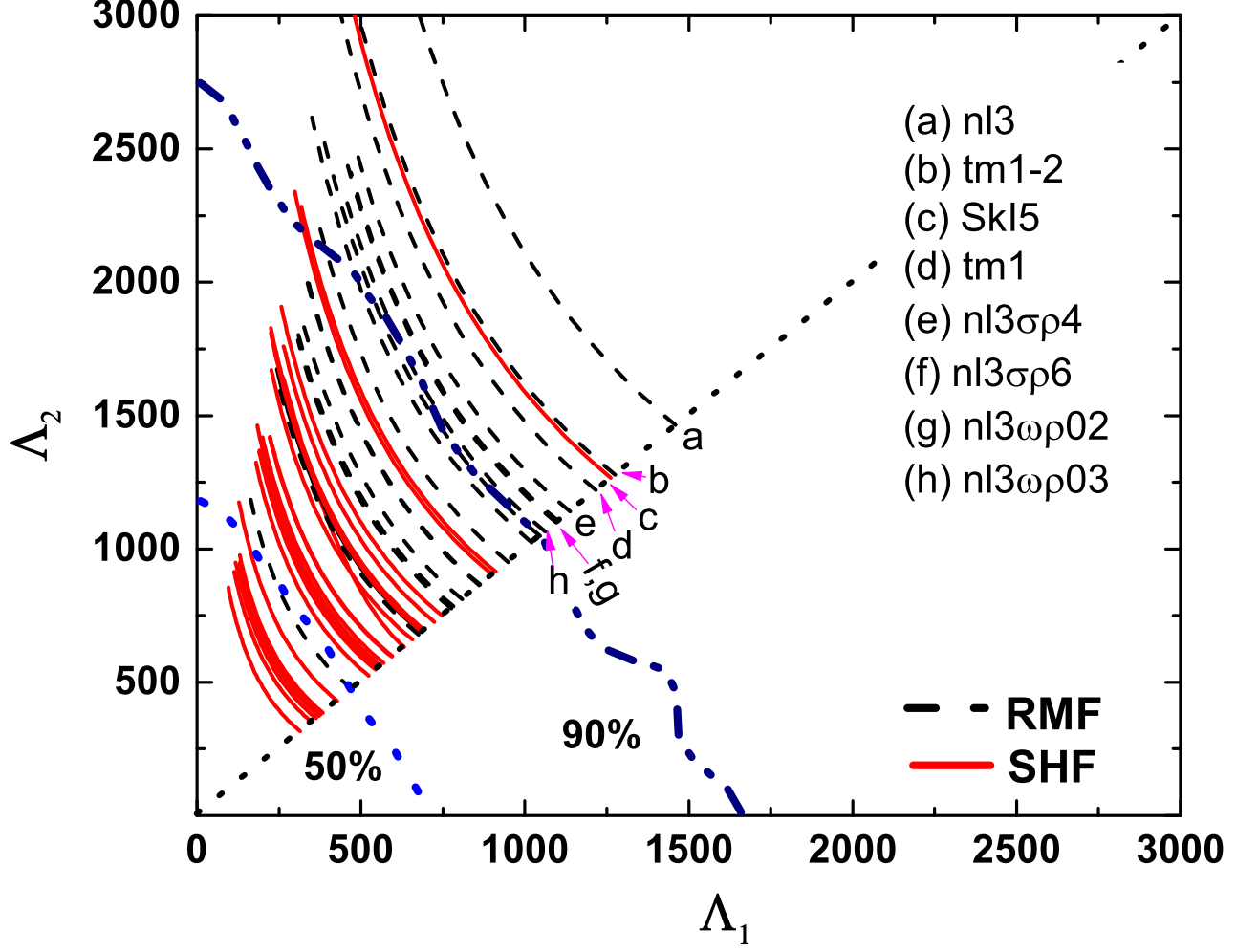


Figure 4.5: Tidal deformability parameters for the case of high mass (Λ_1) and low mass (Λ_2) components of the observed GW170817. The 90% (dot-dot-dashed) and 50% (dot) confidence lines are taken from Ref. [Abbott *et al.* 2017a] corresponding to the low spin priors.

MeV, respectively. For NL3X family the value of M_0 is larger than 3400 MeV and L_0 is in the range of 55-70 MeV except for the base model NL3. Whereas, for TM1X family the value of $M_0 \sim 3100$ MeV and $L_0 \sim 110$ MeV. This indicates that very high value of M_0 and/or L_0 may not be favored by GW170817.

4.4 Nuclear matter parameters and astrophysical observable

In the present section, we study the correlations of the tidal deformability Λ , the Love number k_2 and the radius of NSs R with various nuclear matter parameters. We consider the constraints from the properties of the binary neutron star that satisfy the low spin prior [Abbott *et al.* 2017a]. In our

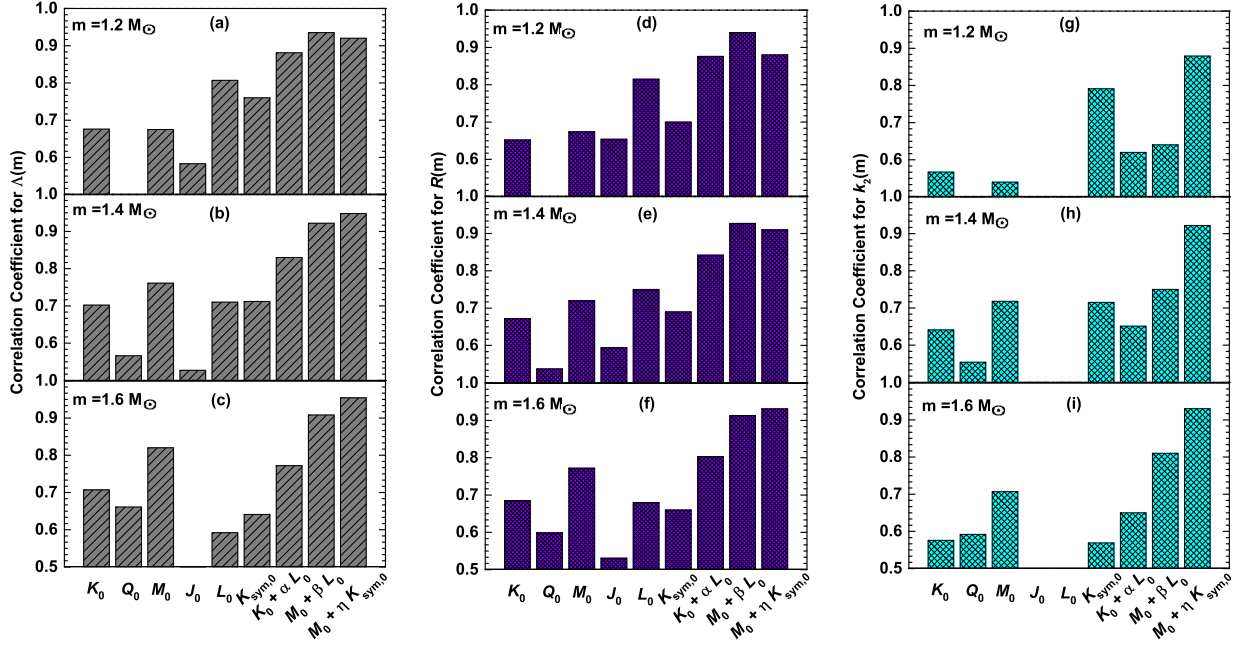


Figure 4.6: Correlation coefficients \mathcal{R} for (a-c) the tidal deformability Λ , (d-f) the radius R , and (g-i) the Love number k_2 with different individual nuclear matter parameters as well as with some selected linear combinations of them obtained for the NS masses $1.2 M_\odot$ (top), $1.4 M_\odot$ (middle) and $1.6 M_\odot$ (bottom). Results are plotted only for the cases with $\mathcal{R} > 0.5$ (see tables 4.3 and 4.4 for details).

analysis, the correlation between a pair of quantities is quantified in terms of Pearson's correlation coefficient, denoted as \mathcal{R} [Brandt 1997]. The magnitude of \mathcal{R} is at most unity indicating that the pair of quantities is completely correlated to each other. For $|\mathcal{R}| < 0.5$, the correlations are usually said to be weak. We calculate the values of the coefficients for the correlation of Λ , k_2 and R with the nuclear matter saturation parameters K_0 , Q_0 , M_0 , J_0 , L_0 , $K_{\text{sym},0}$ and with several linear combinations of two parameters, in particular with $K_0 + \alpha L_0$, $M_0 + \beta L_0$ and $M_0 + \eta K_{\text{sym},0}$. The values of α , β and η are obtained so that, for each NS mass, they yield optimum correlations. Our correlation systematics is determined for NS masses in the range of $1.2 - 1.6 M_\odot$, since, for the low spin prior analysis, these masses are close to the ones involved in the GW170817 event. The results for the values of the \mathcal{R} obtained for the correlation of Λ , k_2 and R with individual nuclear matter parameters are presented in Table 4.3. The Table 4.4 contains the results obtained using the linear combinations of the nuclear matter parameters. The Fig. 4.6 is the pictorial representation of the results presented in Tables 4.3 and 4.4. Only the cases with the correlation coefficients $\mathcal{R} > 0.5$ are displayed. We see from Table 4.3 that for most of the cases, individual EOS parameters seem to be weakly or moderately correlated with the Λ , k_2 and R . Exceptionally, the Λ and R are strongly correlated with the individual nuclear

Table 4.3: The Pearson correlation coefficients, \mathcal{R} obtained for the correlations between various NS and nuclear matter properties. The values of tidal deformability Λ , radius R and the Love number k_2 are evaluated for the NS masses $1.2 - 1.6 M_\odot$. The nuclear matter incompressibility K_0 , the skewness Q_0 , slope of incompressibility M_0 , symmetry energy J_0 , slope of symmetry energy L_0 and the curvature parameters $K_{\text{sym},0}$.

	K_0	Q_0	M_0	J_0	L_0	$K_{\text{sym},0}$
$\Lambda_{1.2}$	0.68	0.46	0.68	0.58	0.81	0.76
$\Lambda_{1.3}$	0.69	0.51	0.72	0.56	0.76	0.74
$\Lambda_{1.4}$	0.70	0.57	0.76	0.53	0.71	0.71
$\Lambda_{1.5}$	0.71	0.62	0.80	0.50	0.65	0.68
$\Lambda_{1.6}$	0.71	0.66	0.82	0.46	0.59	0.64
$R_{1.2}$	0.65	0.48	0.67	0.65	0.82	0.70
$R_{1.3}$	0.66	0.51	0.70	0.62	0.79	0.70
$R_{1.4}$	0.67	0.54	0.72	0.59	0.75	0.69
$R_{1.5}$	0.68	0.57	0.75	0.56	0.72	0.68
$R_{1.6}$	0.68	0.60	0.77	0.53	0.68	0.66
$k_{2,1.2}$	0.57	0.34	0.54	-0.03	0.44	0.79
$k_{2,1.3}$	0.62	0.47	0.65	0.02	0.43	0.76
$k_{2,1.4}$	0.64	0.55	0.72	0.05	0.39	0.72
$k_{2,1.5}$	0.65	0.63	0.77	0.08	0.36	0.66
$k_{2,1.6}$	0.58	0.59	0.71	0.06	0.26	0.57

matter parameters L_0 and M_0 for the NS masses $1.2 M_\odot$ and $1.6 M_\odot$, respectively. Let us point out that the correlation between the radius of low mass NSs and the neutron skin of ^{208}Pb , which is itself correlated with L_0 , was first discussed in [Horowitz & Piekarewicz 2001]. It is seen from Table 4.4, the Λ and R are strongly correlated with $M_0 + \beta L_0$ and $M_0 + \eta K_{\text{sym},0}$ over a wide range of NS masses considered: the values of \mathcal{R} of the order of 0.9. The Love number k_2 is strongly correlated with $M_0 + \eta K_{\text{sym},0}$. The values of α , β and η decrease monotonically with the NS mass. This indicates that the density dependence of symmetry energy is less important in determining the values of Λ and R at higher NS masses. The mass dependence of α , β and η is discussed in some detail in the Appendix A, where, in particular, an exponential dependence of these parameters on the NS mass is proposed. As

Table 4.4: The values of the coefficients \mathcal{R} obtained for the correlations of Λ , R and k_2 with various linear combinations of EOS parameters. The calculations are performed for the NS masses $1.2 - 1.6 M_\odot$.

	$K_0 + \alpha L_0$		$M_0 + \beta L_0$		$M_0 + \eta K_{\text{sym},0}$	
	\mathcal{R}	α	\mathcal{R}	β	\mathcal{R}	η
$\Lambda_{1.2}$	0.88	1.16	0.94	21.22	0.92	6.34
$\Lambda_{1.3}$	0.86	0.93	0.93	17.05	0.94	5.55
$\Lambda_{1.4}$	0.83	0.74	0.92	13.68	0.95	4.83
$\Lambda_{1.5}$	0.80	0.59	0.92	10.91	0.95	4.18
$\Lambda_{1.6}$	0.77	0.45	0.91	8.54	0.95	3.62
$R_{1.2}$	0.88	1.33	0.94	21.75	0.88	5.64
$R_{1.3}$	0.86	1.14	0.93	19.07	0.90	5.33
$R_{1.4}$	0.84	0.98	0.93	16.62	0.91	5.00
$R_{1.5}$	0.82	0.84	0.92	14.38	0.92	4.65
$R_{1.6}$	0.80	0.71	0.91	12.32	0.93	4.31
$k_{2,1.2}$	0.62	0.40	0.64	11.18	0.88	9.15
$k_{2,1.3}$	0.64	0.25	0.70	7.22	0.91	6.83
$k_{2,1.4}$	0.65	0.16	0.75	4.81	0.92	5.31
$k_{2,1.5}$	0.66	0.10	0.79	3.34	0.93	4.20
$k_{2,1.6}$	0.65	0.04	0.81	2.14	0.93	3.52

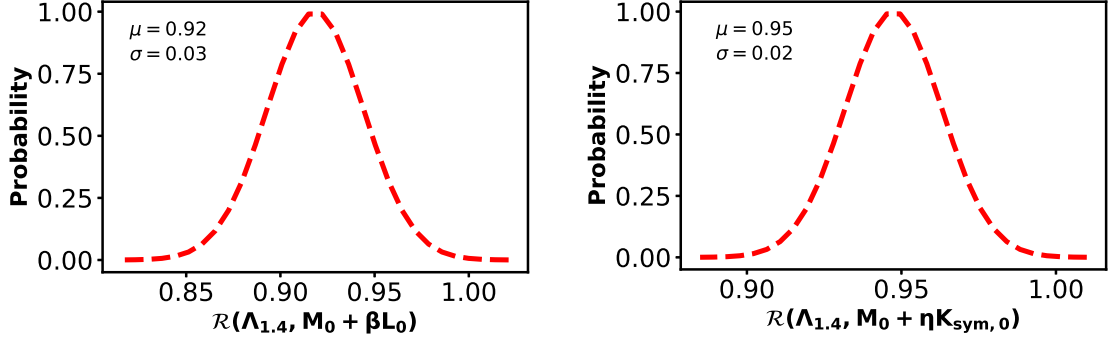


Figure 4.7: The probability distribution for the correlations of $\Lambda_{1.4}$ with $M_0 + \beta L_0$ (left) and $M_0 + \eta K_{\text{sym},0}$ (right) calculated using bootstrap method (see text for details).

an example, in Fig.4.8 we plot $M_0 + \beta L_0$ and $M_0 + \eta K_{\text{sym},0}$ as a function of k_2 and Λ for $1.4 M_\odot$ NS. Since, $\Lambda_{1.4}$ is not very well correlated individually with M_0 , L_0 and $K_{\text{sym},0}$, its strong correlation with $M_0 + \beta L_0$ and $M_0 + \eta K_{\text{sym},0}$ is of particular importance. In Fig 4.7 we plot the probability distribution for the correlations of $\Lambda_{1.4}$ with $M_0 + \beta L_0$ and $M_0 + \eta K_{\text{sym},0}$ calculated using bootstrap method. The bootstrap method is a statistical tool to build a sufficiently large number of data set by re-sampling the original one with random replacement. It was introduced by Efron in 1979 [Efron 1979]. It is based on a simple assumption that the data-set of independent observations contains information on its parent distribution. To evaluate the confidence intervals of any estimated quantity from the data set, one can generate a large number of data sets and find the distribution of the estimated quantity. It has been successfully introduced in nuclear physics [Pastore 2019]. The values of the correlation coefficients given in the figure are obtained with the entire set of RMF and SHF models as presented in section 4.2. In order to check the model dependence of the correlations, we have determined the correlation coefficients for the sets of RMF and SHF models separately. The results are given in Table 4.4 which indicate that the model dependence is only marginal.

The result for the correlations among k_2 , Λ and various nuclear matter properties as depicted in Fig. 4.8 may be understood as follows. In Ref. [Alam *et al.* 2016], it was shown that the NS radius R is strongly correlated with a linear combination of M_0 and L_0 over a wide range of NS masses. This was attributed to the dependence of the pressure on M_0 and L_0 and to the empirical relation of the star radius with the pressure at several reference densities, e.g. $R \times p(\rho)^{-1/4} = \text{constant}$ for $\rho \sim 1.5 \rho_0$ and NS masses, $1 - 1.4 M_\odot$, irrespective of the model [Lattimer & Prakash 2001].

The solid lines in Fig. 4.8 are obtained using linear regression. These linear regressions yield,

$$\frac{M_0}{\text{MeV}} + 13.68 \frac{L_0}{\text{MeV}} = (2.09 \pm 0.14) \Lambda_{1.4} + (2383.12 \pm 96.42), \quad (4.1)$$

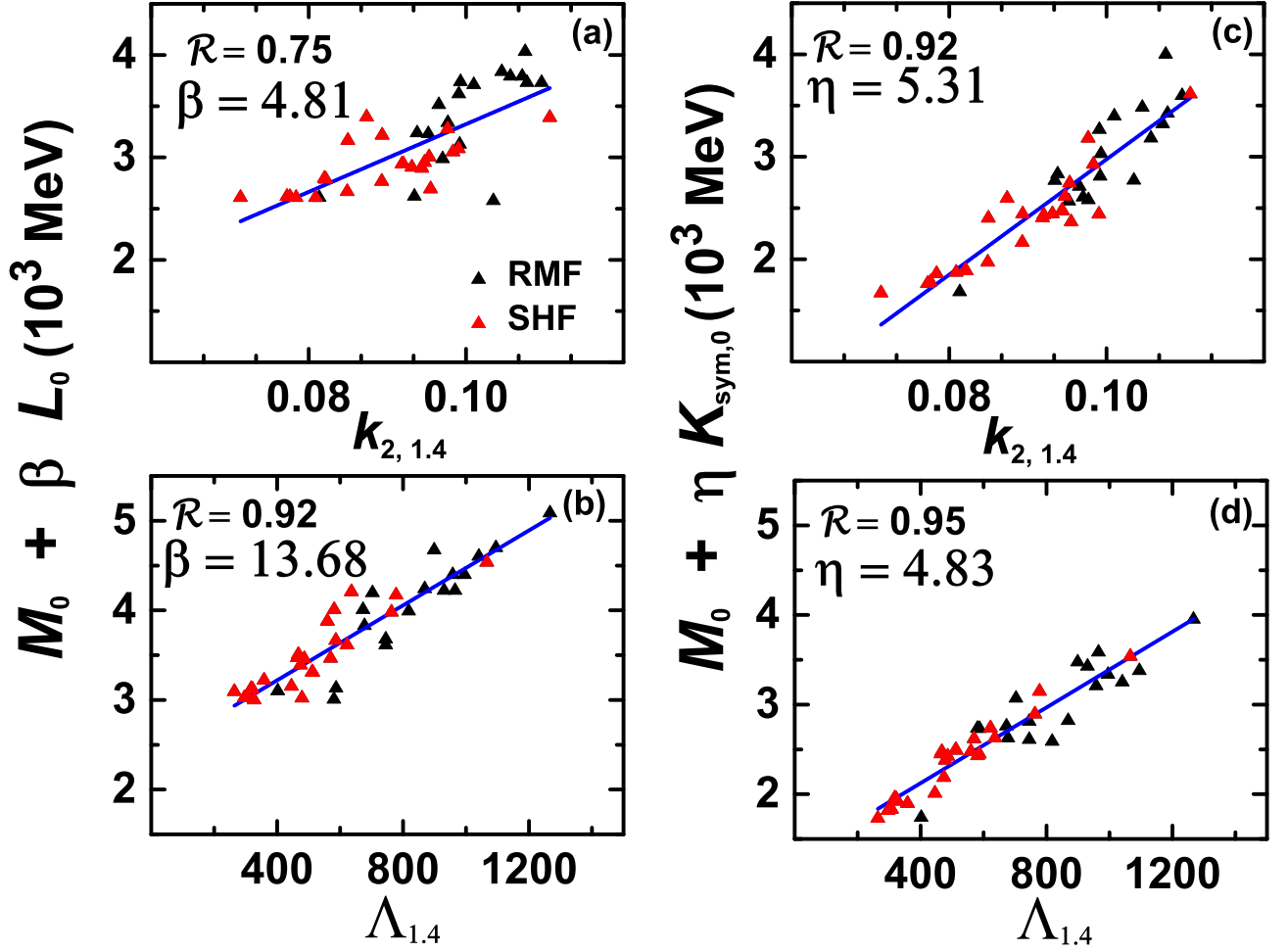


Figure 4.8: (a-b) The $M_0 + \beta L_0$ and (c-d) $M_0 + \eta K_{\text{sym},0}$ versus the tidal Love number $k_{2,1.4}$ (top panels) and dimensionless tidal deformability $\Lambda_{1.4}$ (bottom panels) for a $1.4 M_\odot$ NS, using a set of RMF and SHF models.

$$\frac{M_0}{\text{MeV}} + 4.83 \frac{K_{\text{sym},0}}{\text{MeV}} = (2.11 \pm 0.11) \Lambda_{1.4} + (1278.13 \pm 77.76). \quad (4.2)$$

We need to know the value of $\Lambda_{1.4}$ in order to exploit the correlations, as presented in Fig. 4.8, to estimate the values of nuclear matter properties at the saturation density.

The GW170817 event provides the upper bound on $\tilde{\Lambda}$ as defined by Eq.(2.39). For the low spin prior we have to consider masses such that $q = m_2/m_1 > 0.7$. We have calculated the $\tilde{\Lambda}$ using neutron star masses $m = 1.4, 1.17, 1.6 M_\odot$, which correspond to the canonical mass and the lower and upper mass limits covered by the low spin prior analysis. The neutron star binary companion mass is determined from the chirp mass $\mathcal{M} = 1.188 M_\odot$: $m = 1.17, 1.6 M_\odot$ are, respectively, m_2 and m_1 corresponding to $q = 0.7$; for the canonical mass we get $q = 0.95$ with $m_1 = 1.40 M_\odot$ and $m_2 = 1.33 M_\odot$. Fig. 4.9 shows the variation of $\Lambda_{1.4}$ as a function of $\tilde{\Lambda}$ for all the RMF and SHF models. The correlation between this two quantities is very strong which enables us to express $\Lambda_{1.4}$

Table 4.5: Values for the correlations coefficients for $\Lambda_{1.4}$ and $k_{2,1.4}$ with $M_0 + \beta L_0$ and $M_0 + \eta K_{\text{sym},0}$ obtained separately for the RMF and SHF models. The values of the correlation coefficients corresponding to all the models (ALL) are also listed.

	$M_0 + \beta L_0$			$M_0 + \eta K_{\text{sym},0}$		
	RMF	SHF	ALL	RMF	SHF	ALL
$\Lambda_{1.4}$	0.92	0.90	0.92	0.88	0.97	0.95
$k_{2,1.4}$	0.72	0.68	0.75	0.89	0.91	0.92

in terms of $\tilde{\Lambda}$ as $\Lambda_{1.4} = 0.859 \times \tilde{\Lambda}$. Similar studies were performed for the NS with mass $m = 1.17$ and $1.6 M_\odot$ and we have obtained $\Lambda_{1.17} = 2.452 \times \tilde{\Lambda}$ and $\Lambda_{1.6} = 0.379 \times \tilde{\Lambda}$ with an equally strong correlation. These relations should be compared with the prediction from the expression proposed in [De et al. 2018]

$$\Lambda_1 = \frac{13}{16} \tilde{\Lambda} \frac{q^2(1+q)^4}{12q^2 - 11q + 12}, \quad (4.3)$$

obtained by replacing

$$\Lambda_2 = q^{-6} \Lambda_1 \quad (4.4)$$

in the Eq.(2.39) for $\tilde{\Lambda}$. Eq. (4.4) was obtained assuming that the radii of the stars with masses $1.17 < m < 1.6 M_\odot$ are the same. Using expression (4.3), we get relations between Λ_i and $\tilde{\Lambda}$ for $m_i = 1.17, 1.4, 1.6 M_\odot$ that coincide with ours within the first two digits. We have checked that, in most of the cases, for our set of models the difference between the radii of stars with a mass in that interval is not larger than ~ 0.2 km.

4.5 Constraining M_0 and $K_{\text{sym},0}$

In the following, we want to constraint M_0 and $K_{\text{sym},0}$. We will consider the limits imposed on $\Lambda_{1.4}$. This choice is justified because according to the analysis done in [Abbott et al. 2018, De et al. 2018] the limits obtained for $\tilde{\Lambda}$ are q dependent, and, in particular, in [De et al. 2018] if the double neutron star or galactic neutron star distributions are considered the maximum $\tilde{\Lambda}$ value is obtained, respectively, for $q > 0.9$ ($q > 0.8$). For the lower limit the results of [Perego et al. 2017, Radice et al. 2018] were determined for $q > 0.85$. A lower bound of $\Lambda_{1.4} > 344$ is set by the UV/optical/infrared counterpart of GW170817 that imposes $\tilde{\Lambda} > 400$ [Perego et al. 2017, Radice et al. 2018]. Similarly, the gravitational-wave observations set an upper bound $\Lambda_{1.4} < 687$ or $\Lambda_{1.4} < 859$, respectively from

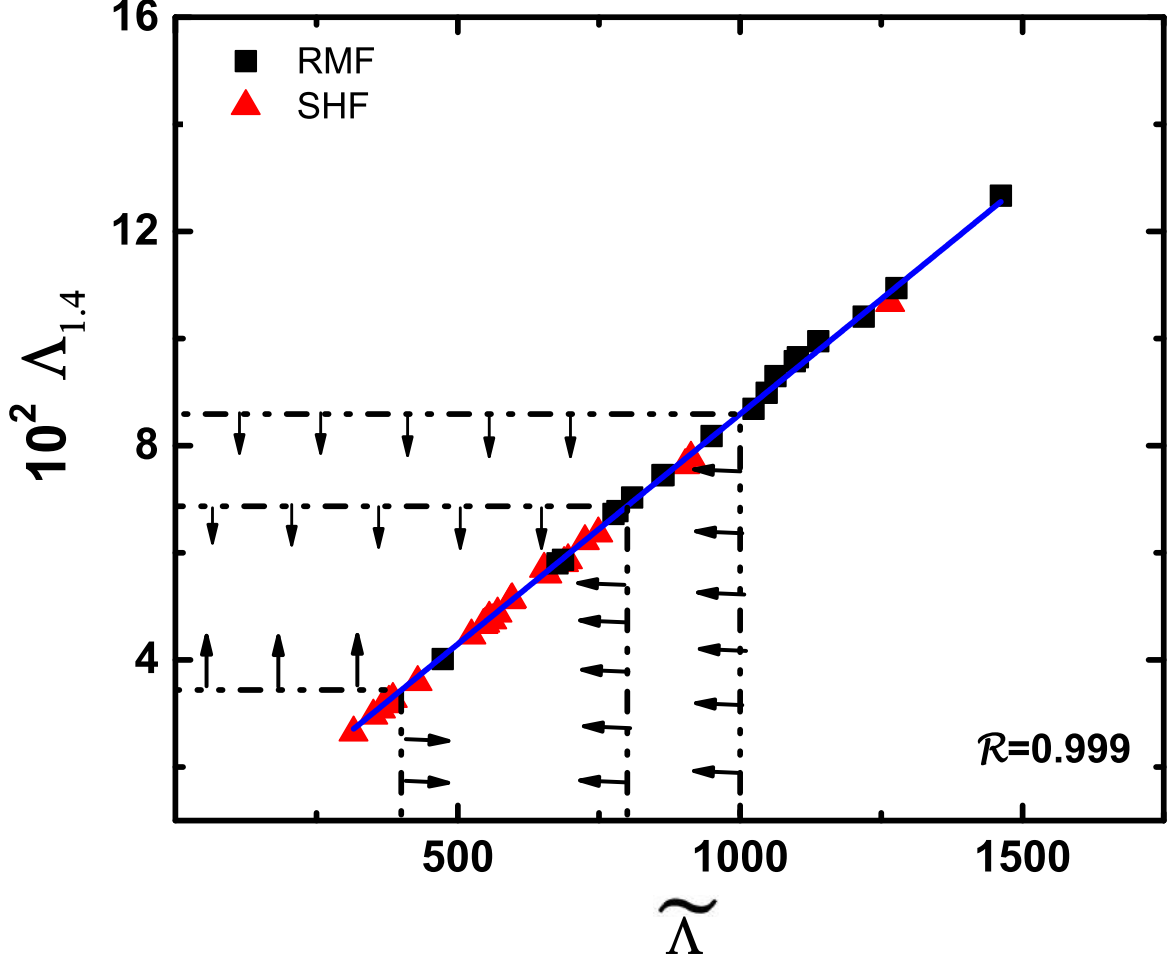


Figure 4.9: The tidal deformability $\Lambda_{1.4}$ versus the weighted average $\tilde{\Lambda}$ as defined in Eq.(2.39) for all the RMF and SHF models. The solid line represents the best fit. The arrows pointing right and up indicate the lower bounds on $\tilde{\Lambda}$ and $\Lambda_{1.4}$, respectively. The upper bounds on $\tilde{\Lambda}$ and $\Lambda_{1.4}$ are denoted by left and down arrows, respectively.

the bounds $\tilde{\Lambda} < 800$ [Abbott *et al.* 2017a] and $\tilde{\Lambda} < 1000$ [De *et al.* 2018]. In what follows, we will use these bounds on $\Lambda_{1.4}$ together with Eqs. (4.1 and 4.2) to constrain the nuclear matter properties.

In Fig. 4.10, the slope of the incompressibility coefficient at the saturation density M_0 is plotted as a function of $\Lambda_{1.4}$ for fixed values of L_0 using Eq. (4.1). The limiting values of L_0 employed in the plot correspond to $L_0 = 51 \pm 11$ MeV [Lattimer & Lim 2013]. This limit on L_0 in conjunction with the bounds on $\Lambda_{1.4}$, as discussed above, constrain the M_0 as listed in Table 4.6. As referred before the lower bound on $\tilde{\Lambda}$ set by [Radice *et al.* 2018] has several associated uncertainties, and, therefore the lower bounds obtained for M_0 and $K_{\text{sym},0}$ suffer from these uncertainties. Notice, however, that independently of the lower value of $\tilde{\Lambda}$ we always have $M_0 > 1500$ (1800) MeV according to the constraints imposed in L_0 in [Lattimer & Lim 2013] ([Oertel *et al.* 2017]). In the same table we also

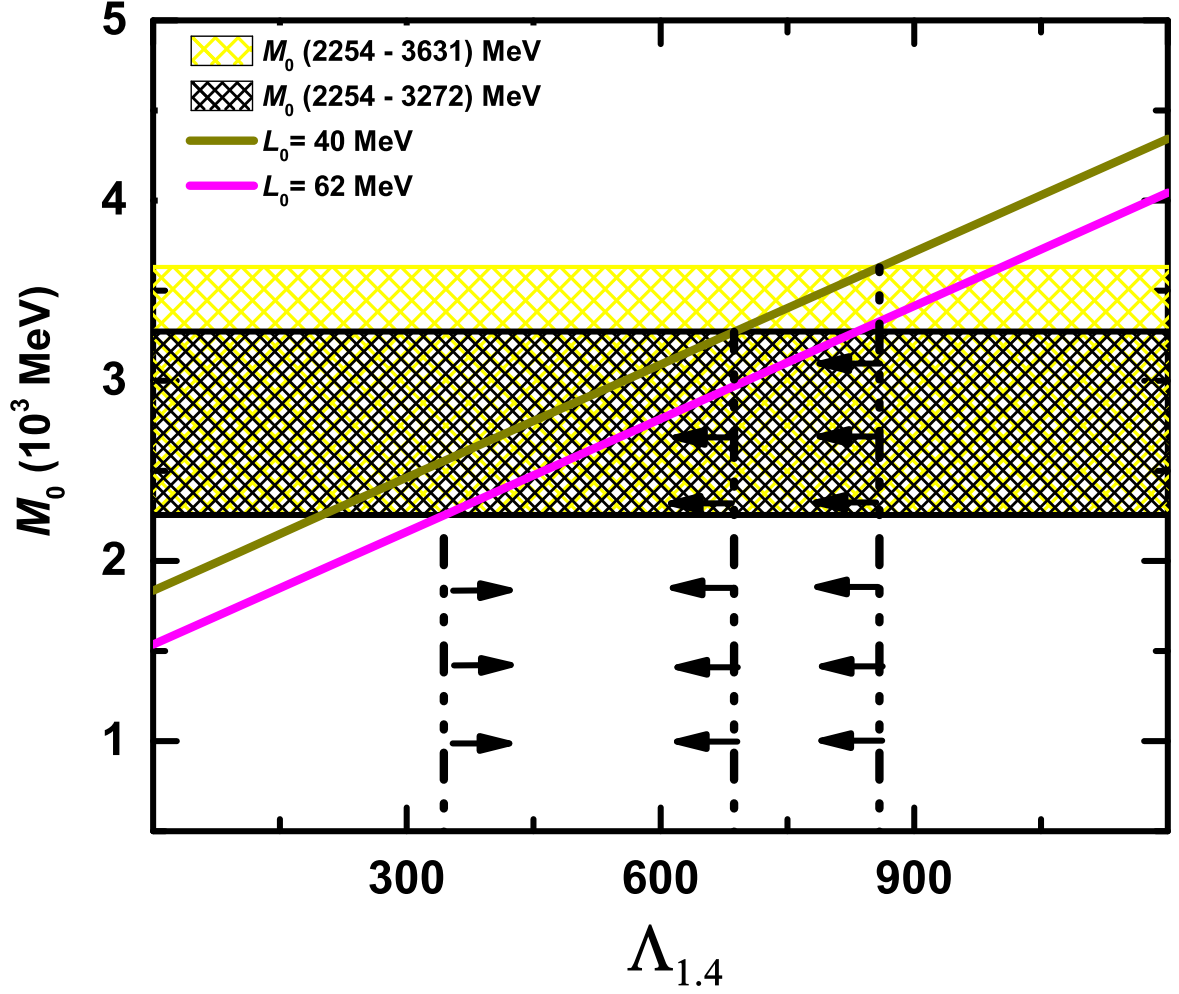


Figure 4.10: Plots for the incompressibility slope parameter M_0 versus tidal deformability $\Lambda_{1.4}$ at fixed values of symmetry energy slope parameter L_0 (solid lines) obtained using Eq.(4.1). The choices for the values of L_0 are discussed in the text. The dot-dot-dashed lines represent the bounds obtained in Fig. 4.9.

present the values of M_0 obtained for $L_0 = 58.7 \pm 28.1$ MeV [Oertel *et al.* 2017]. These values of L_0 take into account terrestrial, theoretical and observational constraints. Our values of M_0 have a reasonable overlap with the values $M_0 = (1800 - 2400)$ MeV obtained empirically in Ref. [De *et al.* 2015]. The value of M_0 in Ref. [De *et al.* 2015] was determined using a Skyrme like energy density functional by imposing the constraint on the incompressibility slope parameter at the crossing density ($\sim 0.1 \text{ fm}^{-3}$) determined from energies of the isoscalar giant monopole resonance in the ^{132}Sn and ^{208}Pb nuclei [Khan & Margueron 2013, Khan *et al.* 2012].

The above analysis is dependent on the star mass used to calculate the tidal deformability. However, it is important to notice that the contribution of M_0 to the linear combination $M_0 + \beta L_0$ is maximum for the larger star masses, so large star masses that satisfy the q constraints should be chosen.

Table 4.6: The empirical values of M_0 and $K_{\text{sym},0}$ derived for different limits on $\Lambda_{1.4}$ and L_0 . The bounds on $\Lambda_{1.4} > 344$ and $< 687(859)$ obtained from Fig. 4.9 are considered. The ranges of $L_0 = 40 - 62$ MeV and $L_0 = 30 - 86$ MeV are taken from Refs. [Lattimer & Lim 2013, Oertel *et al.* 2017].

L_0 (MeV)	$\Lambda_{1.4}$	M_0 (MeV)	$K_{\text{sym},0}$ (MeV)
40 62	344 687	2254 3272	-113 -52
	344 859	2254 3631	-112 -52
30 86	344 687	1926 3409	-141 16
	344 859	1926 3768	-140 16

Taking $\Lambda_{1.6}$ ($q = 0.7$) to constraint M_0 the upper limits would have been $\sim 5 - 10\%$ lower.

We have next considered the range of acceptable values for M_0 just determined, together with the bounds on $\Lambda_{1.4}$ and Eq. (4.2), to set also constraints on $K_{\text{sym},0}$. The results are presented in Table 4.6: the ranges $-113 < K_{\text{sym},0} < -52$ MeV are obtained for the constraints on the symmetry energy slope from [Lattimer & Lim 2013] and $-141 < K_{\text{sym},0} < 16$ MeV imposing the constraints from [Oertel *et al.* 2017]. The symmetry energy curvature is a quantity that is still not constrained experimentally. In [Mondal *et al.* 2017], the authors have obtained from the universality of the correlation structure between the different symmetry energy elements and from some well known nuclear matter properties the range $K_{\text{sym},0} = -111.8 \pm 71.3$ MeV. Our bounds discussed above are in a quite good agreement with these values.

4.6 Neutron star radius and tidal deformability

Fig. 4.11 displays the tidal Love number $k_{2,1.4}$ (top panel) and the dimensionless tidal deformability $\Lambda_{1.4}$ (bottom panel) as a function of NS radius $R_{1.4}$. It is evident from the Eq. (2.34) that the tidal deformability depends mainly on the NS radius and the Love number k_2 . The $\Lambda_{1.4}$ is expected to be strongly correlated with $R_{1.4}$ provided either k_2 is model independent or it is correlated with $R_{1.4}$. We observed from Fig. 4.4 that the value of k_2 is sensitive to the model used which might influence the correlation between $\Lambda_{1.4}$ and $R_{1.4}$. However, the $k_{2,1.4}$ is moderately correlated with $R_{1.4}$ (top panel) which ensures the persistence of the strong correlation ($\mathcal{R} = 0.98$) between $\Lambda_{1.4}$ and $R_{1.4}$ (bottom panel). The solid line in the bottom panel represent the fitted curve with equation $\Lambda_{1.4} = 9.11 \times 10^{-5} \left(\frac{R_{1.4}}{\text{km}}\right)^{6.13}$. This equation can be rewritten in a form similar to the relation obtained in [De *et al.* 2018], that expresses

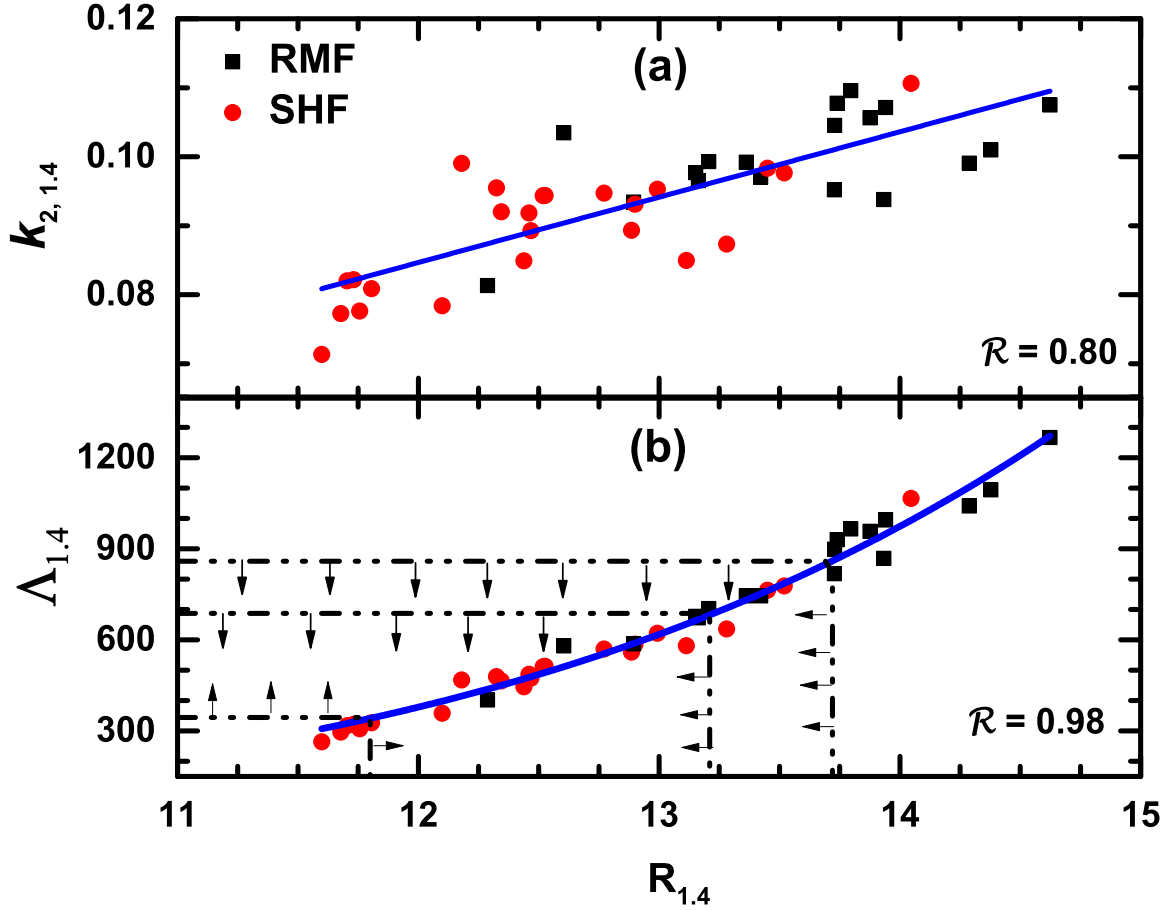


Figure 4.11: (a) The variation of tidal Love number $k_{2,1.4}$ and (b) the dimensionless tidal deformability $\Lambda_{1.4}$ with the radius $R_{1.4}$ obtained for the RMF (black squares) and SHF (red circles) models. The solid lines in the top and bottom panels are the best fitted linear and curve lines, respectively. The horizontal dot-dot-dashed lines represent the bounds obtained in Fig. 4.9.

the tidal deformability in terms of the compactness parameter of the star $\beta = Gm/(Rc^2)$,

$$\Lambda = a\beta^{-6},$$

having the exponent 6.13 instead of 6. We have verified that the exponent is mass dependent although close to 6: taking $m = 1.17 M_{\odot}$ and $m = 1.60 M_{\odot}$ the exponent is respectively, 5.84 and 6.58. In our analysis we use a set of models different from the one used in [De et al. 2018], and besides, we have only considered unified inner crust-core EOS, while in [De et al. 2018] all the EOS have a common crust EOS. These two aspects could explain some of the differences. Using the derived bounds on $\Lambda_{1.4}$, the value of $R_{1.4}$ is found to be in the range 11.82 - 13.22 (11.82 - 13.72) km for $\Lambda_{1.4}$ in the range of 344 - 687 (344 - 859). These ranges for $R_{1.4}$ lie almost within the bounds of 8-14 km and 10.5 - 13.3 km as estimated from GW170817 in Refs. [Abbott et al. 2018, De et al. 2018]. Further, our predictions are in

harmony with $R_{1.4} = 11.5 - 13.6$ km [Li & Steiner 2006] as constrained by the slope of the symmetry energy which was extracted using the terrestrial laboratory data on the isospin diffusion in heavy-ion reactions at intermediate energies.

4.7 Summary

Constraints set on key parameters of the nuclear matter equation of state (EOS) by the values of the tidal deformability, inferred from GW170817, are examined by using a diverse set of relativistic and non-relativistic mean field models. These models are consistent with bulk properties of finite nuclei as well as with the observed lower bound on the maximum mass of neutron star $\sim 2 M_{\odot}$. The tidal deformability shows a strong correlation with specific linear combinations of the isoscalar and isovector nuclear matter parameters associated with the EOS. Such correlations suggest that a precise value of the tidal deformability can put tight bounds on several EOS parameters, in particular, on the slope of the incompressibility and the curvature of the symmetry energy. The tidal deformability obtained from the GW170817 and its UV/optical/infrared counterpart sets the radius of a canonical $1.4 M_{\odot}$ neutron star to be $11.82 \leq R_{1.4} \leq 13.72$ km. In future, precise measurement of tidal deformability will provide an alternative and accurate estimate of nuclear matter parameters.

Chapter 5

Constraining dense matter EOS from terrestrial and astrophysical observations

After the detection of gravitational waves from the GW170817 binary neutron star merger event [Abbott *et al.* 2017a], the rich connection between the very large and the very small nuclear objects has developed more intensely. During the last stages of the inspiral motion of the coalescing neutron stars (NSs), the strong gravity of each of them induces a tidal deformation in the companion star. Decoding the gravitational wave phase evolution caused by that deformation [Flanagan & Hinderer 2008] allows the determination of the dimensionless tidal deformability parameter Λ [Damour *et al.* 2012, Hinderer 2008, Hinderer *et al.* 2010]. It is a measure of the response to the gravitational pull on the neutron star surface correlating with pressure gradients inside the NS and, therefore, it has been proposed as an effective probe of the equation of state (EOS) of nuclear matter relevant for neutron stars [Read *et al.* 2009, Thorne 1987]. A comparatively large value of Λ , for example, points to a neutron star of large radius [Annala *et al.* 2018, De *et al.* 2018, Malik *et al.* 2018a]. This translates into a stiffer nuclear matter EOS and, hence, a comparatively larger neutron skin of a heavy nucleus on the terrestrial plane [Fattoyev *et al.* 2018]. Early analysis of the GW170817 event [Abbott *et al.* 2017a] puts an upper limit to the binary tidal deformability $\tilde{\Lambda}$ at ≈ 800 for the component neutron stars with masses in the range $\approx 1.17 - 1.6 M_{\odot}$ involved in the merger event under the low spin prior scenario. $\tilde{\Lambda}$ is defined as

$$\tilde{\Lambda} = \frac{16}{13} \frac{(12q + 1)\Lambda_1 + (12 + q)q^4\Lambda_2}{(1 + q)^5}, \quad (5.1)$$

where $\Lambda_{1,2}$ are the tidal deformabilities of the neutron stars of masses M_1 and M_2 and $q = M_2/M_1 \leq 1$ is the binary's mass ratio. The masses of the binary components are constrained by the chirp mass $\mathcal{M} = (M_1 M_2)^{3/5} / (M_1 + M_2)^{1/5} = 1.188 M_{\odot}$ for GW170817 event, where M_{\odot} is the solar mass.

When $q = 1$, $\tilde{\Lambda}$ reduces to Λ and is calculated from $\Lambda = \frac{2}{3}k_2[\frac{c^2 R}{GM}]^5$, where k_2 is the second Love number [Abbott *et al.* 2017a], R being the radius of the neutron star. After the initial proposition, the value of $\tilde{\Lambda}$ has gone through several revisions [Abbott *et al.* 2018, 2019, De *et al.* 2018]. Ref. [De *et al.* 2018] reported $\tilde{\Lambda} = 222_{-138}^{+420}$ for a uniform component-mass prior at the 90% credible level; with a few plausible assumptions, a restrictive constraint is now set for a canonical Λ ($=\Lambda_{1.4}$, for a neutron star of mass $1.4M_\odot$) at 190_{-120}^{+390} [Abbott *et al.* 2018] and the radii of both the lighter and the heavier neutron stars in the merger event at $R_{1,2} = 11.9 \pm 1.4$ km. From the spectral parameterization of the defining function $p(\rho)$ (p =pressure) to fit the observational template, the pressure inside the NS at supranormal densities is also predicted. Complementing the electromagnetic probes that determine the maximum mass of neutron stars ($2.01_{-0.04}^{+0.04} \leq M_{\text{NS}}^{\text{max}}/M_\odot \leq 2.16_{-0.15}^{+0.17}$) [Antoniadis & *et al.* 2013, Demorest *et al.* 2010, Rezzolla *et al.* 2018a], GW-based probes of the neutron star structure thus set the stage for exploring the nuclear matter EOS at large densities.

First-principle calculations of nuclear matter EOS at subsaturation densities in chiral effective field theory (CEFT) [Tews *et al.* 2013] and at very high densities in perturbative QCD [Fraga *et al.* 2016, Kurkela *et al.* 2010] are robust. The problem of generating the most generic family of NS-matter EOS at intermediate densities that interpolates between these reliable theoretical estimates consistent with the observational constraints on $M_{\text{NS}}^{\text{max}}$ and the tidal deformability has been recently addressed [Annala *et al.* 2018]. A significant constraint on the nuclear matter EOS is found from the inspection that the low density EOS must be stiff enough to support a NS of mass $\approx 2M_\odot$ but soft enough so that $\tilde{\Lambda} < 800$ [Abbott *et al.* 2019]. Revisiting this problem with a huge number of parametrically constructed plausible different EOSs connecting the low density and the high density end, Most *et al.* [Most *et al.* 2018] find that, for a purely hadronic star, the tidal deformability is constrained at $\Lambda_{1.4} > 375$ at 2σ confidence level. A non-parametric method for inferring the universal neutron star matter EOS from GW observations is also reported recently [Landry & Essick 2019] with the canonical deformability $\Lambda_{1.4} = 160_{-133}^{+448}$ at 90% confidence level. A lower bound on the tidal deformability ≈ 400 is also set from the analysis of the UV-optical-infrared counterpart of GW170817 complemented with numerical relativity results [Radice *et al.* 2018]. Similar analysis, but, with a larger number of models pushes the lower bound to ≈ 200 [Bauswein *et al.* 2017].

Through a combination of laboratory data on light nuclei and sophisticated microscopic modeling of the sub-saturation EOS from CEFT [Lim & Holt 2018, 2019, Tews *et al.* 2018, 2019], attempts have been made to arrive at values of the tidal deformability. Using a relativistic mean field (RMF) inspired family of EOS models calibrated to provide a good description of a set of selective proper-

ties of finite nuclei, the impact of the tidal deformability on the neutron-skin of ^{208}Pb and on the NS mass and radius has also been addressed [Fattoyev *et al.* 2018]. The varying outcomes point to the fact that the connection of the tidal deformability to the laboratory data is not yet fully transparent and that more stringent constraints on the isovector sector of the effective interaction are needed. From new-found strong correlations of $\Lambda_{1.4}$ and $R_{1.4}$ with a set of selective linear combinations of isoscalar and isovector properties of nuclear matter, it is realized that such constraints may be provided by the isovector giant resonances in conjunction with the isoscalar resonances in finite nuclei. To have a better understanding of these particularities, in this communication, we perform an analysis of the suitability of some often-used Skyrme models to explain isoscalar and isovector giant resonance data and examine their predictions for $\Lambda_{1.4}$. Simultaneously, attention is given to the analysis of the astrophysical constraint on the neutron star maximum mass M_{NS}^{\max} [Antoniadis & *et al.* 2013, Demorest *et al.* 2010]; this encodes pressure gradient information from mapping the varying neutron-proton asymmetry over a large density range. Later, by fitting a broader-based set of isoscalar and isovector data along with the observed NS mass constraint, we propose a new EOS with the uncertainties estimated within the covariance analysis and check its compatibility with the GW data. The calculation is model dependent in the sense that the EOS is taken to be a smooth function of density and avoids possibilities of phase transitions to exotic form of matter when more drastic changes in the density behavior of the EOS are considered.

5.1 Motivation from existing trends

We resort to the Skyrme framework for this study. For the suitability analysis of the Skyrme EDFs, we choose among them twenty eight EDFs that are more representative. They include the set of thirteen 'best' EDFs (CSkP set) used in Ref. [Brown 2013]. These are: KDE0v1, LNS, NRAPR, Ska25s20, Ska35s20, SKRA, SkT1, SkT2, SkT3, SQMC700, Sv-sym32, Sly4, SkM*. Another set of thirteen Skyrme EDFs used in Ref. [Alam *et al.* 2016] are also taken to examine the correlation of the neutron star radius with some key parameters of symmetric and asymmetric nuclear matter. They are: Ska, Skb, SkI2, SkI3, SkI5, SkI6, Sly2, Sly230a, Sly9, SkMP, SkOP, SK255 and SK272. To this list of twenty six, two recent EDFs, $\text{Sk}\chi\text{m}^*$ [Zhang *et al.* 2018b] and KDE0-J34 [Roca-Maza *et al.* 2015] are further included; they are compliant with the measured dipole polarizability of few nuclei. The $\text{Sk}\chi\text{m}^*$ EDF, in addition, reproduces the theoretical predictions on properties of asymmetric nuclear matter from CEFT [Wellenhofer *et al.* 2015, 2016]. All these EDFs provide a satisfactory reproduction

of the binding energies of finite nuclei and their charge radii, and obey reasonable constraints on the properties of symmetric nuclear matter such as the energy per nucleon ($e_0 = -15.8 \pm 0.5$ MeV), the saturation density ($\rho_0 = 0.16 \pm 0.01$ fm $^{-3}$), the isoscalar nucleon effective mass ($\frac{m_0^*}{m} = 0.6-1.0$) and the isoscalar nuclear incompressibility ($K_0 = 240 \pm 30$ MeV).

The twenty eight EDFs mentioned above were constructed with emphasis on different biases for the selection of data on finite nuclei and nuclear matter properties. We would like to have a closer look into these EDFs by analyzing their ability to explain few further significant data related to isoscalar and isovector properties of finite nuclei and draw inference on the consistency of the EDFs in explaining observables concerning neutron star masses and their tidal deformability. The experimental data of particular interest for finite nuclei are the centroid energy E_{GMR}^c of the isoscalar giant monopole resonance (ISGMR), the peak energy E_{GDR}^p of the isovector giant dipole resonance (IVGDR) and the dipole polarizability α_D , all for the heavy nucleus ^{208}Pb . The dipole polarizability α_D and the GDR peak energies are measures of the isovector parameter Θ_v that defines the isovector effective nucleon mass $m_{v,0}^*$ [Zhang & Chen 2016] in the Skyrme methodology. In conjunction with the isoscalar effective mass m_0^* , this determines the isovector-splitting of the nucleon effective mass [$\Delta m_0^* \equiv (m_n^* - m_p^*)/m$], which is directly related with the isovector properties of the nuclear interaction. Concerning the astrophysical context, the data include the observed lower limit of the maximum mass $M_{\text{NS}}^{\text{max}}$ of the neutron star [Antoniadis & et al. 2013, Demorest et al. 2010], ($M_{\text{NS}}^{\text{max}} = 2.01 \pm 0.04 M_\odot$).

The constraints provided by these empirical data allow to choose the most plausible EDFs considering the neutron star maximum mass and its radius, and the tidal deformability parameter along with other properties of nuclear matter like m_0^* or Δm_0^* . For the selected twenty eight EDFs, we find the effective mass $\frac{m_0^*}{m}$ lying between $\approx 0.6-1.0$ with Δm_0^* distributed nearly evenly with positive and negative signs. This is shown as (+) and (-) signs for Δm_0^* superimposed on the symbols in Fig.5.1(a) where the calculated values of the maximum neutron star mass $M_{\text{NS}}^{\text{max}}$ are given as a function of the tidal deformability parameter $\Lambda_{1.4}$ for the given EDFs. To focus on the role of m_0^* in determining the ISGMR energy and the maximum mass of the neutron star, $\frac{m_0^*}{m}$ of the EDFs are sorted in three groups, $0.60 \leq \frac{m_0^*}{m} < 0.65$ (red solid circle), $0.65 \leq \frac{m_0^*}{m} < 0.75$ (blue solid square) and $0.75 \leq \frac{m_0^*}{m} \leq 1.0$ (green solid pentagon). The red dashed horizontal lines in all the four panels in Fig.5.1 show the lower bound of the observed maximum value of the NS mass ($= 1.97 M_\odot$) that an acceptable EDF must support. To calculate the neutron star properties, the EOS for its crust is taken from the Baym, Pethick and Sutherland model [Baym et al. 1971] in the density range $\rho \approx 4.8 \times 10^{-9}$ fm $^{-3}$ to 2.6×10^{-4} fm $^{-3}$. The structure of the core is calculated from the EDFs with the assumption of a charge neutral uniform

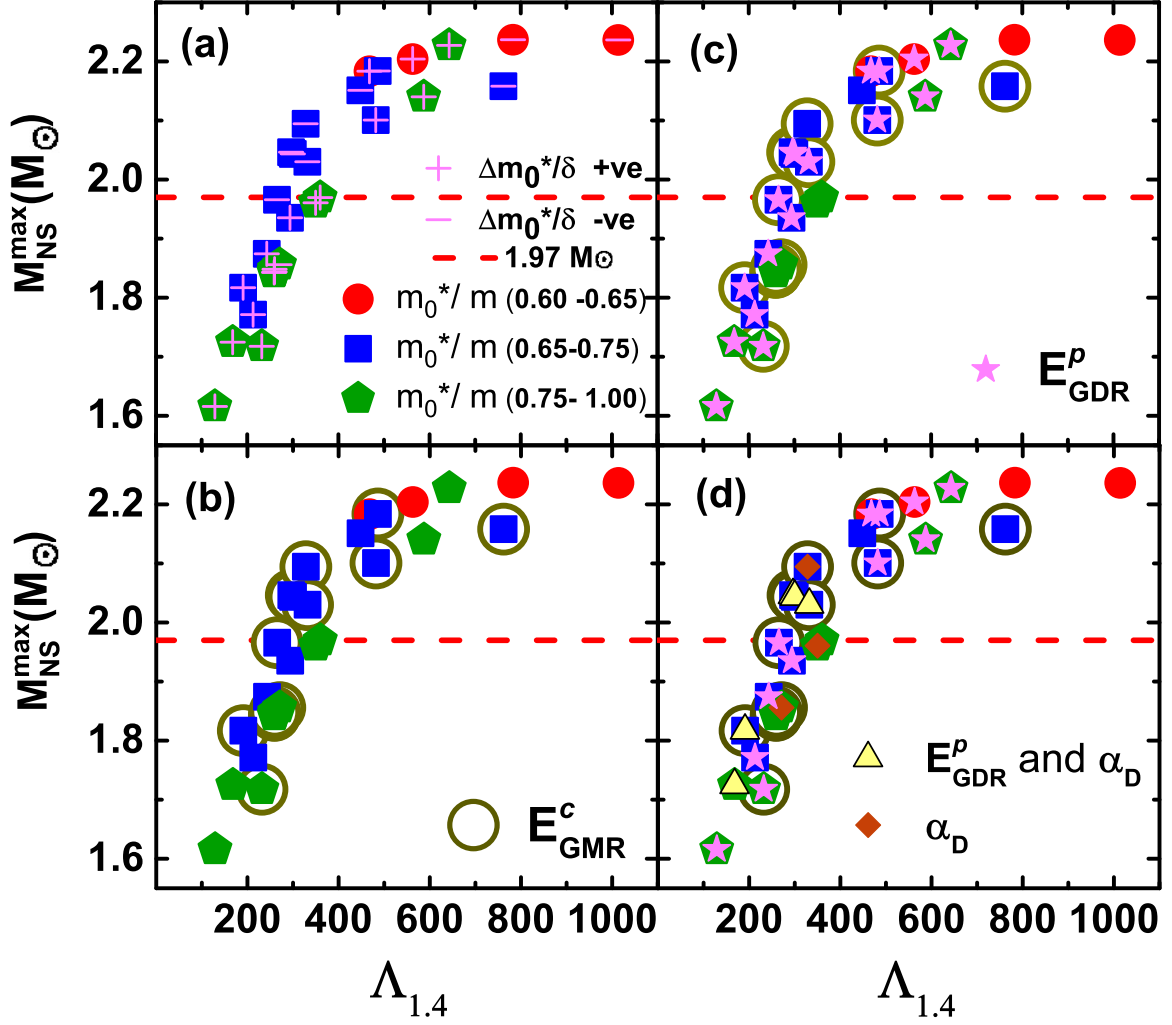


Figure 5.1: The maximum neutron star mass $M_{\text{NS}}^{\text{max}}$ versus the tidal deformability parameter $\Lambda_{1.4}$ obtained from the 28 selected EDFs. The red dashed lines refer to $1.97M_{\odot}$, the observed lower bound for $M_{\text{NS}}^{\text{max}}$. For more details, see text.

plasma of neutrons, protons, electrons and muons in β -equilibrium. The EOS for the region between the inner edge of the outer crust and the beginning of outer core defined by the crust-core transition density is appropriately interpolated using a polytropic form [Carriere *et al.* 2003]. This method may introduce uncertainties in the determination of the radius of low and intermediate NS masses [Fortin *et al.* 2016, Pais & Providencia 2016, Piekarewicz *et al.* 2014]. We have estimated an average uncertainty of $\approx 2\%$ on $\Lambda_{1.4}$ by comparing the present results with the ones obtained from unified EOSs. Fig.5.1(a) shows that the constraint on the NS maximum mass alone filters out some EDFs. A good fraction of the EDFs with effective masses above $0.75m$ fails to achieve the lower bound on $M_{\text{NS}}^{\text{max}}$.

EDFs that fulfill the constraint imposed by the ISGMR centroid energy in ^{208}Pb (14.17 ± 0.28 MeV) are represented by additional open circle in Fig.5.1(b). The EDFs with effective masses in the

lower end of the spectrum (red solid circles, $\frac{m_0^*}{m} < 0.65$) are seen to be excluded from consideration; lower effective masses tend to yield higher values of ISGMR energies than desired. The further constraint of satisfying the IVGDR peak energy (13.43 MeV; in Ref. [Dietrich & Berman 1988], a large width of 4.07 MeV is ascribed to it. We take a conservative estimate of 2 MeV for the width) for ^{208}Pb (marked with further magenta-colored star) eliminates few more EDFs as shown in Fig.5.1(c) and, as is also seen there that, it forces the focus on effective mass values in the middle range $(0.65\text{-}0.75)m$. On top of these, imposition of the next constraint concerning the dipole polarizability α_D for ^{208}Pb ($19.6 \pm 0.6 \text{ fm}^3$) leaves open the question of the suitability of most of the EDFs, as is seen from the inspection of Fig.5.1(d). EDFs satisfying the constraint on α_D are marked by orange diamonds, those satisfying criteria concerning both the IVGDR peak energy and α_D are marked by yellow triangles (see Table I of the Supplemental Material [Malik *et al.* 2019a] for details on 28 EDFs). Fig.5.1(d) shows that among the selected twenty eight EDFs, only three satisfy all the constraints considered. They are the interactions Sly2, Sly4 and KDE0-J34. For these three EDFs, the effective mass is $\approx 0.7m$, and the isovector mass splitting Δm_0^* is negative. It is of interest to note that the constraints on the maximum NS mass and the ISGMR datum in ^{208}Pb can not delineate the sign of the values of Δm_0^* , positive or negative; the extra constraint on the peak energy of IVGDR in ^{208}Pb is in favour of a negative Δm_0^* , the final constraint on the dipole polarizability settles this issue. The value of the nucleon effective mass ($0.7m$) is in very good agreement with that obtained from the optical model analysis of nucleon-nucleus scattering [Li *et al.* 2015], but the negative value of the isospin-splitting effective mass, at variance with most theoretical predictions [Agrawal *et al.* 2017, Baldo *et al.* 2017, Holt *et al.* 2016, Kong *et al.* 2017, Li & Han 2013, Li *et al.* 2018, 2015, Mondal *et al.* 2017, Zhang & Chen 2016], needs possibly a more critical examination. Presently we do not discuss this matter except mentioning that a recent EDF [Malik *et al.* 2018b] based on the Gibbs-Duhem relation and specifically designed to fit a wide variety of 'pseudo data' corresponding to infinite nuclear matter and the experimental energy weighted sum rule for a few nuclei yields a value for the nucleon effective mass that is very close ($\frac{m_0^*}{m} = 0.68$) to what we find from this analysis and also gives a negative value for $\Delta m_0^*(=-0.2\delta)$. Here, δ is the isospin asymmetry of nuclear matter defined as $\delta = (\rho_n - \rho_p)/\rho$, ρ_n and ρ_p being the neutron and proton densities, respectively.

The role of the empirical data in sensitively constraining the tidal deformability parameter Λ should now be stressed. One sees from Fig.5.1 that from the total twenty eight EDFs chosen, $\Lambda_{1.4}$ stretches out from 100 to 1000, the NS mass constraint shrinks the band width to $\approx 270\text{-}1000$, the ISGMR datum shrinks it to $\approx 270\text{-}760$, the IVGDR peak energy squeezes it further to $\approx 270\text{-}590$ and

Table 5.1: Parameters for the model Sk Λ 267 and the resulting nuclear matter and neutron star properties along with their errors in the parenthesis. J_0 is the symmetry energy coefficient, L_0 is related to its density derivative [Malik *et al.* 2018b].

t_0 (MeVfm ³)	t_1 (MeVfm ⁵)	t_2 (MeVfm ⁵)	t_3 (MeVfm ^{3+3α)}	x_0	x_1	x_2	x_3	α	W_0 (MeVfm ⁵)
-2481.08	482.51	-516.17	13778.74	0.93	-0.53	-0.97	1.54	0.167	121.38
(89.05)	(50.41)	(407.22)	(123.72)	(0.28)	(0.89)	(0.20)	(0.58)	(0.018)	(9.35)
e_0 (MeV)	ρ_0 (fm ⁻³)	K_0 (MeV)	m_0^*/m	J_0 (MeV)	L_0 (MeV)	$\Delta m_0^*/\delta$	$\Lambda_{1.4}$	$R_{1.4}$ (km)	$M_{\text{NS}}^{\text{max}}$ (M_\odot)
16.04	0.162	230.2	0.70	31.4	41.1	-0.25	267	11.6	2.04
(0.20)	(0.002)	(6.4)	(0.05)	(3.1)	(18.2)	(0.35)	(144)	(1.0)	(0.15)

$\Lambda_{1.4}$ settles it at ≈ 290 -330 when filtered through the choices of all the data considered; it lies in midway of the observed band width for $\Lambda_{1.4}$ deduced from the GW170817 event [Abbott *et al.* 2018]. This survey suggests that there are models that can endure the constraint on the observed $M_{\text{NS}}^{\text{max}}$, but many of them would not fit the experimental data on the properties of the ISGMR and IVGDR simultaneously due to the weak correlations among them as discussed later. We would like to emphasize that the conclusion drawn from Fig.5.1 is only indicative of the value of the tidal deformability and serves as the motivation for the quantitative investigation that follows.

5.2 Constraining tidal deformability from measured properties of finite nuclei

To reassess the bounds on the tidal deformability more accurately, a new Skyrme EDF calibrated with a wider fit data base is proposed. The constraints include the observed maximum NS mass $M_{\text{NS}}^{\text{max}}$, the binding energies of spherical magic nuclei, their charge radii, the ISGMR energy of ²⁰⁸Pb and its dipole polarizability. In addition, the ISGMR energies of ⁹⁰Zr and ¹²⁰Sn and the dipole polarizability α_D of ⁴⁸Ca, ⁶⁸Ni and ¹²⁰Sn are included in the fitting protocol.

It is observed that for the models employed in Fig.5.1, E_{GMR}^c , α_D and $M_{\text{NS}}^{\text{max}}$ are weakly correlated among themselves (Pearson correlation coefficients r are ≈ 0.5). Simultaneously constraining these quantities may impose strong restrictions on the model parameters. The IVGDR peak energies are left out of the fitting protocol deliberately. Calculations with the selected EDFs reveal the existence of an anti-correlation of E_{GDR}^p for ²⁰⁸Pb with $M_{\text{NS}}^{\text{max}}$ when the EDFs are sorted in groups within narrow windows in m_0^*/m . For illustration, this anti-correlation is displayed in the Fig.5.2(a) for effective masses in the range $0.65 \leq m_0^*/m < 0.75$ with the selected EDFs. The correlation coefficient is

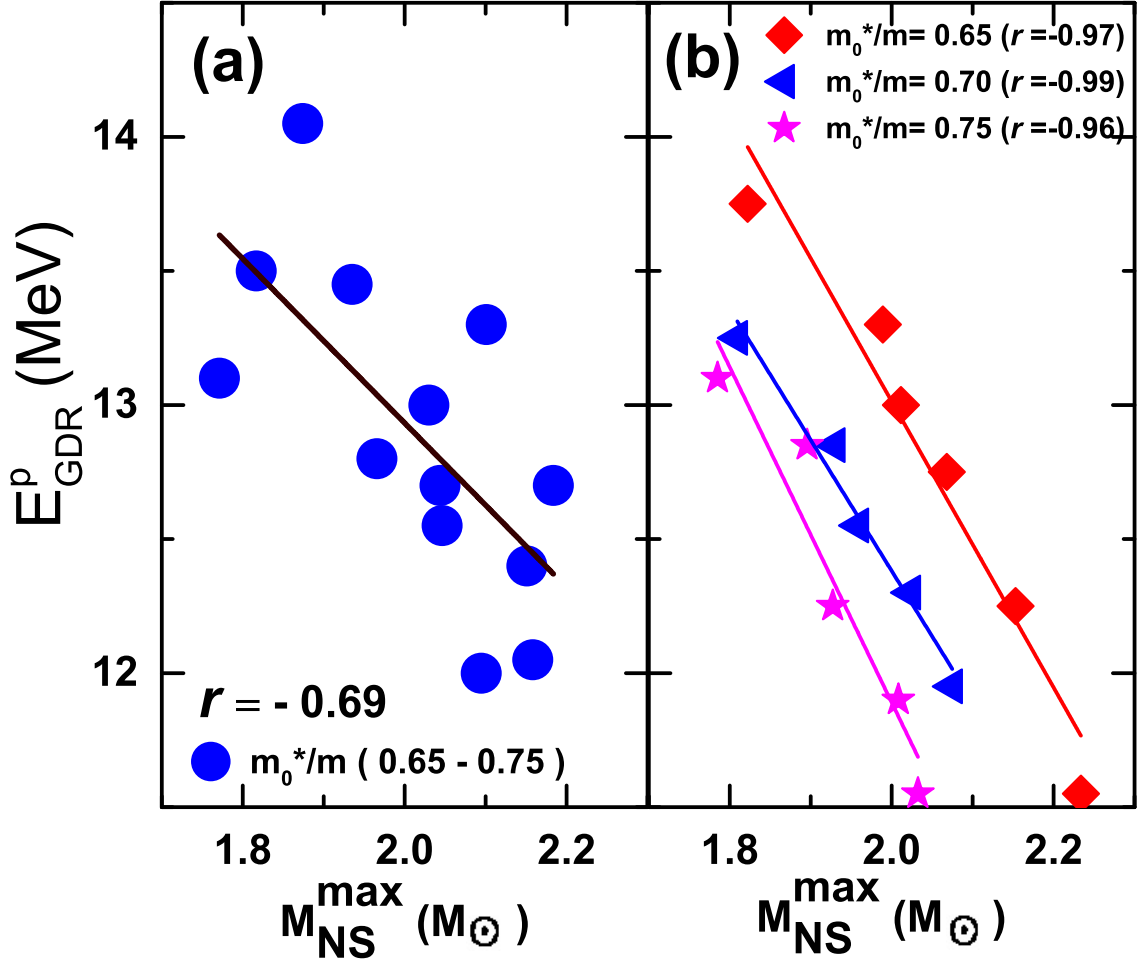


Figure 5.2: Correlation of $E_{\text{GDR}}^{\text{p}}$ and $M_{\text{NS}}^{\text{max}}$ obtained using (a) the set of selected models as in Fig.5.1 with effective mass m_0^*/m in the range 0.65 -0.75 and (b) a set of systematically varied models with chosen fixed effective masses in the present work.

$r = -0.69$. However, we see that the aforesaid correlation shoots up to nearly unity when calculated with the systematically varied models obtained with fixed values of m_0^*/m as displayed in the Fig. 5.2(b). For given values of $M_{\text{NS}}^{\text{max}}$ and m_0^*/m , $E_{\text{GDR}}^{\text{p}}$ is the outcome of the calculation keeping all other data in the fitting protocol unchanged.

The optimized χ^2 -function from the fit to all the input data ($M_{\text{NS}}^{\text{max}}$ and measured properties of finite nuclei as mentioned) yields the EDF parameters. They are listed in Table 5.1 along with their errors obtained within the covariance method [Dobaczewski *et al.* 2014, Mondal *et al.* 2015, Zhang *et al.* 2018b]. Some selected properties of nuclear matter and neutron stars are also presented in the table. Since the central value of $\Lambda_{1.4}$ comes out to be 267, we hereafter name this EDF as Sk Λ 267. The nuclear matter constants obtained for Sk Λ 267 are in excellent agreement with their fiducial values. The lower bound on $M_{\text{NS}}^{\text{max}}$ is comfortably obeyed; the tidal deformability parameter ($\Lambda_{1.4}$) and the NS

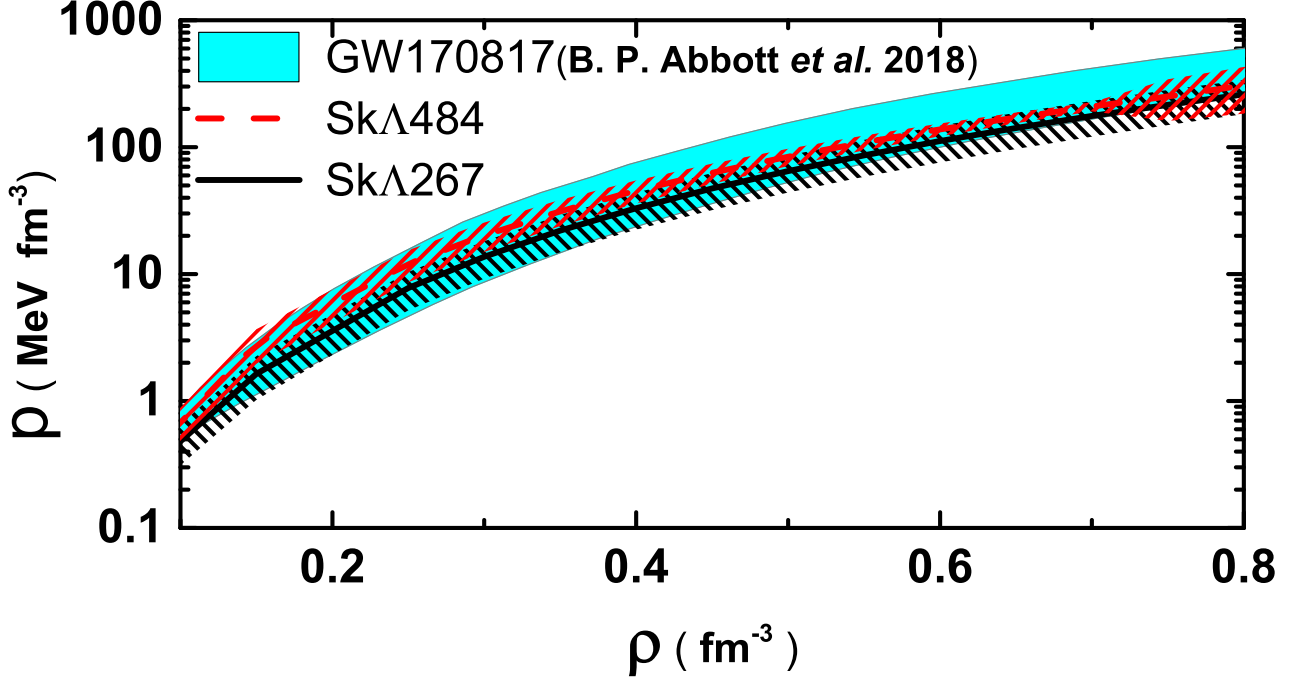


Figure 5.3: Pressure of β -equilibrated neutron star matter displayed as a function of density. The shaded region represents the constraints from GW170817 event (B.P. Abbott *et. al* 2018: [Abbott *et al.* 2018]).

radius $R_{1.4}$ are also found to be in very good agreement with that reported in Ref. [Abbott *et al.* 2018], the errors are more contained though. The value of the neutron-skin Δr_{np} for ^{208}Pb is 0.15 ± 0.05 fm.

Since the experimental value of tidal deformability is not yet settled, tolerance of the fit of the calculated observables with the data is further tested by arbitrarily constraining $\Lambda_{1.4}$ to different values. As a demonstrative example we use an extra constraint in our fit $\Lambda_{1.4} = 500 \pm 100$. The outcome is model Sk Λ 484 with $\Lambda_{1.4} = 484$ (see Table IV of the Supplemental Material [Malik *et al.* 2019a] for the parameters). The model Sk Λ 267 is found to be more compatible with the measured properties of finite nuclei. A comparison of different observables related to nuclear matter and NS properties calculated with Sk Λ 267 and Sk Λ 484 is given in Table III and IV of the Supplemental Material [Malik *et al.* 2019a]. One may note the closeness of the nuclear matter observables obtained from Sk Λ 267 and those from the interaction SLy4 [Chabanat *et al.* 1997]. In SLy4, instead of the IVGDR as fit data as used in this paper, the isotopic properties of forces beyond the β - stability line were dictated by having a good reproduction of neutron-matter EOS obtained variationally by Wiringa *et. al* [Wiringa *et al.* 1988, Wiringa 1993].

The prediction of the EOSs Sk Λ 267 and Sk Λ 484 for the pressure of the neutron star matter as a function of density is displayed in Fig.5.3 and compared with that deduced from the GW170817 event

[Abbott *et al.* 2018]. As expected, Sk Λ 267 is somewhat softer than Sk Λ 484. Overall, the agreement between theory and experiment is very good; the delineation among the two theoretical EOSs is, however, done through the microscopic lens of the measured properties of finite nuclei as already stated. Both EDFs maintain causality in the density range encountered in the interior of the neutron stars; they become acausal beyond $\rho \approx 8\rho_0$ which is slightly higher than the central density $\approx 7.0\rho_0$ for the maximum mass.

5.3 Summary

The agreement of the nuclear equation of state (EOS) deduced from the GW170817 based tidal deformability with the one obtained from empirical data on microscopic nuclei is examined. It is found that suitably chosen experimental data on isoscalar and isovector modes of nuclear excitations together with the observed maximum neutron star mass constrain the EOS which displays a very good congruence with the GW170817 inspired one. The giant resonances in nuclei are found to be instrumental in limiting the tidal deformability parameter and the radius of neutron star in somewhat narrower bounds. At the 1σ level, the values of the canonical tidal deformability $\Lambda_{1.4}$ and the neutron star radius $R_{1.4}$ come out to be 267 ± 144 and 11.6 ± 1.0 km, respectively.

Chapter 6

Conclusion

The equation of state of nuclear matter is determined to take into consideration not only the finite nuclear properties but also neutron star observations. And therefore it is important to pinpoint the symmetry energy at high densities as well as the underlying nuclear interactions. The primary goal of this thesis is to bridge the various aspects of nuclear matter at a various range of densities to the terrestrial experiments whatever available and also the celestial observations. Here we outline the major findings of our work as specified in Chapters 3-5.

In Chapter 3, we presented the extension of the effective chiral model by including $\sigma - \rho$ and $\omega - \rho$ cross-couplings. The motivation was to improve upon the value of symmetry energy both at saturation and the crossing densities. We find that the low-density behavior of PNM EOS for both NCC (no cross coupling) and WR ($\omega - \rho$) models do not match well with the range of values proposed by microscopic calculations [Gezerlis & Carlson 2010, Hebeler *et al.* 2013]. The WR model gives NS maximum mass to be $1.86 M_{\odot}$ which is very less compare to the mass observed for the PSR J0348 + 0432 ($M = 2.01 \pm 0.04 M_{\odot}$) [Antoniadis & *et al.* 2013]. In the case of the SR ($\sigma - \rho$) model, the density dependence of the symmetry energy is found to be consistent with IAS, HIC Sn+Sn and ASY-EOS data. The symmetry energy at the crossing density ($\rho_1 = 0.1 \text{ fm}^{-3}$) is also in harmony with the available empirical data. The value of the symmetry energy slope and the curvature parameters are in accordance with those deduced from the diverse set of experimental data for the finite nuclei. The pure neutron matter EOS at sub-saturation densities passes well through the range of values suggested by the microscopic models [Gezerlis & Carlson 2010, Hebeler *et al.* 2013]. The obtained NS maximum mass is $1.97 M_{\odot}$ which is consistent with the observational data. The value of $R_{1.4}$ (canonical radius) is within the empirical bounds. The SR model satisfies all the discussed constraints which suggest that the inclusion of $\sigma - \rho$ cross-coupling in the effective chiral model is indispensable. We have

also compared our results with a few selected RMF models. In general, it is found that the effects of various cross-couplings within the RMF models are weaker compare to those in the effective chiral model. This effects are more prominent for the models with $\omega - \rho$ cross-coupling.

The tidal deformability inferred from a very recent binary NS mergers event, i.e., GW170817, presents one interesting way to constrain the EOS of dense matter. Complemented with the detection of the UV/optical/infrared counterpart of GW170817, a lower bound on tidal deformability parameter is suggested [Radice *et al.* 2018]. In Chapter 4 we have used a diverse set of relativistic and nonrelativistic mean field models to look for correlations of tidal deformability Λ with several nuclear matter parameters characterizing the EOS such as the nuclear matter incompressibility and symmetry energy coefficients, and their density derivatives. All the models selected are consistent with the bulk properties of finite nuclei as well as with the observation of NS with mass of $\sim 2M_{\odot}$. Nevertheless, across these models, the values of Λ and of the various nuclear matter parameters associated with different EOSs vary over a wide range. The tidal deformability is found to be weakly or only moderately correlated with the individual nuclear matter parameters of the EOS. The stronger correlation of Λ is found only for specific choices of the linear combinations of the isoscalar and isovector EOS parameters. The parameter Λ is strongly correlated with the linear combination of the slopes of incompressibility and symmetry energy coefficients, i.e., $M_0 + \beta L_0$. Further, the parameter Λ and the Love number k_2 both are strongly correlated with the linear combination of $M_0 + \eta K_{\text{sym},0}$. We show that the bound on weighted average of tidal deformability for a system of binary neutron star, obtained from complementary analysis [Abbott *et al.* 2017a, De *et al.* 2018, Radice *et al.* 2018] of GW170817, yields the tidal deformability for NS with mass $1.4 M_{\odot}$ in the range of $344 < \Lambda_{1.4} < 859$. With the aid of the correlations of $\Lambda_{1.4}$ with linear combinations of nuclear matter parameters as considered together with the bounds on $\Lambda_{1.4}$ and the empirical ranges of L_0 obtained in Ref. [Lattimer & Lim 2013, Oertel *et al.* 2017], we have constrained the values of M_0 and $K_{\text{sym},0}$ to lie in the intervals $2254 < M_0 < 3631$ MeV and $-112 < K_{\text{sym},0} < -52$ MeV or $1926 < M_0 < 3768$ MeV and $-140 < K_{\text{sym},0} < 16$ MeV, depending on the constraints set on L_0 . The strong correlation of tidal deformability with the NS radius for a $1.4 M_{\odot}$ NS yields $R_{1.4}$ in the range 11.82 - 13.72 km. The precise measurement of tidal deformability will provide an alternative and accurate estimate for M_0 , $K_{\text{sym},0}$ and $R_{1.4}$.

GW-based measurements of the macroscopic properties of neutron stars offer a very promising means of looking deeper into the nuclear microphysics governing the internal structure of the neutron stars and of obtaining sound informative constraints on the nuclear EOS at subnormal and supranormal densities. In chapter 5, we have explored in this communication how the low density laboratory-

data inspired nuclear matter EOS connects with that obtained from GW-based data. We show that the pressure-density variation deduced from GW analysis is in very good agreement with a parametric form of the EOS designed to comply with properly chosen nuclear observables sensitive to the isoscalar and isovector parts of the nuclear interaction together with the NS mass constraint. The tidal deformability parameter is now constrained at $\approx 267 \pm 144$ (267 ± 236) at 1σ level (90% confidence level). We note that a recent reanalysis [Narikawa *et al.* 2018] of the GW-based data leads to a considerable stretching of the bounds on the tidal deformability although the central value (≈ 200) maintains an extremely good consistency with those obtained earlier or with that obtained by us. On the other hand, the EOS derived from a neural network [Fujimoto *et al.* 2019] having as input observational data from several neutron stars leads to $\Lambda_{1.4} = 320 \pm 120$ which is entirely consistent with the values derived here. Constraining NS properties from low-energy nuclear physics thus seems very meaningful. All nuclear properties, both isoscalar and isovector, derived from our EOS are in very comfortable agreement with their fiducial values. The values of the incompressibility, the symmetry energy and its density derivative indicate that the EOS is soft at densities near saturation; the conformity of the low value of the tidal deformability with the most recent estimates shows that the EOS is soft over a wider range of densities and thus leaves the question open on how to identify a possible phase transition in the neutron star core. Future detection of binary star mergers by the LIGO-Virgo collaboration may settle this issue.

Chapter 7

Future Scope of the Work

In recent years our understanding of the dense matter EOS has been greatly improved. However, there are scope for extension of the present work in the thesis, related to neutron stars. We already have started working on such possible extensions in the light of the results from recent and upcoming developments of the facilities available worldwide and also from different theoretical, observational, experimental or empirical perspectives.

Few of our ongoing works are listed bellow.

- ***On the possibility of having a Dark Matter (DM) in neutron stars***– Observation of the kinematics of self-gravitating objects such as galaxies and clusters of galaxies give a strong hint of the existence of dark matter (DM). Cosmological observations rules out normal baryonic like DM particles. The DM seems to interact very weakly with standard model particles and therefore its coupling is very uncertain. However extensive studies on the particle physics dark matter models have put strong constraints on the coupling constant and mass of the dark matter particles. Among different proposals of dark matter, weakly interacting massive particle (WIMP) scenario has gained favor because it gives the correct prediction of the measured relic abundance of the dark matter today very naturally. The effects of different types of dark matter on dense matter EOS is one of the future scopes of research. The dark matter will softness the EOS, it may possible some ruled out stiff EOS by GW170817 may explain observed neutron star properties with the inclusion of dark matter in the EOS.
- ***Constraints on EOS in a model independent way***– Correlation analysis between nuclear matter parameters and NS properties have been explored using several nuclear models. These correlations studies, however, show a considerable model dependence. Since different models with

similar values of nuclear matter parameters may result in different EOSs. We are interested in further future exploration of correlations of nuclear matter parameters with various astrophysical observables in a model independent approach .

- ***Machine Learning approach to nuclear matter studies***– The correlation analysis are only sensitive to linear dependencies. It may possible that exact dependency of astrophysical observables with nuclear mater parameters are complicated and nonlinear. These non-linear maps can be encoded by supervised machine learning methodology which has already been applied to neutron star physics in , where a Deep Neural Network (DNN) was used as an efficient procedure for mapping from a finite set of mass-radius observational data onto the equation of state plane.
- ***On the possible existence of exotic particle in the core of neutron stars***– The compactness parameter of massive neutron star observed recently indicates a possible existence of baryonic resonances such as $\Lambda^0, \Sigma^{+,0,-}, \Xi^{-,0}, \Omega^-$ in the core of neutron stars. Moreover, Neutrons at very high momentum states will be unstable and therefore it is more likely that baryonic resonances be there at lower momentum states. Their presences will result in more massive stars with smaller radius. Studies has reviled that the presence of exotic particles lowers the pressure and hence one obtains soft EOS at higher densities. Such studies can also through light on the possible interactions between them.
- ***Neutron stars with high magnetic field***– Born out of massive interstellar gases over millions of years, the magnetic field present in these compact structures can be very high, although the origin of these high fields is still not well understood. The typical values of surface magnetic field of neutron stars ranges from 10^{12} to 10^{15} Gauss. It is speculated that the field intensity can be even more at the core. A fraction of the population, having the strongest surface magnetic fields $\sim (10^{12} - 10^{15})$ Gauss are called the magnetars and generally they belong to Soft Gamma Repeaters (SGRs) or Anomalous X-ray Pulsars (AXPs). Therefore, it is desirable to incorporate the magnetic field effects to determine the composition and the gross structural properties of these neutron stars with high magnetic field. Apart from the static structural properties of the magnetars, magnetic fields also play an important role in the physics of compact star mergers. The gravitational waves emitted at the late stage of the merger process can possibly be detected directly and are sensitive to the EOS of the dense matter. The magnetic field in a merger process can possibly become extremely large due to magneto-rotational instability and the magnitude can be large enough to affect the EOS of dense matter.

Appendix A

Mass dependence of correlations parameters

The coefficients α , β and η are obtained in such a way that they optimize the correlations of Λ , for a given NS mass, with the linear combinations $K_0 + \alpha L_0$, $M_0 + \beta L_0$ and $M_0 + \eta K_{\text{sym},0}$. The value of these coefficients are given in Table B.2 for a few selected NS masses. In Figure A.1, we plot the mass

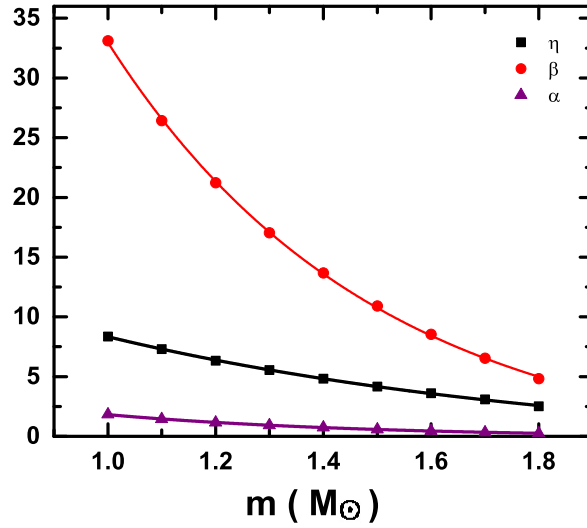


Figure A.1: The values of α , β and η obtained by optimizing the the correlations of Λ with the linear combinations $K_0 + \alpha L_0$, $M_0 + \beta L_0$ and $M_0 + \eta K_{\text{sym},0}$ are plotted as a function of NS mass.

dependence of α , β and η . These coefficients can be easily fitted to the exponential decay like function which can be expressed as $\alpha = -0.13 + 14.87 \exp(-m/0.49)$, $\beta = -1.90 + 265.02 \exp(-m/0.49)$ and $\eta = -1.4 + 29.81 \exp(-m/0.89)$, where the NS mass m is in the unit of solar mass.

Appendix B

The properties of finite nuclei, nuclear matter, and neutron stars

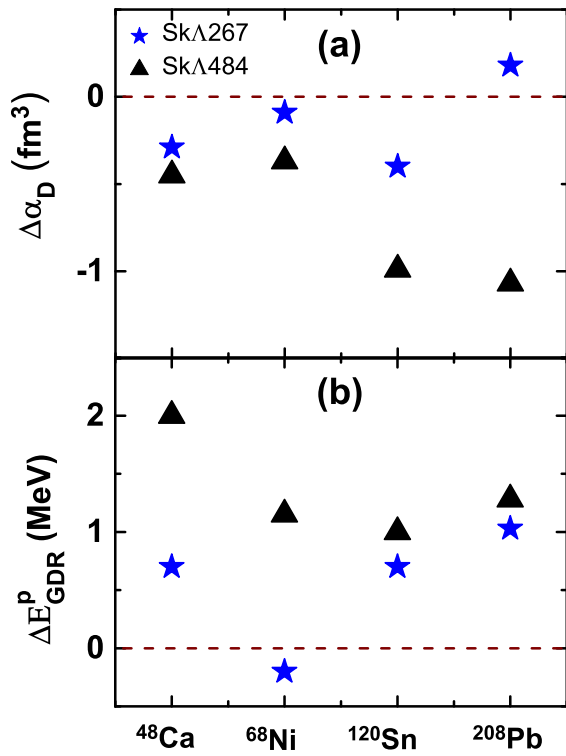


Figure B.1: Deviations of the dipole polarizability $\Delta\alpha_D$ and the peak energy ΔE_{GDR}^p from their experimental values obtained with the Sk Λ 267 and Sk Λ 484 parameter sets are plotted for different nuclei.

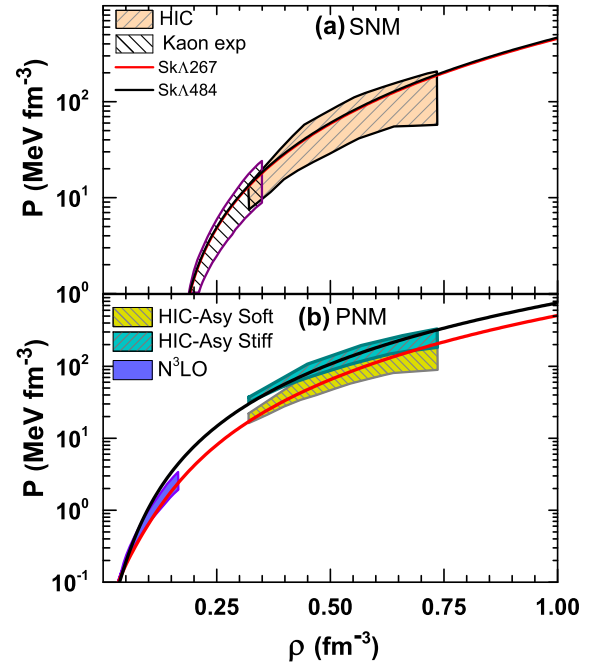


Figure B.2: The pressure $P(\rho)$ for SNM (upper panel) and PNM (lower panel) as a function of baryon density ρ for the parameter sets Sk Λ 267 and Sk Λ 484. Constraints from different previous studies e.g. Kaon exp [Fantina *et al.* 2014, Fuchs 2006], HIC [Danielewicz *et al.* 2002] and N 3 LO [Hebeler *et al.* 2013] are provided for comparison.

Table B.1: Some selected properties of nuclear matter such as binding energy per nucleon e_0 , nuclear matter incompressibility coefficient K_0 , its skewness Q_0 , symmetry energy coefficient J_0 , its slope L_0 , effective mass $\frac{m_0^*}{m}$, isovector splitting of nucleon effective mass $\frac{\Delta m_0^*}{\delta}$ calculated at saturation density ρ_0 for the representative set of Skyrme models considered. The models are arranged according to increasing order of $\frac{m_0^*}{m}$. The values for various quantities associated with ^{208}Pb nucleus and those for neutron star as employed in Fig.1 of the main text are also listed.

Model	ρ_0 (fm^{-3})	e_0 (MeV)	K_0 (MeV)	Q_0 (MeV)	J_0 (MeV)	L_0 (MeV)	$\frac{m_0^*}{m}$	$\frac{\Delta m_0^*}{\delta}$	α_D (fm^3)	E_{GDR}^p (MeV)	E_{GMR}^c (MeV)	$M_{\text{NS}}^{\text{max}}$ (M_\odot)	$R_{1.4}$ (km)	$\Lambda_{1.4}$
SkI3	0.16	-15.98	258.20	-303.88	34.83	100.53	0.58	-0.32	21.99	12.20	14.76	2.24	13.5	783
SkI5	0.16	-15.85	255.80	-301.97	36.64	129.33	0.58	-0.32	23.95	11.90	14.72	2.24	14.0	1014
Skb	0.16	-15.99	263.16	-300.14	23.88	47.54	0.61	0.22	26.86	13.00	15.15	2.18	12.2	468
Ska	0.16	-15.99	263.16	-300.14	32.91	74.62	0.61	0.22	22.31	14.05	14.85	2.20	12.9	563
SkI6	0.16	-15.92	248.60	-327.35	30.09	59.70	0.64	-0.26	20.65	12.70	14.38	2.18	12.5	486
SkMP	0.16	-15.56	230.88	-338.06	29.89	70.31	0.65	0.15	23.82	13.30	14.08	2.10	12.5	482
SLy9	0.15	-15.80	229.85	-350.43	31.98	54.86	0.67	-0.22	20.81	12.40	13.80	2.15	12.4	448
SkI2	0.16	-15.78	240.94	-339.72	33.37	104.34	0.68	-0.20	23.48	12.05	14.37	2.16	13.4	762
NRAPR	0.16	-15.85	225.66	-362.55	32.78	59.63	0.69	0.21	20.58	13.45	13.84	1.94	12.0	294
SLy4	0.16	-15.97	229.92	-363.12	32.00	45.94	0.69	-0.18	19.76	12.55	13.98	2.05	11.7	296
SLy230a	0.16	-15.99	229.89	-364.20	31.99	44.32	0.70	-0.42	19.14	12.00	14.02	2.09	11.8	328
Sly2	0.16	-15.99	229.92	-364.23	32.00	47.45	0.70	-0.18	19.55	12.70	13.99	2.04	11.8	300
KDE0J34	0.16	-16.11	228.84	-373.63	34.00	59.00	0.72	-0.10	19.56	13.00	14.07	2.03	12.1	332
QMC750	0.17	-16.23	231.03	-380.53	34.28	65.43	0.74	0.21	18.61	14.05	14.60	1.87	11.7	243
KDE0v1	0.17	-16.23	227.55	-384.88	34.58	54.69	0.74	-0.13	18.60	12.80	14.06	1.97	11.6	265
SKRA	0.16	-15.78	216.99	-378.78	31.32	53.03	0.75	0.29	21.23	13.10	13.62	1.77	11.4	213
Sk χ m*	0.17	-16.06	230.36	-376.37	30.93	45.55	0.75	0.12	19.68	13.50	14.08	1.82	11.1	191
SK272	0.16	-16.28	271.52	-305.32	37.40	91.67	0.77	0.29	21.00	12.95	14.88	2.23	13.3	643
SkMs	0.16	-15.77	216.62	-386.10	30.03	45.78	0.79	0.33	21.71	13.05	13.56	1.62	10.6	129
SK255	0.16	-16.33	254.94	-350.11	37.40	95.05	0.80	0.37	21.76	12.75	14.41	2.14	13.1	587
LNS	0.18	-15.32	210.79	-382.57	33.43	61.45	0.83	0.22	19.57	12.85	13.80	1.72	11.1	168
SkOp	0.16	-15.75	222.33	-390.77	31.95	68.93	0.90	0.05	21.88	11.80	13.66	1.97	12.3	360
SV-sym32	0.16	-15.94	233.81	-380.13	32.00	57.07	0.90	0.47	20.86	12.60	14.07	1.72	11.6	232
Ska25s20	0.16	-16.07	220.76	-413.47	33.78	63.81	0.98	-0.01	20.02	12.35	14.10	1.86	11.9	271
SkT2	0.16	-15.95	235.74	-382.68	32.00	56.16	1.00	0.00	20.90	11.50	14.22	1.84	11.7	259
SkT1	0.16	-15.98	236.17	-383.54	32.02	56.18	1.00	0.00	20.91	11.50	14.21	1.84	11.7	260
SkT3	0.16	-15.94	235.75	-382.71	31.50	55.31	1.00	0.00	20.79	11.55	14.26	1.85	11.7	260
Ska35s20	0.16	-16.08	240.27	-378.66	33.57	64.83	1.00	0.00	20.06	12.25	14.68	1.96	12.3	350

Table B.2: Experimental values of the fit data and adopted errors on them for Sk Λ 267. For Sk Λ 484 we have taken additional fit data $\Lambda_{1,4} = 500 \pm 100$.

Quantity	Nuclei	Exp. value	Adopted error
Binding energy (MeV)	^{208}Pb	-1636.43	1
	^{40}Ca	-342.05	3
	^{132}Sn	-1102.84	1
	^{16}O	-127.62	4
	^{48}Ca	-416.00	1
	^{56}Ni	-483.99	2
	^{100}Sn	-825.30	2
	$^{24}\text{O} - ^{16}\text{O}$	-41.34	2
charge radii (fm)	^{208}Pb	5.50	0.02
	^{40}Ca	3.48	0.02
	^{132}Sn	4.71	0.02
	^{16}O	2.70	0.04
	^{48}Ca	3.48	0.04
	^{56}Ni	3.75	0.18
α_D (fm 3)	^{208}Pb	19.60	0.6
	^{120}Sn	8.59	0.36
	^{48}Ca	2.07	0.22
E_{GMR}^c (MeV)	^{208}Pb	14.17	0.28
	^{120}Sn	15.70	0.5
	^{90}Zr	17.89	0.2
$M_{\text{NS}}^{\text{max}}$ (M_{\odot})		2.16	0.15

Table B.3: Dipole polarizability α_D , peak energy of IVGDR $E_{\text{GDR}}^{\text{p}}$, centroid energy of ISGMR $E_{\text{GMR}}^{\text{c}}$ for different nuclei [Col *et al.* 2013] and neutron skin thickness Δr_{np} of ^{208}Pb are listed for Sk Λ 267 and Sk Λ 484 models. The corresponding experimental values are also provided for comparison.

Quantity	Nuclei	Experiment	Sk Λ 267	Sk Λ 484
α_D (fm ³)	^{208}Pb	19.6(6)	19.42(50)	20.67(84)
	^{120}Sn	8.59(36)	8.99(25)	9.58(36)
	^{68}Ni	3.88(31)	3.97(12)	4.25(17)
	^{48}Ca	2.07(22)	2.36(16)	2.52(15)
$E_{\text{GDR}}^{\text{p}}$ (MeV)	^{208}Pb	13.43	12.40	12.15
	^{120}Sn	15.00	14.30	14.00
	^{68}Ni	17.10	17.30	15.95
	^{48}Ca	18.90	18.20	16.90
$E_{\text{GMR}}^{\text{c}}$ (MeV)	^{208}Pb	14.17(28)	14.04(11)	13.95(12)
	^{120}Sn	15.70(10)	16.46(13)	16.42(27)
	^{90}Zr	17.81(20)	18.36(12)	18.34(13)
Δr_{np} (fm)	^{208}Pb	0.16(03)*	0.15(05)	0.21(04)

*Obtained from the systematic analysis of measured electric dipole polarizability [Roca-Maza *et al.* 2015].

Table B.4: Values of the parameters for the Sk Λ 267 and Sk Λ 484 models along with their errors. Different properties of nuclear matter and neutron star resulting from both the parameter sets are also listed. Definitions of the different nuclear matter properties are used as in Ref. [Dutra *et al.* 2012].

Quantity	Sk Λ 267	Sk Λ 484
t_0 (MeV fm ³)	-2481.08 ± 89.05	-2488.70 ± 76.02
t_1 (MeV fm ⁵)	482.51 ± 50.41	500.07 ± 30.47
t_2 (MeV fm ⁵)	-516.17 ± 407.22	-503.49 ± 224.21
t_3 (MeV fm ^{3(1+\alpha)})	13778.74 ± 123.72	13675.87 ± 250.29
x_0	0.93 ± 0.28	0.57 ± 0.35
x_1	-0.53 ± 0.89	-0.68 ± 1.22
x_2	-0.97 ± 0.20	-0.97 ± 0.14
x_3	1.54 ± 0.58	1.01 ± 0.77
α	0.167 ± 0.018	0.16 ± 0.01
W_0 (MeV fm ⁵)	121.38 ± 9.35	116.94 ± 13.97
ρ_0 (fm ⁻³)	0.161 ± 0.002	0.161 ± 0.002
e_0 (MeV)	-16.04 ± 0.20	-16.10 ± 0.16
K_0 (MeV)	230.19 ± 6.41	232.32 ± 5.05
Q_0 (MeV)	-366.75 ± 11.96	-363.77 ± 10.23
J_0 (MeV)	31.41 ± 3.13	34.87 ± 3.03
L_0 (MeV)	41.10 ± 18.23	76.32 ± 28.94
$K_{\text{sym},0}$ (MeV)	-123.90 ± 70.19	-28.35 ± 130.68
m_0^*/m_0	0.70 ± 0.05	0.69 ± 0.03
$\Delta m_0^*/\delta$	-0.25 ± 0.35	-0.30 ± 0.51
$M_{\text{max}}^{\text{NS}}/M_{\odot}$	2.04 ± 0.15	2.10 ± 0.04
$R_{1.4}$ (km)	11.6 ± 1.0	13.1 ± 1.1
$\Lambda_{1.4}$	267 ± 144	484 ± 215

Bibliography

- ABBOTT, B.P., ABBOTT, R., ABBOTT, T.D. & ACERNESE, F.*et al.* (2017a). Gw170817: Observation of gravitational waves from a binary neutron star inspiral. *Phys. Rev. Lett.*, **119**, 161101.
- ABBOTT, B.P., ABBOTT, R., ABBOTT, T.D. & ACERNESE, F.*et al.* (2018). Gw170817: Measurements of neutron star radii and equation of state. *Phys. Rev. Lett.*, **121**, 161101.
- ABBOTT, B.P. *et al.* (2017b). Gravitational Waves and Gamma-rays from a Binary Neutron Star Merger: GW170817 and GRB 170817A. *Astrophys. J.*, **848**, L13.
- ABBOTT, B.P. *et al.* (2017c). Multi-messenger Observations of a Binary Neutron Star Merger. *Astrophys. J.*, **848**, L12.
- ABBOTT, B.P. *et al.* (2019). Properties of the binary neutron star merger GW170817. *Phys. Rev.*, **X9**, 011001.
- AGRAWAL, B.K. (2010). Asymmetric nuclear matter and neutron skin in an extended relativistic mean-field model. *Phys. Rev. C*, **81**, 034323.
- AGRAWAL, B.K., SHLOMO, S. & SANZHUR, A.I. (2003). Selfconsistent Hartree-Fock based random phase approximation and the spurious state mixing. *Phys. Rev.*, **C67**, 034314.
- AGRAWAL, B.K., SHLOMO, S. & AU, V.K. (2005). Determination of the parameters of a skyrme type effective interaction using the simulated annealing approach. *Phys. Rev. C*, **72**, 014310.
- AGRAWAL, B.K., DE, J.N. & SAMADDAR, S.K. (2012a). Determining the density content of symmetry energy and neutron skin: an empirical approach. *Phys. Rev. Lett.*, **109**, 262501.
- AGRAWAL, B.K., SULAKSONO, A. & REINHARD, P.G. (2012b). Optimization of relativistic mean field model for finite nuclei to neutron star matter. *Nucl. Phys.*, **A882**, 1–20.

- AGRAWAL, B.K., DE, J.N., SAMADDAR, S.K., COLO, G. & SULAKSONO, A. (2013). Constraining the density dependence of the symmetry energy from nuclear masses. *Phys. Rev.*, **C87**, 051306.
- AGRAWAL, B.K., SAMADDAR, S.K., DE, J.N., MONDAL, C. & DE, S. (2017). Limiting symmetry energy elements from empirical evidence. *Int. J. Mod. Phys.*, **E26**, 1750022.
- ALAM, N., SULAKSONO, A. & AGRAWAL, B.K. (2015). Diversity of neutron star properties at the fixed neutron-skin thickness of ^{208}Pb . *Phys. Rev. C*, **92**, 015804.
- ALAM, N., AGRAWAL, B.K., FORTIN, M., PAIS, H., PROVIDENCIA, C., RADUTA, A.R. & SULAKSONO, A. (2016). Strong correlations of neutron star radii with the slopes of nuclear matter incompressibility and symmetry energy at saturation. *Phys. Rev.*, **C94**, 052801.
- ALAM, N., PAIS, H., PROVIDENCIA, C. & AGRAWAL, B.K. (2017). Warm unstable asymmetric nuclear matter: critical properties and the density dependence of the symmetry energy. *Phys. Rev.*, **C95**, 055808.
- ANNALA, E., GORDA, T., KURKELA, A. & VUORINEN, A. (2018). Gravitational-wave constraints on the neutron-star-matter Equation of State. *Phys. Rev. Lett.*, **120**, 172703.
- ANTONIADIS, J. & *et al.* (2013). A massive pulsar in a compact relativistic binary. *Science*, **340**.
- ARZUMANIAN, Z., GENDREAU, K.C., BAKER, C.L., CAZEAU, T., HESTNES, P., KELLOGG, J.W., KENYON, S.J., KOZON, R.P., LIU, K.C., MANTHRIPRAGADA, S.S., MARKWARDT, C.B., MITCHELL, A.L., MITCHELL, J.W., MONROE, C.A., OKAJIMA, T., POLLARD, S.E., POWERS, D.F., SAVADKIN, B.J., WINTERNITZ, L.B., CHEN, P.T., WRIGHT, M.R., FOSTER, R., PRIGOZHIN, G., REMILLARD, R. & DOTY, J. (2014). The neutron star interior composition explorer (NICER): mission definition. In T. Takahashi, J.W.A. den Herder & M. Bautz, eds., *Space Telescopes and Instrumentation 2014: Ultraviolet to Gamma Ray*, vol. 9144, 579 – 587, International Society for Optics and Photonics, SPIE.
- AVOGADRO, P. & BERTULANI, C.A. (2013). Role of pairing in the description of Giant Monopole Resonances. *Phys. Rev.*, **C88**, 044319.
- BALDO, M., ROBLEDI, L.M., SCHUCK, P. & VIÑAS, X. (2017). Barcelona-catania-paris-madrid functional with a realistic effective mass. *Phys. Rev. C*, **95**, 014318.

- BAUSWEIN, A., JUST, O., JANKA, H.T. & STERGIIOULAS, N. (2017). Neutron-star radius constraints from GW170817 and future detections. *Astrophys. J.*, **850**, L34.
- BAYM, G., PETHICK, C. & SUTHERLAND, P. (1971). The Ground state of matter at high densities: Equation of state and stellar models. *Astrophys. J.*, **170**, 299–317.
- BENNOUR, L., HEENEN, P., BONCHE, P., DOBACZEWSKI, J. & FLOCARD, H. (1989). Charge distributions of 208pb, 206pb, and 205tl and the mean-field approximation. *Phys. Rev. C*, **40**, 2834.
- BINNINGTON, T. & POISSON, E. (2009). Relativistic theory of tidal love numbers. *Phys. Rev. D*, **80**, 084018.
- BIZARRO, D., RABHI, A. & PROVIDENCIA, C. (2015). Effect of the symmetry energy and hyperon interaction on neutron stars. *arXiv*, 1502.04952.
- BOGUTA, J. (1983). ABNORMAL NUCLEI. *Phys. Lett.*, **B128**, 19–23.
- BOGUTA, J. & BODMER, A.R. (1977). Relativistic Calculation of Nuclear Matter and the Nuclear Surface. *Nucl. Phys.*, **A292**, 413–428.
- BOGUTA, J. & STOECKER, H. (1983). Systematics of Nuclear Matter Properties in a Nonlinear Relativistic Field Theory. *Phys. Lett.*, **120B**, 289–293.
- BRANDT, S. (1997). *Statistical and Computational Methods in Data Analysis*. Springer, New York, 3rd English edition.
- BRILLET, A. & *et al.* (VIRGO COLLABORATION) (1989). *Technical Report No. VIR-0517A-15*.
- BROWN, B.A. (2013). Constraints on the Skyrme Equations of State from Properties of Doubly Magic Nuclei. *Phys. Rev. Lett.*, **111**, 232502.
- CARRIERE, J., HOROWITZ, C.J. & PIEKAREWICZ, J. (2003). Low mass neutron stars and the equation of state of dense matter. *Astrophys. J.*, **593**, 463–471.
- CARSON, Z., STEINER, A.W. & YAGI, K. (2019). Constraining nuclear matter parameters with GW170817. *Phys. Rev.*, **D99**, 043010.
- CHABANAT, E. (1995). Ph.D. thesis, University Claude Bernard Lyon-1, Lyon, France.

- CHABANAT, E., BONCHE, P., HAENSEL, P., MEYER, J. & SCHAEFFER, R. (1997). A Skyrme parametrization from subnuclear to neutron star densities. *Nucl. Phys.*, **A627**, 710–746.
- CHABANAT, E., BONCHE, P., HAENSEL, P., MEYER, J. & SCHAEFFER, R. (1998). A Skyrme parametrization from subnuclear to neutron star densities. 2. Nuclei far from stabilities. *Nucl. Phys.*, **A635**, 231–256, [Erratum: *Nucl. Phys.*A643,441(1998)].
- CHEN, L.W., CAI, B.J., KO, C.M., LI, B.A., SHEN, C. & XU, J. (2009). High-order effects on the incompressibility of isospin asymmetric nuclear matter. *Phys. Rev.*, **C80**, 014322.
- CHEN, W.C. & PIEKAREWICZ, J. (2014). Building relativistic mean field models for finite nuclei and neutron stars. *Phys. Rev. C*, **90**, 044305.
- COLO, G., GARG, U. & SAGAWA, H. (2014). Symmetry energy from the nuclear collective motion: constraints from dipole, quadrupole, monopole and spin-dipole resonances. *Eur. Phys. J.*, **A50**, 26.
- COL, G., CAO, L., GIAI, N.V. & CAPELLI, L. (2013). Self-consistent rpa calculations with skyrme-type interactions: The skyrme rpa program. *Computer Physics Communications*, **184**, 142 – 161.
- COULTER, D.A. *et al.* (2017). Swope Supernova Survey 2017a (SSS17a), the Optical Counterpart to a Gravitational Wave Source. *Science*, [Science358,1556(2017)].
- CROMARTIE, H.T. *et al.* (2019). Relativistic Shapiro delay measurements of an extremely massive millisecond pulsar.
- CUTLER, C., APOSTOLATOS, T.A., BILDSTEN, L., FINN, L.S., FLANAGAN, E.E., KENNEFICK, D., MARKOVIC, D.M., ORI, A., POISSON, E., SUSSMAN, G.J. & THORNE, K.S. (1993). The last three minutes: Issues in gravitational-wave measurements of coalescing compact binaries. *Phys. Rev. Lett.*, **70**, 2984–2987.
- DAMOUR, T. & NAGAR, A. (2009). Relativistic tidal properties of neutron stars. *Phys. Rev. D*, **80**, 084035.
- DAMOUR, T., NAGAR, A. & VILLAIN, L. (2012). Measurability of the tidal polarizability of neutron stars in late-inspiral gravitational-wave signals. *Phys. Rev. D*, **85**, 123007.
- DANIELEWICZ, P. & LEE, J. (2014). Symmetry energy ii: Isobaric analog states. *Nuclear Physics A*, **922**, 1 – 70.

- DANIELEWICZ, P., LYNCH, W.G. & LACEY, R. (2002). Determination of the equation of state of dense matter. *Science*, **298**, 1592–1596.
- DE, J.N., SAMADDAR, S.K. & AGRAWAL, B.K. (2015). Reassessing nuclear matter incompressibility and its density dependence. *Phys. Rev. C*, **92**, 014304.
- DE, S., FINSTAD, D., LATTIMER, J.M., BROWN, D.A., BERGER, E. & BIWER, C.M. (2018). Tidal Deformabilities and Radii of Neutron Stars from the Observation of GW170817. *Phys. Rev. Lett.*, **121**, 091102, [Erratum: *Phys. Rev. Lett.* 121, no. 25, 259902 (2018)].
- DEMOREST, P., PENNUCCI, T., RANSOM, S., ROBERTS, M. & HESSELS, J. (2010). Shapiro Delay Measurement of A Two Solar Mass Neutron Star. *Nature*, **467**, 1081–1083.
- DHIMAN, S.K., KUMAR, R. & AGRAWAL, B.K. (2007). Nonrotating and rotating neutron stars in the extended field theoretical model. *Phys. Rev. C*, **76**, 045801.
- DIETRICH, S.S. & BERMAN, B. (1988). Atlas of Photoneutron Cross Sections Obtained with Monoenergetic Photons. *Atom. Data Nucl. Data Tabl.*, **38**, 199–338.
- DOBACZEWSKI, J., NAZAREWICZ, W. & REINHARD, P.G. (2014). Error estimates of theoretical models: a guide. *J. Phys. G: Nucl. Part. Phys.*, **41**, 074001.
- DREVER, R.W.P. (1983). *Gravitational Radiation*. (North-Holland, Amsterdam, 1983) p. 321.
- DUCOIN, C., MARGUERON, J., PROVIDÊNCIA, C. & VIDANA, I. (2011). Core-crust transition in neutron stars: Predictivity of density developments. *Phys. Rev. C*, **83**, 045801.
- DUEZ, M.D. (2010). Numerical relativity confronts compact neutron star binaries: a review and status report. *Class. Quant. Grav.*, **27**, 114002.
- DUTRA, M., LOURENCO, O., SA MARTINS, J.S., DELFINO, A., STONE, J.R. & STEVENSON, P.D. (2012). Skyrme Interaction and Nuclear Matter Constraints. *Phys. Rev.*, **C85**, 035201.
- DUTRA, M., LOURENO, O., AVANCINI, S.S., CARLSON, B.V., DELFINO, A., MENEZES, D.P., PROVIDENCIA, C., TYPEL, S. & STONE, J.R. (2014). Relativistic Mean-Field Hadronic Models under Nuclear Matter Constraints. *Phys. Rev.*, **C90**, 055203.
- EFRON, B. (1979). Bootstrap Methods: Another Look at the Jackknife. *The Annals of Statistics*, **7**, 1–26.

- FABER, J. (2009). Status of neutron star-black hole and binary neutron star simulations. *Class. Quant. Grav.*, **26**, 114004.
- FANTINA, A.F., CHAMEL, N., PEARSON, J.M. & GORIELY, S. (2014). Constraints on the equation of state of cold dense matter from nuclear physics and astrophysics. *EPJ Web of Conferences*, **66**, 07005.
- FATTOYEV, F.J., HOROWITZ, C.J., PIEKAREWICZ, J. & SHEN, G. (2010). Relativistic effective interaction for nuclei, giant resonances, and neutron stars. *Phys. Rev.*, **C82**, 055803.
- FATTOYEV, F.J., CARVAJAL, J., NEWTON, W.G. & LI, B.A. (2013). Constraining the high-density behavior of the nuclear symmetry energy with the tidal polarizability of neutron stars. *Phys. Rev. C*, **87**, 015806.
- FATTOYEV, F.J., PIEKAREWICZ, J. & HOROWITZ, C.J. (2018). Neutron Skins and Neutron Stars in the Multimessenger Era. *Phys. Rev. Lett.*, **120**, 172702.
- FAVATA, M. (2014). Systematic parameter errors in inspiraling neutron star binaries. *Phys. Rev. Lett.*, **112**, 101101.
- FLANAGAN, E.E. & HINDERER, T. (2008). Constraining neutron-star tidal love numbers with gravitational-wave detectors. *Phys. Rev. D*, **77**, 021502.
- FORTIN, M., PROVIDÊNCIA, C., RADUTA, A.R., GULMINELLI, F., ZDUNIK, J.L., HAENSEL, P. & BEJGER, M. (2016). Neutron star radii and crusts: Uncertainties and unified equations of state. *Phys. Rev. C*, **94**, 035804.
- FORTIN, M., AVANCINI, S.S., PROVIDÊNCIA, C. & VIDAÑA, I. (2017). Hypernuclei and massive neutron stars. *Phys. Rev. C*, **95**, 065803.
- FRAGA, E.S., KURKELA, A. & VUORINEN, A. (2016). Neutron star structure from QCD. *Eur. Phys. J.*, **A52**, 49.
- FRIEDRICH, J. & REINHARD, P.G. (1986). Skyrme-force parametrization: Least-squares fit to nuclear ground-state properties. *Phys. Rev.*, **C33**, 335–351.
- FUCHS, C. (2006). Kaon production in heavy ion reactions at intermediate energies. *Prog. Part. Nucl. Phys.*, **56**, 1.

- FUJIMOTO, Y., FUKUSHIMA, K. & MURASE, K. (2019). Mapping neutron star data to the equation of state using the deep neural network.
- FURNSTAHL, R.J. & SEROT, B.D. (1993). Finite nuclei in a relativistic model with broken chiral and scale invariance. *Phys. Lett.*, **B316**, 12–16.
- FURNSTAHL, R.J., SEROT, B.D. & TANG, H.B. (1997). A Chiral effective Lagrangian for nuclei. *Nucl. Phys.*, **A615**, 441–482, [Erratum: *Nucl. Phys.*A640,505(1998)].
- GAITANOS, T., DI TORO, M., TYPEL, S., BARAN, V., FUCHS, C., GRECO, V. & WOLTER, H.H. (2004). On the Lorentz structure of the symmetry energy. *Nucl. Phys.*, **A732**, 24–48.
- GELL-MANN, M. & LEVY, M. (1960). The axial vector current in beta decay. *Nuovo Cim.*, **16**, 705.
- GENDREAU, K.C., ARZOUMANIAN, Z., ADKINS, P.W., ALBERT, C.L., ANDERS, J.F., AYLWARD, A.T. & *et al* (2016). The Neutron star Interior Composition Explorer (NICER): design and development. In J.W.A. den Herder, T. Takahashi & M. Bautz, eds., *Space Telescopes and Instrumentation 2016: Ultraviolet to Gamma Ray*, vol. 9905, 420 – 435, International Society for Optics and Photonics, SPIE.
- GEZERLIS, A. & CARLSON, J. (2010). Low-density neutron matter. *Phys. Rev.*, **C81**, 025803.
- GLENDENNING, N.K. & MOSZKOWSKI, S.A. (1991). Reconciliation of neutron star masses and binding of the lambda in hypernuclei. *Phys. Rev. Lett.*, **67**, 2414–2417.
- GOLDSTEIN, A. *et al.* (2017). An Ordinary Short Gamma-Ray Burst with Extraordinary Implications: Fermi-GBM Detection of GRB 170817A. *Astrophys. J.*, **848**, L14.
- GOMES, R.O., FRANZON, B., DEXHEIMER, V. & SCHRAMM, S. (2017). Many-body forces in magnetic neutron stars. *Astrophys. J.*, **850**, 20.
- GORIELY, S., CHAMEL, N. & PEARSON, J.M. (2010). Further explorations of skyrme-hartree-fock-bogoliubov mass formulas. xii. stiffness and stability of neutron-star matter. *Phys. Rev. C*, **82**, 035804.
- GORIELY, S., CHAMEL, N. & PEARSON, J.M. (2013). Further explorations of skyrme-hartree-fock-bogoliubov mass formulas. xiii. the 2012 atomic mass evaluation and the symmetry coefficient. *Phys. Rev. C*, **88**, 024308.

- GRILL, F., PAIS, H., PROVIDENCIA, C., VIDAA, I. & AVANCINI, S.S. (2014). Equation of state and thickness of the inner crust of neutron stars. *Phys. Rev.*, **C90**, 045803.
- HAENSEL, P., POTEKHIN, A.Y. & YAKOVLEV, D.G. (2007). Neutron stars 1: Equation of state and structure. *Astrophys. Space Sci. Libr.*, **326**, pp.1–619.
- HAGGARD, D., NYNKA, M., RUAN, J.J., KALOGERA, V., BRADLEY CENKO, S., EVANS, P. & KENNEA, J.A. (2017). A Deep Chandra X-ray Study of Neutron Star Coalescence GW170817. *Astrophys. J.*, **848**, L25.
- HALLINAN, G. *et al.* (2017). A Radio Counterpart to a Neutron Star Merger. *Science*, **358**, 1579.
- HARRY, I. & HINDERER, T. (2018). Observing and measuring the neutron-star equation-of-state in spinning binary neutron star systems. *Class. Quant. Grav.*, **35**, 145010.
- HEBELER, K., LATTIMER, J.M., PETHICK, C.J. & SCHWENK, A. (2013). Equation of state and neutron star properties constrained by nuclear physics and observation. *The Astrophysical Journal*, **773**, 11.
- HEIDE, E.K., RUDAZ, S. & ELLIS, P.J. (1994). An Effective Lagrangian with broken scale and chiral symmetry applied to nuclear matter and finite nuclei. *Nucl. Phys.*, **A571**, 713–732.
- HINDERER, T. (2008). Tidal love numbers of neutron stars. *The Astrophysical Journal*, **677**, 1216.
- HINDERER, T., LACKEY, B.D., LANG, R.N. & READ, J.S. (2010). Tidal deformability of neutron stars with realistic equations of state and their gravitational wave signatures in binary inspiral. *Phys. Rev. D*, **81**, 123016.
- HOLT, J.W., KAISER, N. & MILLER, G.A. (2016). Microscopic optical potential for exotic isotopes from chiral effective field theory. *Phys. Rev. C*, **93**, 064603.
- HOROWITZ, C.J. & PIEKAREWICZ, J. (2001). Neutron star structure and the neutron radius of Pb-208. *Phys. Rev. Lett.*, **86**, 5647.
- HOUGH, J. & *et al.* (1989). *MPQ Technical Report No. 147 [GWD/137/JH(89)]*.
- JHA, T.K. & MISHRA, H. (2008). Constraints on nuclear matter parameters of an Effective Chiral Model. *Phys. Rev.*, **C78**, 065802.

- JHA, T.K., RAINA, P.K., PANDA, P.K. & PATRA, S.K. (2006). Neutron star matter in an effective model. *Phys. Rev.*, **C74**, 055803, [Erratum: *Phys. Rev.*C75,029903(2007)].
- JIANG, H., FU, G.J., ZHAO, Y.M. & ARIMA, A. (2012). Volume and surface symmetry energy coefficients. *Phys. Rev.*, **C85**, 024301.
- KHAN, E. & MARGUERON, J. (2013). Determination of the density dependence of the nuclear incompressibility. *Phys. Rev. C*, **88**, 034319.
- KHAN, E., MARGUERON, J. & VIDANA, I. (2012). Constraining the nuclear equation of state at subsaturation densities. *Phys. Rev. Lett.*, **109**, 092501.
- KOCH, V. (1997). Aspects of chiral symmetry. *Int. J. Mod. Phys.*, **E6**, 203–250.
- KOHLER, H. (1976). Skyrme force and the mass formula. *Nuclear Physics A*, **258**, 301.
- KONG, H.Y., XU, J., CHEN, L.W., LI, B.A. & MA, Y.G. (2017). Constraining simultaneously nuclear symmetry energy and neutron-proton effective mass splitting with nucleus giant resonances using a dynamical approach. *Phys. Rev. C*, **95**, 034324.
- KOUVELIOTOU, C. *et al.* (1998). An X-ray pulsar with a superstrong magnetic field in the soft gamma-ray repeater SGR 1806-20. *Nature*, **393**, 235–237.
- KURKELA, A., ROMATSCHKE, P. & VUORINEN, A. (2010). Cold quark matter. *Phys. Rev. D*, **81**, 105021.
- LALAZISSIS, G.A., KONIG, J. & RING, P. (1997). A New parametrization for the Lagrangian density of relativistic mean field theory. *Phys. Rev.*, **C55**, 540–543.
- LALAZISSIS, G.A., NIKŠIĆ, T., VRETENAR, D. & RING, P. (2005). New relativistic mean-field interaction with density-dependent meson-nucleon couplings. *Phys. Rev. C*, **71**, 024312.
- LANDRY, P. & ESSICK, R. (2019). Nonparametric inference of the neutron star equation of state from gravitational wave observations. *Phys. Rev.*, **D99**, 084049.
- LATTIMER, J.M. & LIM, Y. (2013). Constraining the Symmetry Parameters of the Nuclear Interaction. *Astrophys. J.*, **771**, 51.
- LATTIMER, J.M. & PRAKASH, M. (2001). Neutron star structure and the equation of state. *Astrophys. J.*, **550**, 426.

- LATTIMER, J.M. & PRAKASH, M. (2016). The Equation of State of Hot, Dense Matter and Neutron Stars. *Phys. Rept.*, **621**, 127–164.
- LEE, T.D. & MARGULIES, M. (1975). Interaction of a Dense Fermion Medium with a Scalar Meson Field. *Phys. Rev.*, **D11**, 1591, [,401(1974)].
- LEE, T.D. & WICK, G.C. (1974). Vacuum Stability and Vacuum Excitation in a Spin 0 Field Theory. *Phys. Rev.*, **D9**, 2291–2316.
- LI, B.A. (2017). Nuclear Symmetry Energy Extracted from Laboratory Experiments. *Nuclear Physics News*, **27**, 7–11.
- LI, B.A. & HAN, X. (2013). Constraining the neutronproton effective mass splitting using empirical constraints on the density dependence of nuclear symmetry energy around normal density. *Phys. Lett. B*, **727**, 276 – 281.
- LI, B.A. & STEINER, A.W. (2006). Constraining the radii of neutron stars with terrestrial nuclear laboratory data. *Phys. Lett.*, **B642**, 436–440.
- LI, B.A., CAI, B.J., CHEN, L.W. & XU, J. (2018). Nucleon effective masses in neutron-rich matter. *Prog. Part. Nucl. Phys.*, **99**, 29 – 119.
- LI, T. *et al.* (2010). Isoscalar giant resonances in the Sn nuclei and implications for the asymmetry term in the nuclear-matter incompressibility. *Phys. Rev.*, **C81**, 034309.
- LI, X.H., GUO, W.J., LI, B.A., CHEN, L.W., FATTOYEV, F.J. & NEWTON, W.G. (2015). Neutronproton effective mass splitting in neutron-rich matter at normal density from analyzing nucleon-nucleus scattering data within an isospin dependent optical model. *Physics Letters B*, **743**, 408 – 414.
- LIM, Y. & HOLT, J.W. (2018). Neutron star tidal deformabilities constrained by nuclear theory and experiment. *Phys. Rev. Lett.*, **121**, 062701.
- LIM, Y. & HOLT, J.W. (2019). Bayesian modeling of the nuclear equation of state for neutron star tidal deformabilities and gw170817. *arXiv:1902.05502*.
- LOGOTETA, D., VIDAA, I., BOMBACI, I. & KIEVSKY, A. (2015). Comparative study of three-nucleon force models in nuclear matter. *Phys. Rev.*, **C91**, 064001.

- MAKISHIMA, K., ENOTO, T., HIRAGA, J.S., NAKANO, T., NAKAZAWA, K., SAKURAI, S., SASANO, M. & MURAKAMI, H. (2014). Possible Evidence for Free Precession of a Strongly Magnetized Neutron Star in the Magnetar 4U 0142+61. *Phys. Rev. Lett.*, **112**, 171102.
- MALIK, T., ALAM, N., FORTIN, M., PROVIDÊNCIA, C., AGRAWAL, B.K., JHA, T.K., KUMAR, B. & PATRA, S.K. (2018a). Gw170817: Constraining the nuclear matter equation of state from the neutron star tidal deformability. *Phys. Rev. C*, **98**, 035804.
- MALIK, T., MONDAL, C., AGRAWAL, B.K., DE, J.N. & SAMADDAR, S.K. (2018b). Nucleon effective mass and its isovector splitting. *Phys. Rev. C*, **98**, 064316.
- MALIK, T., AGRAWAL, B.K., DE, J.N., SAMADDAR, S.K., PROVIDÊNCIA, C., MONDAL, C. & JHA, T.K. (2019a). See supplemental material at <http://link.aps.org/supplemental/10.1103/physrevc.99.052801> for the compilation of the properties of finite nuclei, nuclear matter, and neutron stars corresponding to the 28 representative edfs as used in the present work along with the result obtained for the newly generated skyrme forces. *Phys. Rev. C* **99**, 052801(Supplemental Material).
- MALIK, T., AGRAWAL, B.K., DE, J.N., SAMADDAR, S.K., PROVIDÊNCIA, C., MONDAL, C. & JHA, T.K. (2019b). Tides in merging neutron stars: Consistency of the GW170817 event with experimental data on finite nuclei. *Phys. Rev.*, **C99**, 052801.
- MELATOS, A. (1999). Bumpy spindown of anomalous x-ray pulsars: the link with magnetars. *Astrophys. J.*, **519**, L77.
- MESSENGER, C. & READ, J. (2012). Measuring a cosmological distance-redshift relationship using only gravitational wave observations of binary neutron star coalescences. *Phys. Rev. Lett.*, **108**, 091101.
- MISHUSTIN, I., BONDORF, J. & RHO, M. (1993). Chiral symmetry, scale invariance and properties of nuclear matter. *Nucl. Phys.*, **A555**, 215–224.
- MONDAL, C., AGRAWAL, B.K. & DE, J.N. (2015). Constraining the symmetry energy content of nuclear matter from nuclear masses: A covariance analysis. *Phys. Rev. C*, **92**, 024302.
- MONDAL, C., AGRAWAL, B.K., DE, J.N., SAMADDAR, S.K., CENTELLES, M. & VIAS, X. (2017). Interdependence of different symmetry energy elements. *Phys. Rev.*, **C96**, 021302.

- MOST, E.R., WEIH, L.R., REZZOLLA, L. & SCHAFFNER-BIELICH, J. (2018). New constraints on radii and tidal deformabilities of neutron stars from gw170817. *Phys. Rev. Lett.*, **120**, 261103.
- MOTCH, C. *et al.* (2013). The Hot and Energetic Universe: End points of stellar evolution.
- NARIKAWA, T., UCHIKATA, N., KAWAGUCHI, K., KIUCHI, K., KYUTOKU, K., SHIBATA, M. & TAGOSHI, H. (2018). Discrepancy in tidal deformability of GW170817 between the Advanced LIGO twin detectors.
- NAZAREWICZ, W., DOBACZEWSKI, J., WERNER, T.R., MARUHN, J.A., REINHARD, P.G., RUTZ, K., CHINN, C.R., UMAR, A.S. & STRAYER, M.R. (1996). Structure of proton drip-line nuclei around doubly magic ^{48}Ni . *Phys. Rev. C*, **53**, 740.
- NIKSIC, T., VRETENAR, D., FINELLI, P. & RING, P. (2002). Relativistic Hartree-Bogolyubov model with density dependent meson nucleon couplings. *Phys. Rev.*, **C66**, 024306.
- NIKSIC, T., VRETENAR, D. & RING, P. (2008). Relativistic Nuclear Energy Density Functionals: Adjusting parameters to binding energies. *Phys. Rev.*, **C78**, 034318.
- OERTEL, M., HEMPEL, M., KLÄHN, T. & TYPPEL, S. (2017). Equations of state for supernovae and compact stars. *Rev. Mod. Phys.*, **89**, 015007.
- OLAUSEN, S.A. & KASPI, V.M. (2014). The McGill Magnetar Catalog. *Astrophys. J. Suppl.*, **212**, 6.
- PAIS, H. & PROVIDENCIA, C. (2016). Vlasov formalism for extended relativistic mean field models: The crust-core transition and the stellar matter equation of state. *Phys. Rev.*, **C94**, 015808.
- PAPAZOGLU, P., SCHAFFNER, J., SCHRAMM, S., ZSCHIESCHE, D., STOECKER, H. & GREINER, W. (1997). Phase transition in the chiral sigma - omega model with dilatons. *Phys. Rev.*, **C55**, 1499–1508.
- PAPAZOGLU, P., SCHRAMM, S., SCHAFFNER-BIELICH, J., STOECKER, H. & GREINER, W. (1998). Chiral Lagrangian for strange hadronic matter. *Phys. Rev.*, **C57**, 2576–2588.
- PASTORE, A. (2019). An introduction to Bootstrap for nuclear physics. *J. Phys.*, **G46**, 052001.
- PEARSON, J.M., CHAMEL, N. & GORIELY, S. (2010). Breathing-mode measurements in Sn isotopes and isospin dependence of nuclear incompressibility. *Phys. Rev.*, **C82**, 037301.

- PEREGO, A., RADICE, D. & BERNUZZI, S. (2017). AT 2017gfo: An Anisotropic and Three-component Kilonova Counterpart of GW170817. *Astrophys. J.*, **850**, L37.
- PIEKAREWICZ, J., FATTOYEV, F.J. & HOROWITZ, C.J. (2014). Pulsar glitches: The crust may be enough. *Phys. Rev. C*, **90**, 015803.
- POSTNIKOV, S., PRAKASH, M. & LATTIMER, J.M. (2010). Tidal love numbers of neutron and self-bound quark stars. *Phys. Rev. D*, **82**, 024016.
- PRAKASH, M., AINSWORTH, T.L. & LATTIMER, J.M. (1988). Equation of state and the maximum mass of neutron stars. *Phys. Rev. Lett.*, **61**, 2518–2521.
- PROVIDÊNCIA, C. & RABHI, A. (2013). Interplay between the symmetry energy and the strangeness content of neutron stars. *Phys. Rev. C*, **87**, 055801.
- RADICE, D. & DAI, L. (2019). Multimessenger parameter estimation of gw170817. *The European Physical Journal A*, **55**, 50.
- RADICE, D., PEREGO, A., ZAPPA, F. & BERNUZZI, S. (2018). Gw170817: Joint constraint on the neutron star equation of state from multimessenger observations. *The Astrophysical Journal Letters*, **852**, L29.
- READ, J.S., MARKAKIS, C., SHIBATA, M., URYU, K., CREIGHTON, J.D.E. & FRIEDMAN, J.L. (2009). Measuring the neutron star equation of state with gravitational wave observations. *Phys. Rev.*, **D79**, 124033.
- READ, J.S., BAIOTTI, L., CREIGHTON, J.D.E., FRIEDMAN, J.L., GIACOMAZZO, B., KYUTOKU, K., MARKAKIS, C., REZZOLLA, L., SHIBATA, M. & TANIGUCHI, K. (2013). Matter effects on binary neutron star waveforms. *Phys. Rev.*, **D88**, 044042.
- REINHARD, P.G. (1999). Skyrme forces and giant resonances in exotic nuclei. *Nucl. Phys.*, **A649**, 305–314.
- REINHARD, P.G. & FLOCARD, H. (1995). Nuclear effective forces and isotope shifts. *Nucl. Phys.*, **A584**, 467–488.
- REZZOLLA, L., MOST, E.R. & WEIH, L.R. (2018a). Using gravitational-wave observations and quasi-universal relations to constrain the maximum mass of neutron stars. *Astrophys. J. Lett.*, **852**, L25.

- REZZOLLA, L., PIZZOCHERO, P., JONES, D.I., REA, N. & VIDAA, I. (2018b). *The Physics and Astrophysics of Neutron Stars. Astrophys. Space Sci. Libr.*, **457**.
- ROCA-MAZA, X., CENTELLES, M., VINAS, X. & WARDA, M. (2011). Neutron skin of ^{208}Pb , nuclear symmetry energy, and the parity radius experiment. *Phys. Rev. Lett.*, **106**, 252501.
- ROCA-MAZA, X., BRENNA, M., AGRAWAL, B.K., BORTIGNON, P.F., COL, G., CAO, L.G., PAAR, N. & VRETENAR, D. (2013a). Giant Quadrupole Resonances in ^{208}Pb , the nuclear symmetry energy and the neutron skin thickness. *Phys. Rev.*, **C87**, 034301.
- ROCA-MAZA, X., CENTELLES, M., VIAS, X., BRENNA, M., COL, G., AGRAWAL, B.K., PAAR, N., PIEKAREWICZ, J. & VRETENAR, D. (2013b). Electric dipole polarizability in ^{208}Pb : Insights from the droplet model. *Phys. Rev.*, **C88**, 024316.
- ROCA-MAZA, X., VIÑAS, X., CENTELLES, M., AGRAWAL, B.K., COLÒ, G., PAAR, N., PIEKAREWICZ, J. & VRETENAR, D. (2015). Neutron skin thickness from the measured electric dipole polarizability in ^{68}Ni , ^{120}Sn , and ^{208}Pb . *Phys. Rev. C*, **92**, 064304.
- RUSSOTTO, P., GANNON, S., KUPNY, S., LASKO, P., ACOSTA, L. & *et all* (2016). Results of the asy-eos experiment at gsi: The symmetry energy at suprasaturation density. *Phys. Rev. C*, **94**, 034608.
- SAGAWA, H., YOSHIDA, S., ZENG, G.M., GU, J.Z. & ZHANG, X.Z. (2007). Isospin dependence of incompressibility in relativistic and non-relativistic mean field calculations. *Phys. Rev.*, **C76**, 034327, [Erratum: *Phys. Rev.*C77,049902(2008)].
- SAHU, P.K. & OHNISHI, A. (2000). SU(2) chiral sigma model and the properties of neutron stars. *Prog. Theor. Phys.*, **104**, 1163–1171.
- SAHU, P.K., BASU, R. & DATTA, B. (1993). High density matter in the chiral sigma model. *Astrophys. J.*, **416**, 267–275.
- SAHU, P.K., JHA, T.K., PANDA, K.C. & PATRA, S.K. (2004). Hot nuclear matter in asymmetry chiral sigma model. *Nucl. Phys.*, **A733**, 169–184.
- SAHU, P.K., TSUBAKIHARA, K. & OHNISHI, A. (2010). Nuclear Matter and Finite Nuclei in the Effective Chiral Model. *Phys. Rev.*, **C81**, 014002.

- SAMMARRUCA, F., CORAGGIO, L., HOLT, J.W., ITACO, N., MACHLEIDT, R. & MARCUCCI, L.E. (2015). Toward order-by-order calculations of the nuclear and neutron matter equations of state in chiral effective field theory. *Phys. Rev. C*, **91**, 054311.
- SCHRAMM, S. (2002). Deformed nuclei in a chiral model. *Phys. Rev.*, **C66**, 064310.
- SEROT, B.D. & WALECKA, J.D. (1997). Recent progress in quantum hadrodynamics. *Int. J. Mod. Phys.*, **E6**, 515–631.
- SHLOMO, S., KOLOMIETZ, V.M. & COLÒ, G. (2006). Deducing the nuclear-matter incompressibility coefficient from data on isoscalar compression modes. *Eur. Phys. J. A*, **30**, 23–30.
- SKYRME, T.H.R. (1956). CVII. The nuclear surface. *Phil. Mag.*, **1**, 1043–1054.
- STONE, J.R., STONE, N.J. & MOSZKOWSKI, S.A. (2014). Incompressibility in finite nuclei and nuclear matter. *Phys. Rev.*, **C89**, 044316.
- SULAKSONO, A. & AGRAWAL, B.K. (2012). Existence of hyperons in the pulsar PSRJ1614-2230. *Nucl. Phys.*, **A895**, 44–58.
- TAYLOR, J.H. & WEISBERG, J.M. (1982). A new test of general relativity: Gravitational radiation and the binary pulsar PS R 1913+16. *Astrophys. J.*, **253**, 908–920.
- TEWS, I., KRÜGER, T., HEBELER, K. & SCHWENK, A. (2013). Neutron matter at next-to-next-to-next-to-leading order in chiral effective field theory. *Phys. Rev. Lett.*, **110**, 032504.
- TEWS, I., MARGUERON, J. & REDDY, S. (2018). Critical examination of constraints on the equation of state of dense matter obtained from gw170817. *Phys. Rev. C*, **98**, 045804.
- TEWS, I., MARGUERON, J. & REDDY, S. (2019). Confronting gravitational-wave observations with modern nuclearphysics constraints. *arXiv:1901.09874 [nucl-th]*.
- THOMAS, A.W., GUICHON, P.A.M., LEINWEBER, D.B. & YOUNG, R.D. (2004). Towards a connection between nuclear structure and QCD. *Prog. Theor. Phys. Suppl.*, **156**, 124–136.
- THORNE, K. (1987). *Three Hundred Years of Gravitation*. Cambridge, UK: Univ. Pr. 684 p.
- TODD-RUTEL, B.G. & PIEKAREWICZ, J. (2005). Neutron-Rich Nuclei and Neutron Stars: A New Accurately Calibrated Interaction for the Study of Neutron-Rich Matter. *Phys. Rev. Lett.*, **95**, 122501.

- TRIPPA, L., COLÒ, G. & VIGEZZI, E. (2008). The Giant Dipole Resonance as a quantitative constraint on the symmetry energy. *Phys. Rev.*, **C77**, 061304.
- TROJA, E. *et al.* (2017). The X-ray counterpart to the gravitational wave event GW 170817. *Nature*, **551**, 71–74, [Nature551,71(2017)].
- TSANG, M.B., ZHANG, Y., DANIELEWICZ, P., FAMIANO, M., LI, Z., LYNCH, W.G. & STEINER, A.W. (2009). Constraints on the density dependence of the symmetry energy. *Phys. Rev. Lett.*, **102**, 122701.
- TSANG, M.B., ZHANG, Y., DANIELEWICZ, P. & *et al.* (2010). Constraints on the density dependence of the symmetry energy. *Int. Jour. of Mod. Phys. E*, **19**, 1631–1638.
- TSUBAKIHARA, K. & OHNISHI, A. (2007). A Chiral symmetric relativistic mean field model with logarithmic sigma potential. *Prog. Theor. Phys.*, **117**, 903–921.
- TSUBAKIHARA, K., MAEKAWA, H. & OHNISHI, A. (2007). Hypernuclei and nuclear matter in a chiral SU(3) RMF model. *Eur. Phys. J.*, **A33**, 295–298.
- TSUBAKIHARA, K., MAEKAWA, H., MATSUMIYA, H. & OHNISHI, A. (2010). Lambda hypernuclei and neutron star matter in a chiral SU(3) relativistic mean field model with a logarithmic potential. *Phys. Rev.*, **C81**, 065206.
- TYPEL, S. & WOLTER, H.H. (1999). Relativistic mean field calculations with density dependent meson nucleon coupling. *Nucl. Phys.*, **A656**, 331–364.
- TYPEL, S., ROPKE, G., KLAHN, T., BLASCHKE, D. & WOLTER, H.H. (2010). Composition and thermodynamics of nuclear matter with light clusters. *Phys. Rev. C*, **81**, 015803.
- VAUTHERIN, D. & BRINK, D.M. (1972). Hartree-Fock calculations with Skyrme’s interaction. 1. Spherical nuclei. *Phys. Rev.*, **C5**, 626–647.
- WALECKA, J.D. (1974). A Theory of highly condensed matter. *Annals Phys.*, **83**, 491–529.
- WATTS, A.L. *et al.* (2019). Dense matter with eXTP. *Sci. China Phys. Mech. Astron.*, **62**, 29503.
- WEINBERG, S. (1972). *Gravitation and cosmology*. Wiley, New York.
- WEISSENBORN, S., CHATTERJEE, D. & SCHAFFNER-BIELICH, J. (2012). Hyperons and massive neutron stars: the role of hyperon potentials. *Nucl. Phys.*, **A881**, 62–77.

- WELLENHOFER, C., HOLT, J.W. & KAISER, N. (2015). Thermodynamics of isospin-asymmetric nuclear matter from chiral effective field theory. *Phys. Rev. C*, **92**, 015801.
- WELLENHOFER, C., HOLT, J.W. & KAISER, N. (2016). Divergence of the isospin-asymmetry expansion of the nuclear equation of state in many-body perturbation theory. *Phys. Rev. C*, **93**, 055802.
- WILSON-HODGE, C.A. *et al.* (2016). Large Observatory for x-ray Timing (LOFT-P): a Probe-class mission concept study. *Proc. SPIE Int. Soc. Opt. Eng.*, **9905**, 99054Y.
- WIRINGA, R., FIKS, V. & FABROCINI, A. (1988). Equation of state for dense nucleon matter. *Phys. Rev.*, **C38**, 1010–1037.
- WIRINGA, R.B. (1993). From deuterons to neutron stars: variations in nuclear many-body theory. *Rev. Mod. Phys.*, **65**, 231–242.
- Y.SUGAHARA & H.TOKI (1994). Relativistic mean field theory for unstable nuclei with nonlinear sigma and omega terms. *Nucl. Phys.*, **A579**, 557–572.
- ZDUNIK, J.L., FORTIN, M. & HAENSEL, P. (2017). Neutron star properties and the equation of state for the core. *Astron. Astrophys.*, **599**, A119.
- ZHANG, N.B. & LI, B.A. (2019a). Delineating Effects of Nuclear Symmetry Energy on the Radii and Tidal Polarizabilities of Neutron Stars. *J. Phys.*, **G46**, 014002.
- ZHANG, N.B. & LI, B.A. (2019b). Extracting Nuclear Symmetry Energies at High Densities from Observations of Neutron Stars and Gravitational Waves. *Eur. Phys. J.*, **A55**, 39.
- ZHANG, N.B., LI, B.A. & XU, J. (2018a). Combined Constraints on the Equation of State of Dense Neutron-rich Matter from Terrestrial Nuclear Experiments and Observations of Neutron Stars. *Astrophys. J.*, **859**, 90.
- ZHANG, Z. & CHEN, L.W. (2016). Isospin splitting of the nucleon effective mass from giant resonances in ^{208}Pb . *Phys. Rev. C*, **93**, 034335.
- ZHANG, Z., LIM, Y., HOLT, J.W. & KO, C.M. (2018b). Nuclear dipole polarizability from mean-field modeling constrained by chiral effective field theory. *Phys. Lett.*, **B777**, 73–78.

Curriculum Vitae (CV)

Contact Information

Research Scholar

Department of Physics
BITS Pilani K K Birla Goa Campus
Room No- B 109
State: Goa, PIN:403 726, Country: India.

Office: +91 832-2580150
mobile: +91 8967619343
e-mail: p20140402@goa.bits-pilani.ac.in
Skype ID : **tuhin.malik_3**

Permanent Address

Jiarah, Bandpur, Hooghly
Chanditala
City: Kolkata ; State: West Bengal,
PIN: 712 701; Country: India

Home: + 91 8007998333
e-mail: tuhin.malik@gmail.com

Education

- **Ph.D.** (2014– Present) Birla Institute of Science & Technology – Pilani, Goa, India
(Ph. D thesis submitted for review at 10th Dec 2019)
- **Masters of Science (M.Sc) Physics:** (2014) Indian School of Mines (IIT Dhanbad), Dhanbad, India
- **Bachelor of Science (B.Sc) Physics:** (2011) Scottish Church College, University of Calcutta, Kolkata, India
- **Higher Secondary Exam:** (2007) Akuni B. G. Beharilal Institution, Hooghly, India
- **Secondary Exam:** (2005) Akuni B. G. Beharilal Institution, Hooghly, India

Research Interests

- Nuclear Astrophysics.
- Compact Star.
- Gravitational Wave & tidal deformation of neutron star merger.

Awards

- International Travel Support (ITS) awarded by SCIENCE & ENGINEERING RESEARCH BOARD (SERB), Govt. of India for participating in “XXII International Conference on Few-Body Problems in Physics (FB22), France (09 July, 2018 to 13 July, 2018)“
- International Travel Grant (TG) awarded by COUNCIL OF SCIENTIFIC AND INDUSTRIAL RESEARCH (CSIR), HUMAN RESOURCE DEVELOPMENT, Govt. of India for participating “TALENT course 11 Learning from Data: Bayesian Methods and Machine Learning, in University of York, UK, June 10-28, 2019“

Conferences, Seminar and workshops attended

- TALENT workshop course 11, Learning from Data: Bayesian Methods and Machine Learning, in University of York, United Kingdom, June 10-28, 2019
- XXII International Conference on Few-Body Problems in Physics (FB22) 2018, France.
- Advances in Astroparticle Physics and Cosmology (AAPCOS-2018) workshop, India.
- DAE Symposium on Nuclear Physics, India in 2013, 2014, 2015, 2016, 2017 and 2018
- XXII DAE-BRNS high energy physics symposium 2016, India.

Research Visit

- Departamento de Física, University of Coimbra, Coimbra, Portugal
- Saha Institute of Nuclear Physics (SINP), Kolkata, India
- Physical Research Laboratory (PRL), Ahmedabad, India
- Institute of Physics (IOP), Bhubaneswar, India

Publications

Journals

- **“Tides in merging neutron stars: Consistency of the GW170817 event with experimental data on finite nuclei”**
Tuhin Malik, B. K. Agrawal, J. N. De, S. K. Samaddar, C. Providencia, C. Mondal and T. K. Jha.
arXiv:1901.04371 [nucl-th]
[DOI:10.1103/PhysRevC.99.052801](https://doi.org/10.1103/PhysRevC.99.052801)
Phys. Rev. C **99**, no. 5, 052801(R) (2019)
[2 citations counted in INSPIRE as of 29 Oct 2019](#)

- “Nucleon effective mass and its isovector splitting”
Tuhin Malik, C. Mondal, B. K. Agrawal, J. N. De and S. K. Samaddar.
arXiv:1811.09077 [nucl-th]
[DOI:10.1103/PhysRevC.98.064316](https://doi.org/10.1103/PhysRevC.98.064316)
Phys. Rev. C **98**, no. 6, 064316 (2018)
[1 citations counted in INSPIRE as of 29 Oct 2019](#)
- “Confronting nuclear equation of state in the presence of dark matter using GW170817 observation in relativistic mean field theory approach”
A. Das, Tuhin Malik and A. C. Nayak.
arXiv:1807.10013 [hep-ph]
[DOI:10.1103/PhysRevD.99.043016](https://doi.org/10.1103/PhysRevD.99.043016)
Phys. Rev. D **99**, no. 4, 043016 (2019)
[5 citations counted in INSPIRE as of 29 Oct 2019](#)
- “GW170817: constraining the nuclear matter equation of state from the neutron star tidal deformability”
Tuhin Malik, N. Alam, M. Fortin, C. Providencia, B. K. Agrawal, T. K. Jha, B. Kumar and S. K. Patra.
arXiv:1805.11963 [nucl-th]
[DOI:10.1103/PhysRevC.98.035804](https://doi.org/10.1103/PhysRevC.98.035804)
Phys. Rev. C **98**, no. 3, 035804 (2018)
[62 citations counted in INSPIRE as of 29 Oct 2019](#)
- “Nuclear symmetry energy with mesonic cross-couplings in the effective chiral model”
Tuhin Malik, K. Banerjee, T. K. Jha and B. K. Agrawal.
arXiv:1708.07291 [nucl-th]
[DOI:10.1103/PhysRevC.96.035803](https://doi.org/10.1103/PhysRevC.96.035803)
Phys. Rev. C **96**, no. 3, 035803 (2017)
[3 citations counted in INSPIRE as of 29 Oct 2019](#)
- “Spectroscopy of low-lying states in odd-odd ^{146}Eu ”
T. Bhattacharjee, D. Banerjee, S.K. Das, Tuhin Malik, S. Chanda, A. Chowdhury, P. Das, S. Bhattacharyya, R. Guin
[DOI:10.1103/PhysRevC.88.014313](https://doi.org/10.1103/PhysRevC.88.014313)
Phys. Rev. C **88**, no. 1, 014313 (2013).
[7 citations counted in INSPIRE as of 29 Oct 2019](#)

Conferences proceedings

- “Determination of the nuclear incompressibility and symmetry energy from neutron star tides”;
Tuhin Malik, N. Alam, M. Fortin, C. Providencia, B.K. Agrawal, T.K. Jha, Bharat Kumar and S.K. Patra
Proceedings of the [DAE Symp.Nucl.Phys. 63 \(2018\) 816-817](#)
- “Effects of mesonic cross-coupling on symmetry energy : effective chiral model”; Tuhin Malik, Kinjal Banerjee, T.K. Jha, B.K. Agrawal.
Proceedings of the [DAE Symp.Nucl.Phys. 62 \(2017\) 678-679](#)
- “Modified chiral potential and neutron stars”; Tuhin Malik, Kinjal Banerjee, T.K. Jha, B.K. Agrawal.
Proceedings of the [DAE Symp.Nucl.Phys. 61 \(2016\) 872-873](#)
- “Effect of non-linear vector interactions in nuclear matter” ; Tuhin Malik, Kinjal Banerjee, T.K. Jha.
Proceedings of the [DAE Symp.Nucl.Phys. 60 \(2015\) 878-879](#)
- “Gamma Spectroscopy with a digital oscilloscope ”; Tuhin Malik, Krithika Raman, Rutuparna Rath, Rohan Biswas, Dibyadyuti Pramanik, Abhijit Bisoi, Shinjinee Dasgupta, Maitreyee Saha Sarkar.
Proceedings of the [DAE Symp.Nucl.Phys. 59 \(2014\) 984-985](#)

- “Neutron Pulse-Shape Discrimination and Time -of - Flight Measurements with a Digital Oscilloscope”; Uttiyoarnab Saha, Krithika Raman, Rutuparna Rath, **Tuhin Malik**, Abhijit Bisoi, Maitreyee Saha Sarkar.
Proceedings of the **DAE Symp.Nucl.Phys. 59 (2014) 986-987**
- “Lifetime measurement with LaBr3 (Ce) Detector ”; D. Banerjee, A. Saha, **T. Malik**, T. Bhattacharjee, S.R.Banerjee, S.K.Das.
Proceedings of the **DAE Symp.Nucl.Phys. 58 (2013) 888-889**

Manuscript in Preparation

- “The Equation of State (EOS) for magnetized nuclear matter and tidal deformability in neutron star merger”
- “The nuclear matter EOS from neutron star properties and finite nuclei : a deep learning approach”

Teaching

- Teaching Assistance (TA) at BITS-Pilani Goa
- CMNSR2018, School cum First Collaboration Meeting on Computational Nuclear Structure and Reactions, VECC & SINP, Kolkata (2nd -22nd January 2018) on Advanced Fortran 90 Programming.

Competence with programming language known languages

- FORTRAN 90, Python, Wolfram Mathematica, C, Linux Shell scripting, L^AT_EX.
- English, Bengali and Hindi

Personal Details

- Name of Father : Mr. Sibnath Malik (Senior Section Engineer, Indian Railway).
- Name of Mother : Mrs. Sephali Malik
- Date of Birth : 16th April, 1990
- Nationality : Indian
- Marital Status : Married

Referees

Prof. B K Agrawal
Professor H
Theory Division
Saha Institute of Nuclear Physics, Kolkata
India
e-mail: *bijay.agrawal@saha.ac.in*

Prof. Jadu Nath De
Visiting Scientist
Theory Division
Saha Institute of Nuclear Physics, Kolkata
India
e-mail: *jn.de@saha.ac.in*

Dr. T K Jha
Assistant Professor
Physics Department
Birla Institute of Technology & Science, Pilani
K K Birla Goa Campus, India
e-mail: *tkjha@goa.bits-pilani.ac.in*

Prof. Hiranmaya Mishra
Senior Professor & Chairperson
Theoretical Physics Division
Physical Research Laboratory
India
e-mail: *hm@prl.res.in*

Prof. Constana Providncia
Full Professor
Departamento de Fsica
Universidade de Coimbra, Coimbra
Portugal
e-mail: *cp@uc.pt*

Dr. Tarun Kumar Jha

Assistant Professor, Physics Department
Birla Institute of Technology & Science, Pilani
K K Birla Goa Campus, Zuarinagar - 403 726, Goa; India

e-mail: tkjha75@gmail.com / tkjha@goa.bits-pilani.ac.in

Ph : +91 832 2580177 (O) / +91 95270 57533 (Cell)

Research Interest:

I work in the domain of Nuclear-Astrophysics. Here I am interested in working on problems related to Neutron stars, such as

- Symmetry energy & its implication on Equation of State of dense nuclear matter,
- Neutron star structure, composition and dynamics,
- Gravitational waves from Neutron Stars.

Personal Profile:

Date of Birth : 15th of December 1975

Sex : Male

Marital Status: Married

Nationality : India

Academic Profile:

Assistant Professor (August 2009 - cont.)

Affiliation : BITS Pilani; K K Birla Goa Campus

Post Doctoral Fellow (August 2007 - August 2009)

Institute : Physical Research Laboratory, Ahmedabad

Ph. D. in Physics (2008)

Thesis Title : Relativistic Nuclear Equation of State in an Effective Model.

Affiliation : Indian Institute of Technology - Kharagpur.

Thesis Supervisor : Prof. P. K. Raina; Dept. of Physics & Meteorology; IIT Kharagpur.

Master of Science (Nuclear Physics, 1999)

Affiliation : Sambalpur University

Marks Obtained : 70 %

Bachelor of Science (Physics (Honors), 1996)

Affiliation : G. M. College, Sambalpur

Marks Obtained : 60 %

Senior Secondary Examination (Physics, Chemistry, Mathematics, 1993)

Affiliation : Atomic Energy Central School, Jaduguda

Marks Obtained : 69.4 %

Higher Secondary Examination (1991)

Affiliation : Atomic Energy Central School, Jaduguda

Marks Obtained : 68 %

Teaching Experience: 4 Years: at the BITS Pilani - K K Birla Goa Campus

Sl. no	Courses	Book	# Taught	UG / PG
Ist Semester				
1	Physics I Mech., Oscill., & Waves	Klepner & Kolenkow A P French	2010, 2011, 2012, 2013	UG
2	Measurement Techniques I (LAB)	–	2009,2010,2011,2012	UG
IInd Semester				
3	Nuclear Physics	V Devnathan H S Hans	2010,2011,2012	UG
4	Astrophysics	IGNOU Baidyanath Basu	2010,2011,2013	PG
5	Atomic & Molecular Spectroscopy	B.H. Bransden & C.J. Joachain	2013	UG
6	Electromagnetic Theory	John R. Reitz, Milford & Robert W. Christy	2013	UG
7	Electric, Magnetic & Optics Laboratory	–	2013	UG
8	SOP/ COP/ LOP Projects	–		

Computational Skills:

- Operating systems: Linux, DOS, Windows
- Application Packages:
 - Typesetting Softwares: LaTeX, RevTeX, PCTex
 - Graphical Interface: XmGrace, Gnuplot, Origin, Excel
 - Scientific Packages: Scientific WorkPlace, Mathematica
 - Programming languages: Fortran & C

Research Experience:

- Post Doctoral experience of 2 years at Physical Research Laboratory, Ahmedabad.
- Research experience of more than 2 years (January 2002 - February 2004) at Institute of Physics, Bhubaneswar (India), under the supervision of Dr. S. K. Patra in the Relativistic Mean Field Theory.

Other Information:

1. Doctoral Thesis was selected among the best four thesis at National DAE Nuclear Physics Symposium (December 2007) held at Sambalpur University.
2. Nominated twice in Category A speaker in Nuclear Physics of Theoretical Physics Seminar Circuit (TPSC) in **2003-04 & 2006-07**, meant to deliver talks at various research institutes in India.
3. Senior Research Fellow (SRF) at IIT Kharagpur (**March 2004 - April 2007**).

4. Experience of one and half years (3 semesters) in taking laboratory assignments for the M.Sc. Ist year and Nuclear Physics experiments at IIT- Kharagpur.
5. Undertook the M.Sc. Project in “Linear electron accelerator” during Post Graduation, at Inter University Consortium for Department of Atomic Energy Facilities, Kolkata center (IUC DAEF-Kolkata), under the supervision of Dr. J. V. M. Krishna.

References:

1. **Prof. P. K. Raina**

HOD, Department of Physics
Indian Institute of Technology, Ropar
Nangal Road, Rupnagar, Punjab, 140001 INDIA

e-mail : pkraina@phy.iitkgp.ernet.in

Ph : +91 3222 283836 (O) / +91 9434023776 (Cellular)

Fax : +91 3222 282700

2. **Dr. Hiranmaya Mishra**

Theoretical Physics Division
Physical Research Laboratory, Ahmedabad
Gujarat - 380 009; INDIA

e-mail : hm@prl.res.in

Ph : +91 79 2631 4477 (O) / +91 9426408039 (Cellular)

Fax : +91 79 2631 1502

3. **Prof. S. Kar**

Department of Physics and Meteorology
Indian Institute of Technology, Kharagpur
West Bengal - 721 302; INDIA

e-mail : sayan@phy.iitkgp.ernet.in

Ph : +91 3222 283822 (O)

Fax : +91 3222 283857

4. **Dr. S. K. Patra**

Institute of Physics
Sachivalaya Marg, Bhubaneswar
Orissa - 751 005; INDIA

e-mail : patra@iopb.res.in

Ph : +91 674 230 1058 (extn-231) (O) / +91 674 230 1083 (Home)

Fax : +91 674 230 0142

5. **Dr. P. K. Rath**

Department of Physics
Lucknow University, Lucknow
Uttar Pradesh - 226 007; INDIA

e-mail : pkrath@hotmail.com

Ph : +91 9415419455 (Cellular)

List Of Publications:

1. “Bulk viscosity in hyperonic star and r-mode instability” by **T. K. Jha**, H. Mishra and V. Sreekanth. Physical Review C, **82**, (2010) 025803. Preprint: nucl-th/ 1002.4253.
2. “Constraints on nuclear matter parameters of an Effective chiral model” by **T. K. Jha** and H. Mishra. Physical Review C, **78**, (2008) 065802. Preprint: nucl-th/ 0811.4233.
3. “Attributes of a rotating Neutron star with a Hyperon core” by **T. K. Jha**, H. Mishra and V. Sreekanth. Physical Review C **77**, (2008) 045801. Preprint: nucl-th/ 0710.5392.
4. “Neutron star matter in an effective model” by **T. K. Jha**, P. K. Raina, P. K. Panda and S. K. Patra. Physical Review C **74**, (2006) 055803. Preprint: nucl-th/0608013.
5. “Hot nuclear matter in asymmetry chiral sigma model” by P. K. Sahu, **T. K. Jha**, K. C. Panda and S. K. Patra. Nuclear Physics A **733** (2004), 169.
6. “Shape change in Hf, W and Os-isotopes: A non-relativistic Hartree-Fock versus relativistic Hartree approximation” by Z. Naik, B. K. Sharma, **T. K. Jha**, P. Arumugam and S. K. Patra. Pramana- Journal of Physics, **62** (2004), 827.
7. “Potential energy surfaces for $N = Z, 20^{Ne} - 112^{Ba}$ nuclei” by M. S. Mehta, **T. K. Jha**, S. K. Patra and Raj. K. Gupta. Pramana- Journal of Physics, **62** (2004), 841.
8. “A relativistic mean-field study of magic numbers in light nuclei” from neutron to proton drip-lines by **T. K. Jha**, M. S. Mehta, S. K. Patra, B. K. Raj and Raj. K. Gupta, Pramana- Journal of Physics, **61** (2003), 517.

Prof. Bijay Kumar Agrawal

Date of birth: Nov. 3, 1964
Designation: Prof.'H',
Saha Institute of Nuclear Physics, Kolkata India.
Marital status: Married

ADDRESSES FOR CORRESPONDENCE :

Theory Division,
Saha Institute of Nuclear Physics,
1/AF, Bidhan Nagar
Kolkata - 700 064. INDIA
Mobile - 09433030328
Phone No.-091-33-23374321 (Ext. 2343), Fax - 091-233-3374637
E-mail - bijay.agrawal@saha.ac.in

ACADEMIC RECORD :

Year	Degree Obtained	University, Place Country	Main Subjects	Grade
1986	B. Sc.	Kurukshetra University, Kurukshetra, India	Physics, Maths Electronics & Hindi	First Division (Gold Medal)
1988	M. Sc.	Kurukshetra University, Kurukshetra, India	Electronics & Nuclear Physics	First Division
1989	Post M. Sc.	Institute of Physics, Bhubaneswar, India	Particle Physics, Solid State Physics & Nuclear Physics	
Jan. 1996	Ph. D.	Utkal University, Bhubaneswar, India	Nuclear Structure Physics	

TITLE OF THESIS : Study of hot rotating nuclei in a functional integral approach

THESIS SUPERVISOR : Professor A. Ansari

AREA OF RESEARCH INTEREST :

Nuclear Structure, Nuclear Astrophysics

Awards and Honours

- BSc. Gold Medal
- SINP Foundation Day Award 2014

POST DOCTORAL EXPERIENCE

1. May 1996 - April 1997 : Visiting Scientists at Bhabha Atomic Research Centre, Bombay.
2. May 1997 - August 1997 : Visiting Fellow at Institute of Physics, Bhubaneswar.
3. September 1997 - September 2000 : Research associate at Saha Institute of Nuclear Physics, Kolkata.
4. November 2001 - December 2004 : Research associate at Cyclotron Institute, Texas A&M University, USA.

ACADEMIC VISITS

1. RIKEN, Nishina Center for Accelerator Based Science, Japan March 15th - 31st, 2014.
2. Institute of Physics, Bhubaneswar, India, May 18th- 2nd June 2013.
3. Dipartimento di Fisica, Universit degli Studi di Milano, Italy from May 18th - 25th June , 2012.
4. Radioactive Ion Beam Facility, Oak Ridge National Laboratory, USA 9th-29th March 2011.
5. Institute of Mathematical Sciences, Chennai, July 12 - 20, 2007.
6. Vellore Institute of Technology, Vellore, July 25 - August 1, 2007.
7. Himachal Pradesh University, Shimla, May 22nd- 30th June, 2006.

Invited Talks

1. The journey from terrestrial nuclei to extraterrestrial neutron stars Banasthali Vidyapith, 28th March, 2017
2. The journey from finite nuclei to neutron stars, University of Rajasthan, Dept. of Physics, 30th March 2017
3. The journey from terrestrial nuclei to extraterrestrial neutron stars, BITS Pilani Goa Campus, 22nd March, 2016.
4. Sensitivity of symmetry energy content of nuclear matter to the properties of neutron rich systems, Recent Trends in Nuclear Structure and its implication in Astrophysics 2016 Puri Jan. 4-8 2016.
5. Probing the nuclear symmetry energy, Academic session of the Annual function of Alumni Association, Institute of Physics, 3rd Sept. 2015
6. Nuclear Physics Meet 2015, Institute of Physics, Bhubaneswar 26th -30th June, 2015
7. Nuclear symmetry energy from nuclear observables, RIKEN, Nishina Center for Accelerator Based Science, Japan March 25th 2014.
8. Density content of symmetry energy from neutron-skin, nuclear masses and giant resonances, DAE Symposium on Nuclear Physics Dec.2-6 2013 BARC, Mumbai.
9. Probing the density content of nuclear symmetry energy, National Conference on Nuclear Physics School of Physics, March 01-03, 2013 Sambalpur University Sambalpur, Odisha, India
10. Nuclear symmetry energy at nuclear saturation, Nuclear Dynamics and Nuclear Astrophysics' February 5-6, 2013, Department of Physics, University of Calcutta, India
11. Recent updates on Nuclear Symmetry Energy , BARC, 27th Dec. 2012, Mumbai.

12. Nuclear Symmetry Energy :An overview "International Conference on Recent Trends in Nuclear Physics-2012" Nov. 19-21, 2012 Chitkara University,Solan India.
13. "Existence of Hyperons in the PSRJ1614-2230, "The nuclear dipole polarizability and its impact on nuclear structure and astrophysics" ECT* Trento, Italy, June 18-22, 2012.
14. "Can Hyperons exist in the $2M_{\odot}$ pulsar?", INFN, Milano, Italy June 8 2012.
15. "Some results for the Extended Relativistic mean field models" Workshop on Neutron Skin and E1 Strength", Oak Ridge National Laboratory USA, 18 March 2011.
16. "Quarks in Astrophysics and Cosmology" in Toshali Sands", Puri, India, 15-17 February, 2008
17. "Neutron Stars : An Astrophysical Laboratory", Vellore Institute of Technology, Vellore, July 27th, 2007.
18. "Skyrme interactions: Past, Present and Future" Institute of Physics, Bhubaneswar, Jan. 30th, 2005.
19. "Breathing mode energy and nuclear matter incompressibility coefficient within the relativistic and nonrelativistic models", International conference on Exotic Nuclei and Atomic Masses, Callway Garden Atlanta, USA, Sept. 12-16 2004.
20. "Path integral approach to nuclear partition function and its application", 3rd national workshop on nuclear structure physics, Pantnagar India, Dec. (1996).

Invited Talks

1. Spectroscopic properties of nuclei in generalized seniority scheme, Bhoomika Maheshwari and Bijay Kumar Agrawal, CRC Press
2. Symmetry energy of warm nuclear system, B. K. Agrawal, J. N. De, S. K. Samaddar, M. Centelles and X. Vinas, Eur. Phys. J. A50, 19 (2014).

Research Guidance

A. Ph. D. Thesis

1. Tuhin Malik, BITS Pilani, K. K. Birla, Goa Campus, working under my supervision (as co-guide) for his Ph. D. thesis work. We are looking the various issues concerning the tidal deformability inferred from the observation of the gravitational waves from GW170817 event. We wish to implement Bayesian methods to extend our work and extract reasonable constraint on the equation of state using the gravitational wave data from LIGO-Virgo collaboration planned for the future.
2. Chiranjib Mondal has completed his Ph. D. thesis work under my supervision at Saha Institute of Nuclear Physics. We have developed an improved nuclear energy density functional with particular emphasis on the error propagation and the covariance analysis. We have shown using a simple form for the nuclear energy density functional that the curvature of symmetry energy can be expressed conveniently in terms of the symmetry energy and its slope. The universality of this analytical finding is verified using the results from 500 different nuclear energy density functionals consistent with the nuclear properties.
3. Naosad Alam has completed his Ph. D. thesis work under my supervision at Saha Institute of Nuclear Physics. We have mainly focussed on probing the equation of state (EOS) of dense matter in terms of the the correlations of the various bulk properties of neutron star with the key parameters of the EOS.
4. I have provided research guidance to O. Pochivalov who is a Ph. D. student of Prof. S. Shlomo at Texas A& M University, Texas, USA. I first trained him to carryout HF based RPA calculations for the response function for various giant multipole resonance. Then, our next step was to use the microscopic transition densities (obtained from HF-RPA) to calculate the cross-section for the various isoscalar giant multipole resonances excited by the inelastic scattering of α -particles.

5. I have supervised V. Kim Au who is Ph. D. student of Prof. S. Shlomo at Texas A& M University, Texas. I trained him to carry out numerical calculations using Hartree-Fock approach applied to the Skyrme type effective nucleon-nucleon interaction. Later on we published an article in which we provided for the first time the solution to the problem associated with the value of the nuclear matter incompressibility yielded by the relativistic and non-relativistic HF-RPA calculations.
6. I have supervised Raj Kumar Jagota, H. P. University, Shimla. We have studied the naturalness behaviour of the parameters of the extended field theoretical (EFT) model which includes the self and mixed interaction terms for the σ , ω and ρ mesons upto the quartic order. We show that the ω meson self coupling not only modifies the high density behaviour of the equation of state, but, it also affects crucially the overall naturalness of the parameters of the EFT model. Next, we studied in detail that up to what extent the properties of non-rotating and rotating neutron stars can be affected when the high density behaviour of the equations of state is appropriately varied within the EFT model.

B. Post M. Sc. review & summer projects

1. Tanmoy Ghosh, SINP, P. MSc. project on 'The beryllium anomaly and new physics, January - March, 2019.
2. Rashika Gupta, SINP, P. MSc. project on 'Anomaly of Beryllium', April - June, 2018.
3. Upalparna Banerjee, IIT Kharagpur, completed her summer project Numerical solution of Woods-Saxon potential using basis expansion method, during May - June, 2018.

TEACHING

1. Six lectures on 'Microscopic methods in nuclei' to the P. MSc. students, SINP Jan. -March, 2019.
2. Four lectures on 'Developing Skyrme-Hartee Fock code', during 'School cum First collaboration Meeting on computational Nuclear Structure & Reaction' during Jan. 2 - 22, 2018 (CMNSR2018), Saha Institute of Nuclear Physics / Variable Energy Cyclotron Center, Kolkata.
3. Six lectures on "Nuclear Energy Density Functionals within Relativistic Mean Field approach and their parameterizations", "SERC School on Modern Microscopic Approaches in Nuclear Physics", University of Kashmir, Srinagar, 17th May-6th June, 2016.
4. Three lectures for the "CNT lectures on Selected Topics in Nuclear Theory"(STNT2016) during 15th-25th February, 2016, on Numerical Optimization and Error Analysis"
5. Two lectures for the Post M.Sc. 2015-2016 as a part of the course on the Numerical Method.

Organization of school/conference

Proposed and organized 'School cum First collaboration Meeting on computational Nuclear Structure & Reaction' during Jan. 2 - 22, 2018 (CMNSR2018), Saha Institute of Nuclear Physics / Variable Energy Cyclotron Center, Kolkata.

The CMNSR2018 was proposed by me with the following motivation in the mind. Most of the theoretical work in the area of nuclear structure and reactions carried out at present in our country are based mainly on the computer codes developed at foreign institutions / universities. Consequently, our Ph. D. students are gradually losing skills of developing their own computer codes.

During the three week long school we trained the 40 students in learning some basic numerical techniques essential in developing useful codes for the study of nuclear structure and reactions. Long computer sessions were organized to encourage the students to develop their own computer codes.

REVIEW WORK

1. Examined 4 Ph. D. thesis.
2. Reviewed a book proposal: Recent Highlights in Nuclear Structure Physics : A Theoretical Treatise for CRC Press — Taylor & Francis Group.
3. Reviewed manuscripts for the following journals
 - (a) Pramana, Journal of Physics
 - (b) Indian Journal of Physics
 - (c) Journal of Nuclear Physics, Material Sciences, Radiation and Applications
 - (d) Physical Review C.
 - (e) European journal Physics.
 - (f) Zeitschrift fur Physik A.
 - (g) International Journal of Modern Physics
4. Reviewed research proposals submitted to:
 - (a) Department of Science & Technology Government of India
 - (b) National Science Center, Poland.

Best Cited Articles (according to Google scholar)

Journal Ref.	Times cited
Physical Review C 85, 041302 ,2012	193
Physical Review C 72 , 014310, 2005	167
Physical Review C 68, 031304, 2003	132
Physical Review C 88, 024316,2013	99
Physical Review C 87, 034301 ,2013	99
Physical Review C 92, 064304, 2015	90
Physical Review C 73, 034316, 2006	90
Physical Review C 81, 034323 ,2010	76
Physical Review C 76, 045801, 2007	71
Physical Review C 73, 034319, 2006	71
Physical review letters 109 , 262501, 2012	67
Physical Review C 98, 035804, 2018	56